AFWAL-TR-81-3154
VOLUME I

DESIGN METHODOLOGY FOR BONDED-BOLTED COMPOSITE JOINTS Vol. I. Analysis Derivations and Illustrative Solutions

L. J. Hart-Smith

Douglas Aircraft Company
McDonnell Douglas Corporation
Long Beach,
California 90846

February 1982

TECHNICAL REPORT AFWAL-TR-81-3154
Final Report for Period August 1979 - June 1981

FLIGHT DYNAMICS LABORATORY
AIR FORCE WRIGHT AERONAUTICAL LABORATORIES
AIR FORCE SYSTEMS COMMAND
WRIGHT-PATTERSON AIR FORCE BASE, OHIO 45433

NOTICE

When Government drawings, specifications, or other data are used for any purpose other than in connection with a definitely related Government procurement operation, the United States Government thereby incurs no responsibility nor any obligation whatsoever; and the fact that the government may have formulated, furnished, or in any way supplied the said drawings, specifications, or other data, is not to be regarded by implication or otherwise as in any manner licensing the holder or any other person or corporation, or conveying any rights or permission to manufacture use, or sell any patented invention that may in any way be related thereto.

This report has been reviewed by the Office of Public Affairs (ASD/PA) and is releasable to the National Technical Information Service (NTIS). At NTIS, it will be available to the general public, including foreign nations.

This technical report has been reviewed and is approved for publication.

VIPPERLA B. VENKAYYA
Project Engineer

FREDERICK A. PICCHIONI, Lt Col, USAF
Chief, Analysis & Optimization Branch

FOR THE COMMANDER

RALPH L. KUSTER, JR., Col, USAF
Chief, Structures & Dynamics Div.

"If your address has changed, if you wish to be removed from our mailing list, or if the addressee is no longer employed by your organization please notify AFWAL/FIBRA, W-PAFB, OH 45433 to help us maintain a current mailing list".

Copies of this report should not be returned unless return is required by security considerations, contractual obligations, or notice on a specific document.

Unclassified

SECURITY CLASSIFICATION OF THIS PAGE (When Data Entered)

REPORT DOCUMENTATION PAGE

READ INSTRUCTIONS BEFORE COMPLETING FORM

1. REPORT NUMBER: AFWAL-TR-81-3154, Vol I	2. GOVT ACCESSION NO.: AD-A117342
3. RECIPIENT'S CATALOG NUMBER:	
4. TITLE (and Subtitle): DESIGN METHODOLOGY FOR BONDED-BOLTED COMPOSITE JOINTS Volume I. Analysis Derivations and Illustrative Solutions	5. TYPE OF REPORT & PERIOD COVERED: Final Report August 1979 - June 1981
	6. PERFORMING ORG. REPORT NUMBER:
7. AUTHOR(s): L. J. Hart-Smith, Ph.D.	8. CONTRACT OR GRANT NUMBER(s): F33615-79-C-3212
9. PERFORMING ORGANIZATION NAME AND ADDRESS: Douglas Aircraft Company / McDonnell Douglas Corporation Long Beach, California 90846	10. PROGRAM ELEMENT, PROJECT, TASK AREA & WORK UNIT NUMBERS: P.E. 62201F Project 2401 02 28
11. CONTROLLING OFFICE NAME AND ADDRESS: Flight Dynamics Laboratory (AFWAL/FIBRA) AF Wright Aeronautical Laboratories Wright-Patterson AFB, OH 45433	12. REPORT DATE: February 1982
	13. NUMBER OF PAGES: 99
14. MONITORING AGENCY NAME & ADDRESS (if different from Controlling Office):	15. SECURITY CLASS. (of this report): Unclassified
	15a. DECLASSIFICATION/DOWNGRADING SCHEDULE:

16. DISTRIBUTION STATEMENT (of this Report)

Approved for public release; distribution unlimited.

17. DISTRIBUTION STATEMENT (of the abstract entered in Block 20, if different from Report)

18. SUPPLEMENTARY NOTES

19. KEY WORDS (Continue on reverse side if necessary and identify by block number)

Adhesive Bonded Joints
Bolted Joints
Bonded/Bolted Joints
Composite Joints
Computer Programs
Joint Analysis
Joint Design
Repairs

20. ABSTRACT (Continue on reverse side if necessary and identify by block number)

This report contains recent developments in three aspects of joints in advanced fibrous composite structures: (1) nonlinear analysis of adhesively-bonded stepped-lap joints and doublers, (2) multirow mechanically fastened joints in aerospace structures, and (3) nonlinear analysis of combined bonded and bolted joints. The methods developed include nonlinearities needed for metal structures as well as those for composites. The analyses are based on continuum mechanics techniques and have been coded into three Fortran IV

DD FORM 1 JAN 73 1473 EDITION OF 1 NOV 65 IS OBSOLETE

Unclassified

SECURITY CLASSIFICATION OF THIS PAGE (When Data Entered)

20. ABSTRACT (Continued)

digital computer programs A4EI, A4EJ, and A4EK respectively. The report contains explanations of the derivations of the solutions as well as sample worked problems to illustrate both the capabilities of the programs and the behavior characteristics of the real structures.

PREFACE

This report presents the results of the investigation into Design Methodology for Bonded-Bolted Composite Joints, Contract F33615-79-C-3212. The work was performed by the Douglas Aircraft Company, McDonnell Douglas Corporation, Long Beach, California during the period August 1979 to June 1981. Dr. L. J. Hart-Smith was the Principal Investigator.

This work was sponsored by the Air Force Flight Dynamics Laboratory, Wright-Patterson Air Force Base, Ohio. Dr. V. B. Venkayya and Lt. P. J. Conrad were the Project Engineers.

The computer coding for the programs A4EI, A4EJ and A4EK will be made available through the Aerospace Structures Information Analysis Center.

TABLE OF CONTENTS

TABLE OF CONTENTS (Concluded)

LIST OF ILLUSTRATIONS

LIST OF ILLUSTRATIONS (Continued)

LIST OF ILLUSTRATIONS (Concluded)

TABLE

SECTION 1

SUMMARY

It has long been recognized that the critical feature of aerospace structural design is the joints between the elements. They often represent reductions in static strength, and stress-concentration sites where fatigue damage can initiate. These situations are even more demanding for advanced composite structures because they are brittle and lack the ductility to redistribute loads (and mask imperfections in analysis) which is so characteristic of conventional metal alloys used widely throughout the industry.

This report examines three aspects of the analysis and design of joints in advanced fibrous composite structures: (1) nonlinear analysis of adhesively-bonded stepped-lap joints and doublers, (2) multirow mechanically fastened joints in aerospace structures, and (3) nonlinear analysis of combined bonded and bolted joints. The methods developed include nonlinearities needed for metal structures as well as those for composites. The analyses are based on continuum mechanics techniques and have been coded into three Fortran IV digital computer programs A4EI, A4EJ, and A4EK, respectively. This work builds upon prior contract research for the NASA Langley Research Center and the USAF Flight Dynamics Laboratory in which elastic-plastic analyses were developed for adhesively-bonded stepped-lap joints and doublers and coded as the A4EG and A4EH programs.

The material in Section 2 on nonlinear analysis of adhesive-bonded stepped-lap joints and doublers contains derivations for elastic, elastic-plastic, and bilinear adhesive models. The analyses have been coded into the computer program A4EI which is used to demonstrate many of the characteristics of thick stepped-lap bonded joints between metal and fibrous composites. The sample solutions cover the effect of the type of load application, tension, compression, or in-plane shear; the residual thermal stresses due to curing the adhesive at elevated temperature or to co-cure and bonding of the composite to the metal; the improvement of joint strength by

optimizing the joint proportions, particularly those of the end metal tab; the changes in critical failure mode with temperature and/or the nature of the applied loads; and the load redistribution around and across flaws. The importance of having such an analysis method available is emphasized in terms of experimental evidence as to the problems and weaknesses associated with unsuitably proportioned stepped-lap joints.

The nonlinearities included in the new analysis method in Section 3 for multirow mechanically fastened joints in aerospace structures include the fastener load-deflection characteristics, the provision for clearance around fasteners, the elastomechanical deformation of the members between the fasteners, and the interaction between bearing and bypass loads in establishing the failure loads at each station. The analysis has been coded into a Fortran IV digital computer program A4EJ. The solution is by continuum mechanics rather than finite elements, and the computer run times are therefore extremely short. This greater definition of the internal load transfer within such a joint requires considerably greater input data than older simpler analyses and the report indicates just what data will be required to be generated. Sample solutions are presented, to cover thick fibrous composite structure, and thin metal structure, to illustrate the capabilities of the analysis.

The combined bonded/bolted joint analysis in Section 4 of this report needs no new derivations beyond those in Sections 2 and 3. The illustrative examples show how the combination is typically no better than a nominally perfect adhesive-bonded joint alone, because the adhesive is typically so much stiffer than the fasteners. However, the combination is shown to have substantial benefits in the context of repair of improperly bonded structure prior to delivery, of the in-service repair of damaged structure, and of damage confinement in thick fibrous composites or bonded laminated metal structures. While it is widely recognized that bonded/bolted joints are difficult to justify for perfect structures, there are thus several situations which warrant having the capability to design and analyze such structures when allowance is made for real-world defects and damage. The separate analyses A4EI for bonded joints and A4EJ for bolted joints have been combined into the single computer program A4EK for combined bonded/bolted

joints. The sample solutions presented pertain to fibrous composite structures, but the program is equally applicable to all-metal structures.

If one highlight were to be singled out from the new developments in this investigation, it would have to be the use of fasteners in thick fibrous composite (or laminated metal) structures to provide fail-safety by preventing the wide-spread delaminations that could otherwise be initiated by quite local damage. While the fasteners carry virtually no load as long as the bond and laminate are intact, they enable any remaining adhesive after damage to work more efficiently as well as accept load themselves to relieve the load on the bonds or resin interfaces. This condition could arise anywhere in the structure, not just at the locations of the original splices. The examples shown for this problem encourage the belief that, with the analyses generated by the A4EK program, it should be possible to thus design sufficient fail-safety into thick composite structures. The residual strength of the damaged structure could be so high as to permit safe operation at the original strain level with only a loss of effective area in the damaged area, with no notch effect to reduce the load carrying capability of the structure outside that area.

SECTION 2

NONLINEAR ANALYSIS OF ADHESIVE-BONDED STEPPED-LAP JOINTS AND DOUBLERS

2.1 INTRODUCTION

The elastic-plastic analysis for the internal stresses and strains in the stepped-lap adhesive-bonded joints is documented in References 1 and 2. Those analyses are modified here to account for the features added since then. The original solution in Reference 1 produced the digital computer program A4EG for bonded joints. This was expanded in Reference 3 to produce the program A4EH for bonded doublers as well as bonded joints. The difference between the two is that, for bonded joints, the entire load is transferred through the adhesive while, for bonded doublers, only a fraction of the load is so transferred, with the remainder staying in the continuous member. As part of the Primary Adhesively Bonded Structure Technology (PABST) program, these earlier programs were expanded to include variable adhesive properties along with the earlier variable adherend properties. This new analysis, coded as the Fortran IV program A4EI is reported in Reference 2. (The earlier programs should now be considered superseded.) For the first time it became possible to analyze such effects as load redistribution around bond flaws, the strength loss due to pinch off of the adhesive at the edges of the overlap, and the consequences of porosity. Also, the logic was improved to reduce the already short run times and to minimize the amount of data input.

The nonlinear analysis presented here covers all of the material in Reference 2, as coded in the program A4EI, as well as new developments not yet coded. These include the bilinear adhesive model used for double-lap joints in Reference 4. This is not necessary for improved accuracy, but facilitates the generation of a set of solutions for a range of applied loads. The solution here also includes a variable bond width along the length of the joint, as with finger doublers, which is incorporated in the combined program

A4EK for bonded-bolted joints.

2.2 SYMBOLS

A, B, C, H, J, K A', B', C', D'	Integration constants
D	Effective disbonding (zero to unity range)
E_1, E_2	Young's moduli of adherends
F	Number of adhesively bonded surfaces (one or two)
G_{el}, G_{pl}	Adhesive shear moduli
ℓ	Total overlap (length of bond)
ℓ_{step}	Length of individual step in joint
p_1, p_2	Running loads introduced along length of joint
T_1, T_2	Direct stress resultants in adherends
ΔT	Temperature change ($T_{operating} - T_{cure}$)
t_1, t_2	Thicknesses of adherends
w, w_1, w_2	Widths of adherends
x	Axial (longitudinal) coordinate parallel to load direction
x_p	Length of plastic portion of step
α_1, α_2	Coefficients of thermal expansion of adherends
γ	Adhesive shear strain
γ_e, γ_p	Elastic and plastic adhesive shear strains
δ_1, δ_2	Axial (longitudinal) displacements of adherends
η	Thickness of adhesive layer
λ, λ'	Exponents of elastic and bilinear adhesive shear stress distribution
τ	Adhesive shear stress
τ_{el}, τ_p	Elastic and plastic peak adhesive shear stresses

Subscripts

1, 2	Different adherends at each end of joint
e, el, p, pl	Elastic and plastic adhesive behavior
ref	Value of quantity at start of step (x = 0)

2.3 NONLINEAR ANALYSIS OF ADHESIVE-BONDED STEPPED-LAP JOINTS

A representative idealized stepped-lap joint is shown in Figure 1, along with the sign convention and nomenclature necessary for the analysis. The analysis of this joint is conveniently subdivided into two to four stages, depending on the adhesive strain.

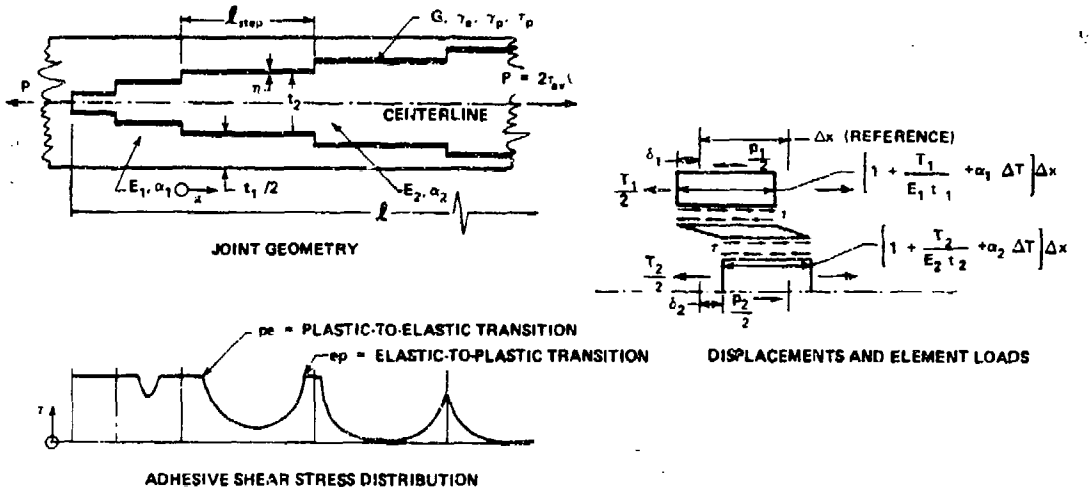

FIGURE 1. NOTATION AND GEOMETRY FOR ADHESIVE-BONDED STEPPED-LAP JOINT ANALYSIS

Equilibrium And Compatibility Equations

The analysis begins with the equilibrium equations for a differential element of one of the steps.

$$\frac{dT_1}{dx} - p_1 + F(1-D)\tau w = 0, \tag{1}$$

$$\frac{dT_2}{dx} + p_2 - F(1-D)\tau w = 0, \tag{2}$$

in which w is the bond width.

$$w \text{ is the lesser of } w_1 \text{ and } w_2 \tag{3}$$

The factor F is used to distinguish between single and double adhesive bond

surfaces.

$$\left.\begin{array}{l} F = 1 \text{ for one layer of adhesive (single shear)} \\ F = 2 \text{ for two layers of adhesive (double shear)} \end{array}\right\} \qquad (4)$$

The term D represents the effective disbond or porosity at that step, and the shear stress τ characterizes the adhesive on the reduced area that is fully stressed. The factor 1-D is needed to relate the adhesive shear stress τ to the differential motion between the adherends in terms of adhesive stress-strain characteristics measured on unflawed adhesive bonds. The adherend forces T_1 and T_2 refer to the total load in the adherends, rather than the loads per unit width modelled in Reference 2. Those loads may actually be in one or two physical members, depending on the number of adhesive-bonded surfaces.

The thermoelastic relations for the adherends are:

$$\frac{d\delta_1}{dx} = \frac{T_1}{E_1 t_1 w_1} + \alpha_1(\Delta T), \quad \frac{d\delta_2}{dx} = \frac{T_2}{E_2 t_2 w_2} + \alpha_2(\Delta T), \qquad (5)$$

in which

$$\Delta T = T_{operating} - T_{stress\text{-}free} \simeq T_{operating} - T_{cure} \qquad (6)$$

and is usually negative.

As a first approximation, the adhesive shear strain is represented as

$$\gamma = (\delta_2 - \delta_1) / \eta \qquad (7)$$

and is assumed to be constant across the thickness of the adhesive. This approximation violates the stress-free edges of the adhesive and results in a significant overestimate of the elastic adhesive shear stresses at the ends of the overlap; however, the error becomes progressively smaller as the adhesive is strained more into the nonlinear or plastic state. Differentiation of Equation (7) and the elimination of the displacements via Equations (5) leads to the result

$$\frac{d\gamma}{dx} = \frac{1}{\eta}\left(\frac{d\delta_2}{dx} - \frac{d\delta_1}{dx}\right) = \frac{1}{\eta}\left(\frac{T_2}{E_2 t_2 w_2} - \frac{T_1}{E_1 t_1 w_1} + (\alpha_2 - \alpha_1)\Delta T\right). \qquad (8)$$

A further differentiation of Equation (8), in conjunction with Equations (1) and (2), leads to the expression

$$\frac{d^2\gamma}{dx^2} - \frac{F(1-D)w}{\eta}\left(\frac{1}{E_1t_1w_1} + \frac{1}{E_2t_2w_2}\right)\tau = -\frac{1}{\eta}\left(\frac{p_1}{E_1t_1w_1} + \frac{p_2}{E_2t_2w_2}\right). \qquad (9)$$

Within the elastic region of adhesive behavior, as with light applied loads or near the middle of the bonded overlap, the adhesive stress is related to the shear strain by the equation

$$\tau = G_{el}\gamma \qquad (\text{for } \gamma \leq \gamma_e) \qquad (10)$$

while, throughout any plastic adhesive areas,

$$\tau = \tau_p = \text{constant.} \qquad (\text{for } \gamma \geq \gamma_e) \qquad (11)$$

For the nonlinear behavior of a bilinear elastic model,

$$\tau = \tau_{el} + G_{pl}(\gamma-\gamma_e) = (G_{el}-G_{pl})\gamma_e + G_{pl}\gamma. \qquad (\text{for } \gamma \geq \gamma_e) \qquad (12)$$

These various adhesive models are shown in Figure 2. There is no need for any more complicated adhesive models.

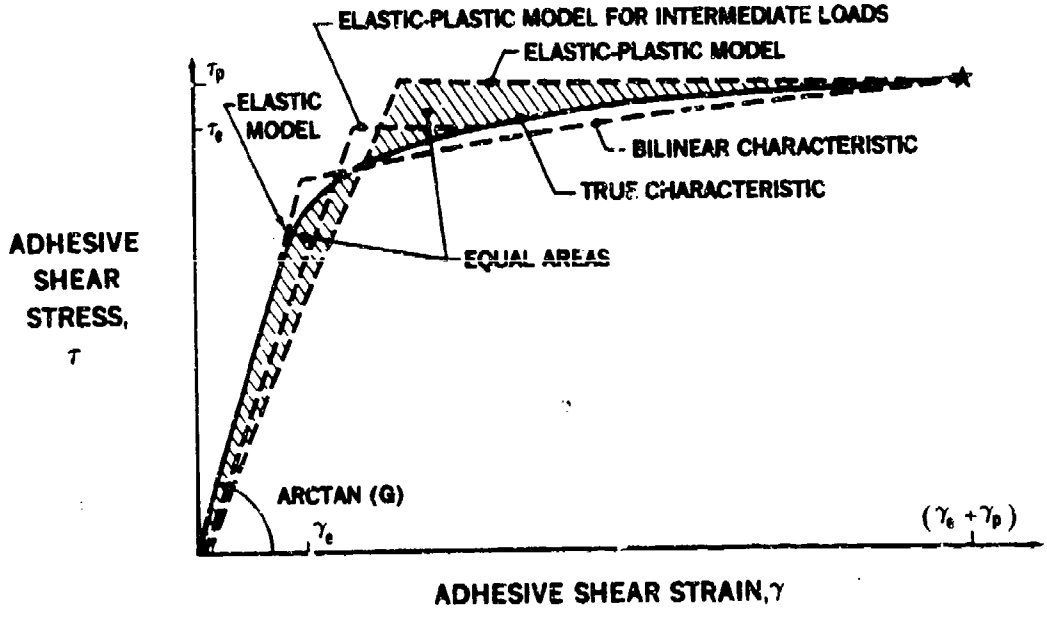

FIGURE 2. REPRESENTATIONS OF ADHESIVE NONLINEAR SHEAR BEHAVIOR

Elastic Solution

The combination of Equations (9) and (10) yields, as the governing differential equation for the elastic behavior,

$$\frac{d^2\gamma}{dx^2} - F(1-D)\frac{G_{el}w}{\eta}\left(\frac{1}{E_1t_1w_1} + \frac{1}{E_2t_2w_2}\right)\gamma = -\frac{1}{\eta}\left(\frac{p_1}{E_1t_1w_1} + \frac{p_2}{E_2t_2w_2}\right) \qquad (13)$$

or, on introducing the coefficient

$$\lambda^2 = F(1-D)\frac{G_{el}w}{\eta}\left(\frac{1}{E_1t_1w_1} + \frac{1}{E_2t_2w_2}\right), \qquad (14)$$

$$\frac{d^2\gamma}{dx^2} - \lambda^2\gamma = \text{constant}. \qquad (15)$$

The elastic adhesive shear strains are then expressed as

$$\gamma = A\cosh(\lambda x) + B\sinh(\lambda x) + C\ , \qquad (16)$$

in which

$$C = \frac{1}{\lambda^2\eta}\left(\frac{p_1}{E_1t_1w_1} + \frac{p_2}{E_2t_2w_2}\right). \qquad (17)$$

Integration of Equations (1) and (2) in turn, making use of Equation (10), leads to the expressions

$$T_1 = T_{1_{ref}} + p_1x - F(1-D)G_{el}w\left[\frac{A}{\lambda}\sinh(\lambda x) + \frac{B}{\lambda}\left(\cosh(\lambda x)-1\right) + Cx\right], \qquad (18)$$

and

$$T_2 = T_{2_{ref}} - p_2x + F(1-D)G_{el}w\left[\frac{A}{\lambda}\sinh(\lambda x) + \frac{B}{\lambda}\left(\cosh(\lambda x)-1\right) + Cx\right]. \qquad (19)$$

The values of the integration constant $T_{1_{ref}}$ and $T_{2_{ref}}$ depend on the origin adopted for x. In the coding of the computer program A4EI, it is convenient to adopt the start of each step as the origin of x for that step. Integrating Equations (18) and (19) again and substituting the integrals into Equations (5) yields the following

$$\delta_1 = \delta_{1_{ref}} + \alpha_1(\Delta T)x + \frac{1}{E_1 t_1 w_1}\left\{T_{1_{ref}}x + \frac{p_1 x^2}{2} - F(1-D)G_{el}w\right.$$

$$\left.\left[\frac{A}{\lambda^2}\left(\cosh(\lambda x)-1\right) + \frac{B}{\lambda^2}\left(\sinh(\lambda x) - \lambda x\right) + \frac{Cx^2}{2}\right]\right\} \qquad (20)$$

and

$$\delta_2 = \delta_{2_{ref}} + \alpha_2(\Delta T)x + \frac{1}{E_2 t_2 w_2}\left\{T_{2_{ref}}x - \frac{p_2 x^2}{2} + F(1-D)G_{el}w\right.$$

$$\left.\left[\frac{A}{\lambda^2}\left(\cosh(\lambda x)-1\right) + \frac{B}{\lambda^2}\left(\sinh(\lambda x) - \lambda x\right) + \frac{Cx^2}{2}\right]\right\} . \qquad (21)$$

The subroutine in the FORTRAN IV digital computer program A4EI used to solve the equations above (or, more strictly, those in Reference 2 without the variable width effect) for the elastic adhesive behavior employs the following analysis technique to determine the integration constants A and B. The notation ref is used to identify the start of any step or bonded zone within the overlap. The constant A in Equation (16) follows from evaluation of Equation (16) at $x = 0$. Thus

$$A = \gamma_{ref} - C, \qquad (22)$$

with the constant C given in Equation (17). The other constant B can be deduced by differentiating Equation (16) once and equating the result to that given by Equation (8). Thus

$$\frac{d\gamma}{dx} = A\lambda \sinh(\lambda x) + B\lambda \cosh(\lambda x) = \frac{1}{\eta}\left(\frac{T_2}{E_2 t_2 w_2} - \frac{T_1}{E_1 t_1 w_1} + (\alpha_2-\alpha_1)\Delta T\right) \qquad (23)$$

so that at $x = 0$

$$B = \frac{1}{\lambda\eta}\left(\frac{T_{2_{ref}}}{E_2 t_2 w_2} - \frac{T_{1_{ref}}}{E_1 t_1 w_1} + (\alpha_2-\alpha_1)\Delta T\right). \qquad (24)$$

The values of γ, τ, T_1, T_2, δ_1 and δ_2 at the end of that step then follow from Equations (16), (10), (18), (19), (20), and (21), respectively. These, in turn, specify the initial conditions for the next step.

For the special case of the first step of the joint, it is necessary to assume, or prescribe, a complete set of initial conditions. However, the actual conditions which must be satisfied are shared between both ends of the overlap. So it is necessary to adjust one of the initial conditions iteratively until the other boundary condition is satisfied at the far end of the bonded overlap.

Plastic Solution

The inclusion of plastic nonlinear behavior in the analysis is similar to that above for the elastic solution, with one of the major complications being the unknown location of any transitions between elastic and plastic behavior. The plastic adhesive shear stesss is constant throughout that portion (or all) of the step, as given in Equation (11). Therefore, Equation (9) becomes, for the plastic zones,

$$\frac{d^2\gamma}{dx^2} = \frac{\lambda^2}{G_{el}}\tau_p - \frac{1}{\eta}\left(\frac{P_1}{E_1t_1w_1} + \frac{P_2}{E_2t_2w_2}\right). \tag{25}$$

Thus, throughout the plastic adhesive areas,

$$\frac{d^2\gamma}{dx^2} = H = \frac{\lambda^2}{G_{el}}\tau_p - \frac{1}{\eta}\left(\frac{P_1}{E_1t_1w_1} + \frac{P_2}{E_2t_2w_2}\right) = \text{constant}, \tag{26}$$

so that

$$\gamma = \tfrac{1}{2}Hx^2 + Jx + K. \tag{27}$$

The other constants J and K are determined by directly analogous techniques with those used for the elastic solution. Thus

$$K = \gamma_{ref} = \gamma\Big|_{x=0} \tag{28}$$

and, from equations (27) and (8),

$$J = \frac{d\gamma}{dx}\Big|_{x=0} = \frac{1}{\eta}\left(\frac{T_{2_{ref}}}{E_2t_2w_2} - \frac{T_{1_{ref}}}{E_1t_1w_1} + (\alpha_2-\alpha_1)\Delta T\right). \tag{29}$$

The adherend loads in the plastic zone follow from integration of Equations (1) and (2), by means of Equation (11), as

$$T_1 = T_{1_{ref}} + p_1 x - F(1-D)w\tau_p x \tag{30}$$

and

$$T_2 = T_{2_{ref}} - p_2 x + F(1-D)w\tau_p x. \tag{31}$$

Equations (5) may then be integrated to yield

$$\delta_1 = \delta_{1_{ref}} + \alpha_1(\Delta T)x + \frac{1}{E_1 t_1 w_1}\left(T_{1_{ref}} x + \frac{p_1 x^2}{2} - F(1-D)w\tau_p \frac{x^2}{2}\right) \tag{32}$$

and

$$\delta_2 = \delta_{2_{ref}} + \alpha_2(\Delta T)x + \frac{1}{E_2 t_2 w_2}\left(T_{2_{ref}} x - \frac{p_2 x^2}{2} + F(1-D)w\tau_p \frac{x^2}{2}\right). \tag{33}$$

Very few individual steps of stepped-lap bonded joints or doublers have fully plastic behavior throughout. Any plastic (or other nonlinear) behavior is frequently confined to the ends of the outermost steps, because in order to achieve the excellent fatigue behavior for which bonded structures are renowned, it is desireable not to operate the adhesive beyond its proportional limit for frequently recurring loads. (The plastic strength is best reserved for overloads and for local load redistribution around flaws.) Therefore, in performing elastic-plastic analyses of adhesively-bonded stepped-lap joints, it is necessary to compute the extent of the step under consideration to see whether there is a transition to elastic behavior.

The various possible behaviors are shown in Figure 3. Starting from Equations (27) and (28),

$$\gamma = \tfrac{1}{2}Hx^2 + Jx + \gamma_{ref}, \tag{34}$$

in which the constant J is given by equation (29). It is necessary to find the lesser value of x for which

$$\gamma = \gamma_e. \tag{35}$$

Equation (34) is first rearranged to read

$$\tfrac{1}{2}Hx_p^2 + Jx_p + (\gamma_{ref} - \gamma_e) = 0, \tag{36}$$

so that the maximum extent of plastic adhesive zone is given by

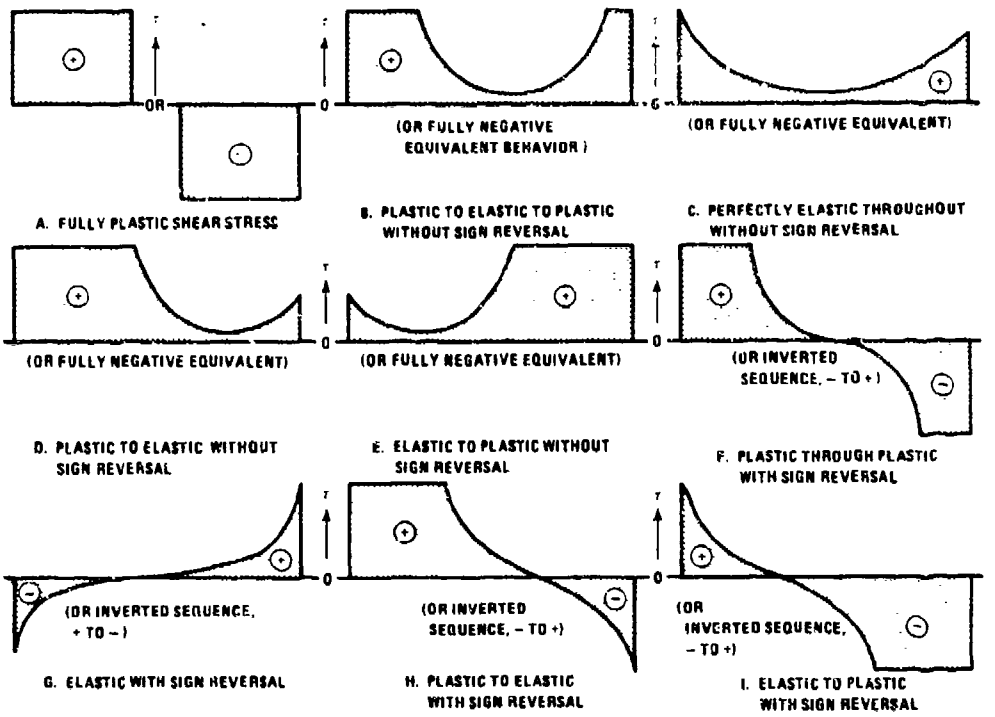

FIGURE 3. EIGHTEEN TYPES OF ADHESIVE BEHAVIOR IN BONDED JOINTS

$$x_p = -\frac{J}{H} \pm \sqrt{\left(\frac{J}{H}\right)^2 - \frac{2(\gamma_{ref} - \gamma_e)}{H}} \,. \tag{37}$$

The minus sign in front of the radical holds whenever $d\gamma/dx$ is less than zero, as at the near end of the joint. Now, if the loading is such that γ is negative and $d\gamma/dx$ positive at the start of the joint, the appropriate answer is the lesser of

$$x_p = -\frac{J'}{H'} \pm \sqrt{\left(\frac{J'}{H'}\right)^2 - \frac{2(\gamma_{ref} + \gamma_e)}{H'}} \,. \tag{38}$$

In evaluating this dimension, it is important to note that the expression for H in Equation (26) is modified by reversing the sign of the term containing the plastic shear stress τ_p. Likewise, the expression for J in Equation (29) is altered because the adherend loads T_1 and T_2 are negative. After x_p has been computed from Equation (37) or (38), it is compared with the actual step length ℓ_{step}. If $x_p > \ell_{step}$, that particular step is fully plastic

throughout, and the values of the various quantities at the far end of the step are evaluated from Equations (27), (11), (30), (31), and (33).

Should x_p be less than ℓ_{step}, the difference is examined elastically to see whether the step remains elastic thoughout the remainder or becomes plastic again at the far end. It is necessary that $d\gamma/dx$ be maintained at any plastic-to-elastic or elastic-to-plastic transitions in order to ensure equilibrium, as can be seen from Equation (29). In solving for the maximum possible length of the elastic adhesive zone, one must provide both for the case of shear strains of the same sign (positive or negative) at each end of the step and for the case of a reversal of sign in the shear stress. The latter can arise physically in the presence of adherend thermal mismatch (as between fibrous composites and metals) but occurs most frequently as a result of an imbalance between the known and assumed boundary conditions at the start of the analysis. The procedure to determine the length of the elastic zone is thus reduced to an iterative solution of the distance required for the adhesive strain to become

$$\gamma = \gamma_e \text{ or } -\gamma_e. \tag{39}$$

If the elastic zone does not extend beyond the far end of the step being analyzed, it is necessary to compute the load transferred between the adherends throughout the elastic trough. In doing so, it is simple to take the length computed for the elastic zone and substitute it back into Equations (16), (10), (18), (19), (20), and (21) for the standard elastic analysis of that portion. Should the elastic trough not extend to the far end of the step, Equations (27), (11), (30), (31), (32) and (33) are then employed for the plastic zone to the end of the step.

Bilinear Solution

The linear portion of the bilinear adhesive model shown in Figure 2 is given by the elastic analysis above, just as for the elastic-plastic model. So it is necessary to discuss only the nonlinear portion here. In this case Equation (9) becomes

$$\frac{d^2\gamma}{dx^2} - \frac{w}{\eta} F(1-D)\left(\frac{1}{E_1 t_1 w_1} + \frac{1}{E_2 t_2 w_2}\right) G_{pl}\gamma =$$

$$\frac{w}{\eta} F(1-D)\left(\frac{1}{E_1 t_1 w_1} + \frac{1}{E_2 t_2 w_2}\right)(G_{el}-G_{pl})\gamma_e - \frac{1}{\eta}\left(\frac{p_1}{E_1 t_1 w_1} + \frac{p_2}{E_2 t_2 w_2}\right) \quad (40)$$

or, in terms of Equation (14),

$$\frac{d^2\gamma}{dx^2} - \frac{G_{pl}}{G_{el}}\lambda^2\gamma = \left(1 - \frac{G_{pl}}{G_{el}}\right)\lambda^2\gamma_e - \frac{1}{\eta}\left(\frac{p_1}{E_1 t_1 w_1} + \frac{p_2}{E_2 t_2 w_2}\right). \quad (41)$$

It can be seen that this has the same basic form as Equation (15) for the linear elastic solution. It is sensible to introduce the notation

$$(\lambda')^2 = \frac{G_{pl}}{G_{el}}(\lambda)^2 \quad (42)$$

so that the solution of Equation (41) is

$$\gamma = \gamma_e + A' \cosh(\lambda' x) + B' \sinh(\lambda' x) + C' \quad (43)$$

in which

$$C' = \frac{1}{(\lambda')^2 \eta}\left(\frac{p_1}{E_1 t_1 w_1} + \frac{p_2}{E_2 t_2 w_2}\right) - \frac{G_{el}}{G_{pl}}\gamma_e \quad (44)$$

The adhesive shear stress then follows from Equation (12) as

$$\tau = G_{el}\gamma_e + A' G_{pl} \cosh(\lambda' x) + B' G_{pl} \sinh(\lambda' x) + C' G_{pl}. \quad (45)$$

$$\tau = A' G_{pl} \cosh(\lambda' x) + B' G_{pl} \sinh(\lambda' x) + D' G_{pl}, \quad (46)$$

where

$$D' = \frac{1}{(\lambda')^2 \eta}\left(\frac{p_1}{E_1 t_1 w_1} + \frac{p_2}{E_2 t_2 w_2}\right) = \frac{G_{el}}{G_{pl}} C. \quad (47)$$

The loads in the adherends then follow from the integration of Equations (1) and (2) as

$$T_1 = T_{1_{ref}} + p_1 x - F(1-D) G_{pl} w \left[\frac{A'}{\lambda'} \sinh(\lambda' x) + \frac{B'}{\lambda'}\left(\cosh(\lambda' x) - 1\right) + D' x\right] \quad (48)$$

and

$$T_2 = T_{2_{ref}} - p_2 x + \Gamma(1-D)G_{pl}w\left[\frac{A'}{\lambda'}\sinh(\lambda' x) + \frac{B'}{\lambda'}\left(\cosh(\lambda' x)-1\right) + D'x\right]. \quad (49)$$

The displacements then can be evaluated from Equations (5) in the form

$$\delta_1 = \delta_{1_{ref}} + \alpha_1(\Delta T)x + \frac{1}{E_1 t_1 w_1}\left\{T_{1_{ref}}x + \frac{p_1 x^2}{2} - F(1-D)G_{pl}w\right.$$
$$\left.\left[\frac{A'}{(\lambda')^2}\left(\cosh(\lambda' x)-1\right) + \frac{B'}{(\lambda')^2}\left(\sinh(\lambda' x)-\lambda' x\right) + \frac{D'x^2}{2}\right]\right\} \quad (50)$$

and

$$\delta_2 = \delta_{2_{ref}} + \alpha_2(\Delta T)x + \frac{1}{E_2 t_2 w_2}\left\{T_{2_{ref}}x - \frac{p_2 x^2}{2} + F(1-D)G_{pl}w\right.$$
$$\left.\left[\frac{A'}{(\lambda')^2}\left(\cosh(\lambda' x)-1\right) + \frac{B'}{(\lambda')^2}\left(\sinh(\lambda' x)-\lambda' x\right) + \frac{D'x^2}{2}\right]\right\}. \quad (51)$$

These equations are employed in much the same way as those above for the elastic and plastic solutions. The constant A' follows from Equation (43), evaluated at $x = 0$. That is

$$A' = \gamma_{ref} - \gamma_e - C'. \quad (52)$$

Similarly, the constant B' is determined in exactly the same form as in Equation (24). Thus

$$B' = \frac{1}{(\lambda')\eta}\left(\frac{T_{2_{ref}}}{E_2 t_2 w_2} - \frac{T_{1_{ref}}}{E_1 t_1 w_1} + (\alpha_2-\alpha_1)\Delta T\right). \quad (53)$$

Just as with the plastic analysis above, it is necessary to compare the extent of each step with the length over which the nonlinear adhesive behavior can occur. The procedure is first to evaluate Equation (43) over the entire step length and determine whether or not the strain at the far end of the step lies in the linear or nonlinear regime. The step can be subdivided into nonlinear and linear zones as necessary.

In-Plane Shear Loading

The derivations above have been presented for in-plane tensile or compressive loading across the bonded joint. The governing equations for in-plane shear loading (Figure 4) have precisely the same form, as explained in Reference 1. Only two changes are needed. The adherend extensional moduli E_1 and E_2 must be replaced by the shear moduli G_1 and G_2. This causes an increase in the distribution parameters λ and λ' which, in turn, results in higher peak adhesive shear strains than if the same load intensity were applied in tension or compression. However, since the adherend materials are usually weaker under in-plane shear than under direct in-plane tension or compression, the adhesive is still usually not the weak link in the structure. It is necessary also to delete the inclusion of the adherend thermal mismatch terms for in-plane shear loading, since those residual stress effects do not induce in-plane shear preloading in the adherends. That effect must be ignored until some more complex analysis is formulated to account for local effects which peak in two corners of the bond area rather than all along two edges. With ductile adhesives, the resultant effect of a small preload strain orthogonal to those induced by the basic applied load is often insignificant anyway.

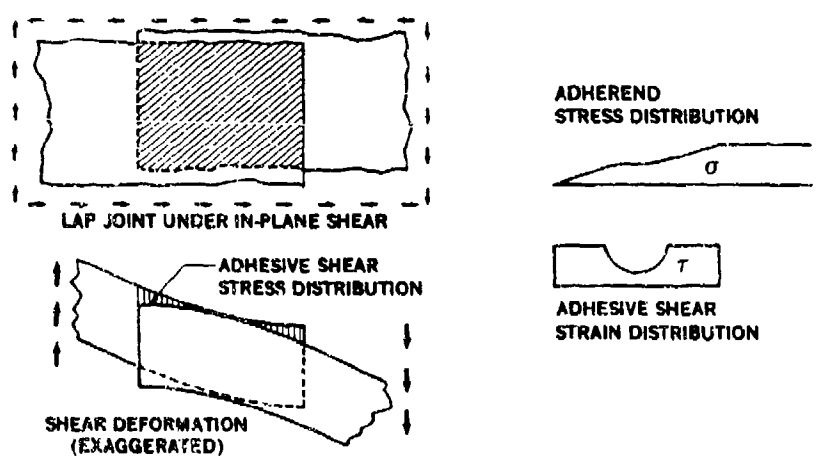

FIGURE 4. ADHESIVE-BONDED JOINT LOADED BY IN-PLANE SHEAR

2.4 SAMPLE SOLUTIONS

The sample solutions for adhesive-bonded steppped-lap joints and doublers which are given below are mostly concerned with variations on one basic high-load-intensity titanium to graphite-epoxy joint. The capabilities of the computer program A4EI are illustrated in terms of the different solutions for elastic, ultimate, and potential bond strengths, of the residual thermal stresses induced during cool-down after cure, of the different strengths in tensile and compressive load application, and of the load redistribution due to various bond flaws. Part 4 of this report uses this same basic joint as a means of showing how effective mechanical fastening is on its own, in conjuntion with the adhesive, and as a substitute for the adhesive in disbonded areas. References 1, 2, 3, 5, and 6 contain different sample solutions which augment the information about the features and capabilities of this program.

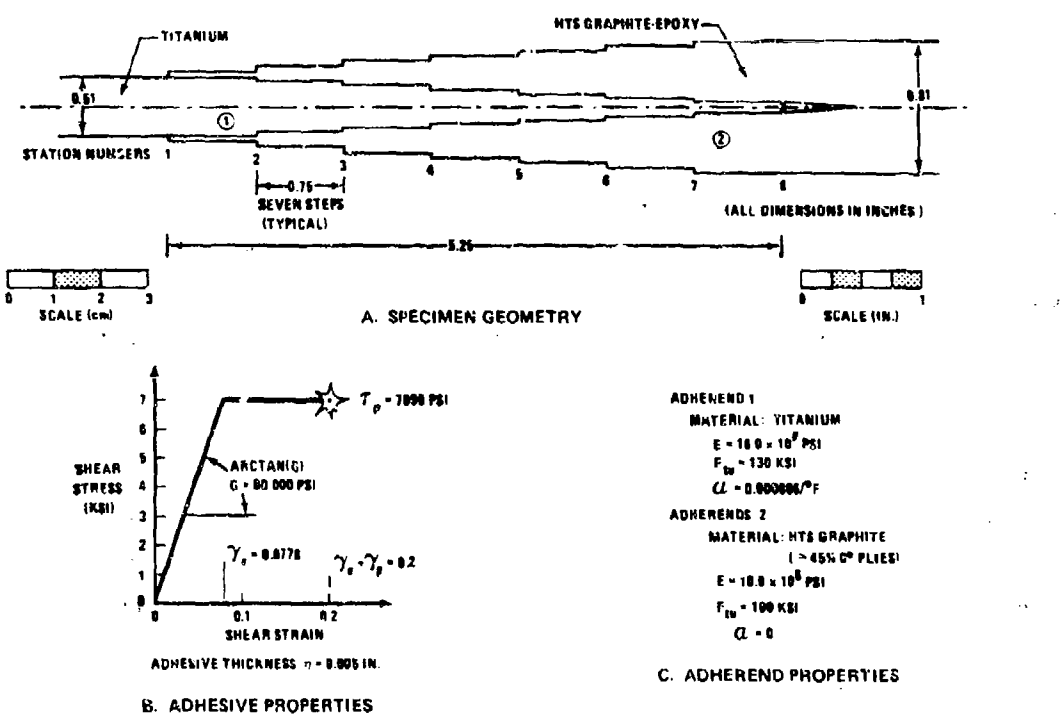

FIGURE 5. STEPPED-LAP ADHESIVE BONDED JOINT

Basic Joint Description

This basic joint is shown in Figure 5. It is a hypothetical joint, deliberately not optimized, to expose the design problems. The adhesive properties are not specific to any particular adhesive but representative of an adhesive which has a higher service temperature capability than the ductile adhesives used on the PABST program, in conjunction with somewhat more ductility than exhibited by the first generation of high-temperature brittle adhesives.

The following illustrative example solutions perform two functions. They demonstrate the capabilities of the analysis program A4EI and, in the process, explain many of the important considerations in the design and analysis of stepped-lap adhesive-bonded joints. The computer code itself is listed in Volume II of this report, along with the user instructions.

Solutions In Absence Of Residual Thermal Stresses

Figure 6 shows the adhesive shear stresses and strains associated with the simplest solution of the joint in Figure 5, neglecting the thermal stresses. (Strictly, for this case, the adhesive properties used in the analysis should have been those which apply at the stress-free temperature, about 300°F, but these curves are to be compared later with equivalent solutions accounting for the residual thermal stress effects and it would be confusing to cover two perturbations simultaneously.) Three curves are shown in Figure 6; for the adhesive elastic capability, for the failure of the joint in the adherend, and for the potential bond strength of the adhesive had the adherends been stronger. This information is typical of the answers obtained when the joint strength is sought. Note how, in the strain curves on the right, there is none of the flattening out associated with the stress curves on the left. The peaks of the stress and strain curves occur at the steps (discontinuities) in adherend properties at each station. It can be seen from the strain curves, on the right, that even at ultimate load only a small fraction of the adhesive is loaded beyond the elastic adhesive strain, so the accumulation of creep under sustained load is improbable. Indeed, over half of the adhesive is strained to less than 15 percent of its failure strain prior to failure of the adherend.

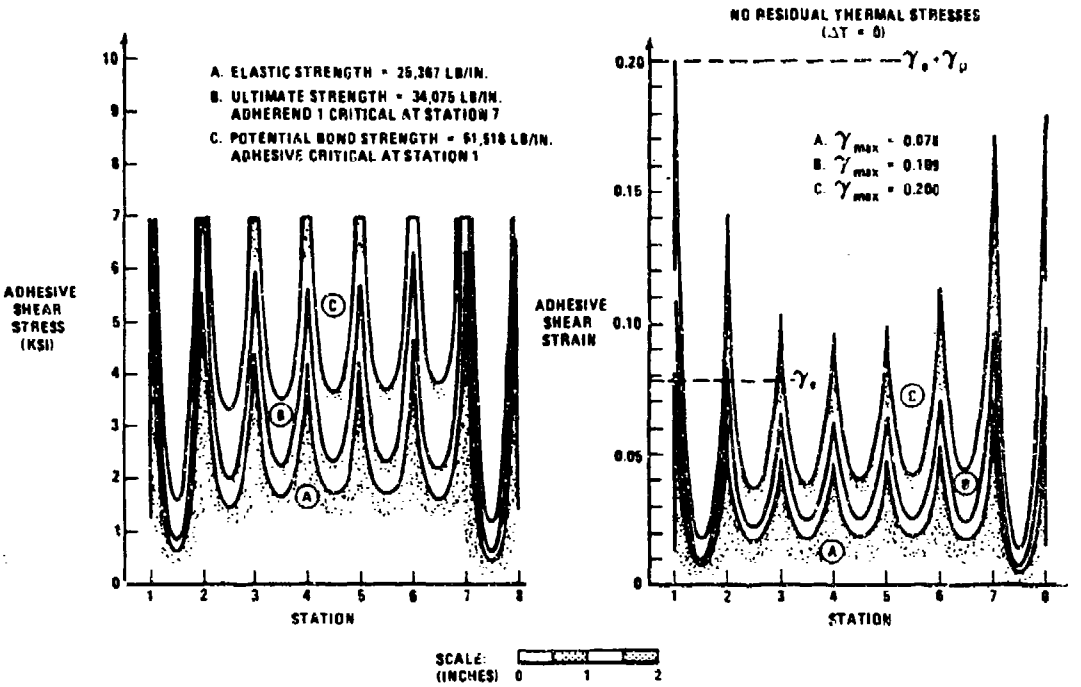

FIGURE 6. ADHESIVE SHEAR STRESSES AND STRAINS IN STEPPED-LAP BONDED JOINT

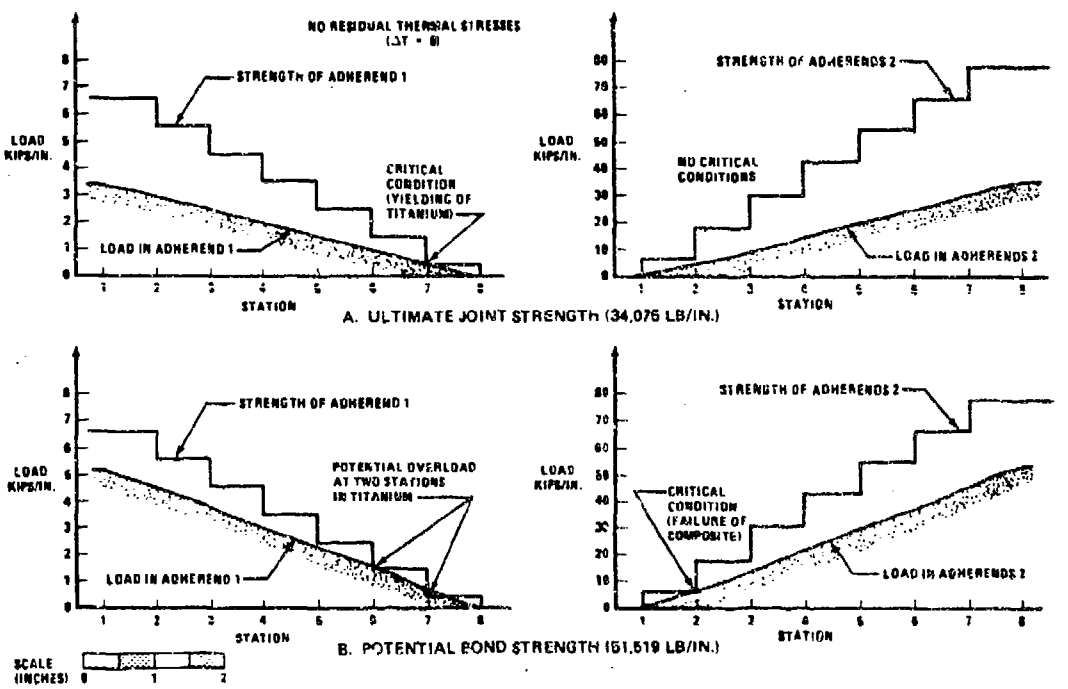

FIGURE 7. ADHEREND STRESSES IN STEPPED-LAP BONDED JOINT

This design in Figure 5 was deliberately not optimized, to highlight some characteristics of stepped-lap adhesive-bonded joints. The ultimate strength is limited not by the adhesive, but by the thin, excessively long end step on the titanium plate, as shown in Figure 7. This end step frequently fails in fatigue if the joint proportions are not sized carefully. Figure 7 shows the further information, beyond that in Figure 6, which is provided by the analysis of such joints with the program A4EI.

Improvement Of Joint Strength By Optimizing Proportions

Armed with information of the type shown in Figures 6 and 7, one would set about modifying the design to improve the joint strength. It is evident that, since the adhesive shear strains at each end of the joint are roughly equal, the overall stiffness balance is good. Any further impovement in that regard would probably be thwarted by the constraint that the fibrous composite laminate must consist of an integral number of plies. The need for stiffness balance is why there is such a pronounced thickness buildup at the right side of Figure 5. However, since the titanium end step is either too thin, too long, or both, it should be modified. It is preferable not to make it too thick, lest it joggle the fibers in the laminate and thereby weaken the other member more than it is strengthened itself. A tip thickness in the range 0.030 inch to 0.050 inch is usually found to be optimal. So a redesign should shorten that step, as well as lengthening some of the middle steps to decrease the minimum adhesive shear stress there. Since the composite adherend is weakest at its end step, as shown in Figure 7, that also should be shortened. Figure 8 depicts the results of such a reanalysis, showing how the ultimate strength was increased from 34075 lbs/in. to 38033 lbs/in. This is a rather small increase, and was sufficient to reduce the potential bond strength from 51519 lbs/in. to 38033 lbs/in., since the adhesive is now critical rather than the adherends. Therefore, one should perform a further redesign of the joint with the only variable left - an increase in the number of steps. The results of such a further design iteration are shown in Figure 9. The ultimate (and potential bond) strength was increased to 46363 lbs/in. This represents a substantial increase over the 34075 lbs/in. of the initial design in Figure 6, showing how important it is to properly proportion the step details. However, it must be recorded

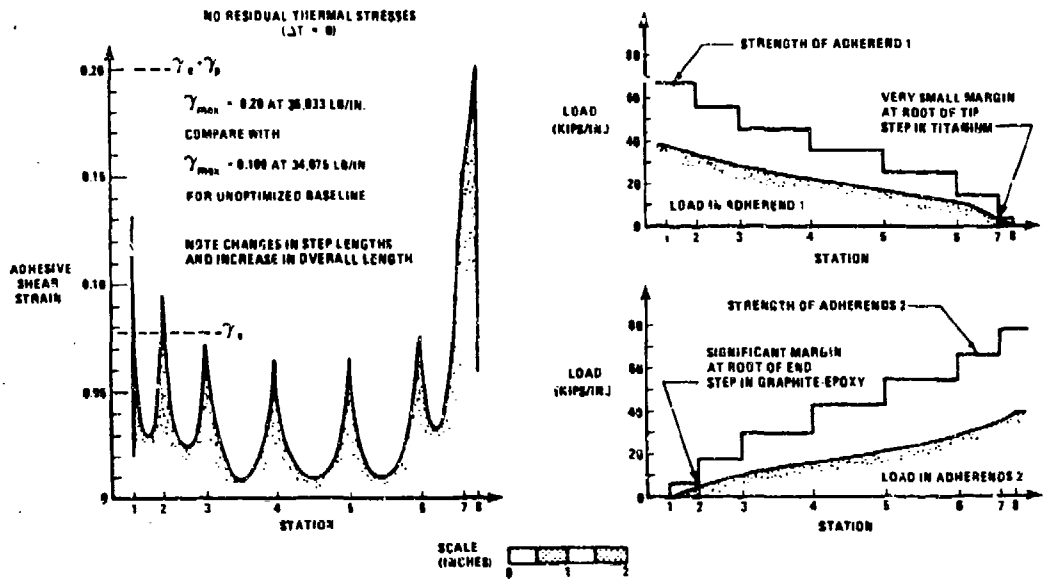

FIGURE 8. IMPROVEMENTS DUE TO FIRST REDESIGN OF STEPPED-LAP BONDED JOINT

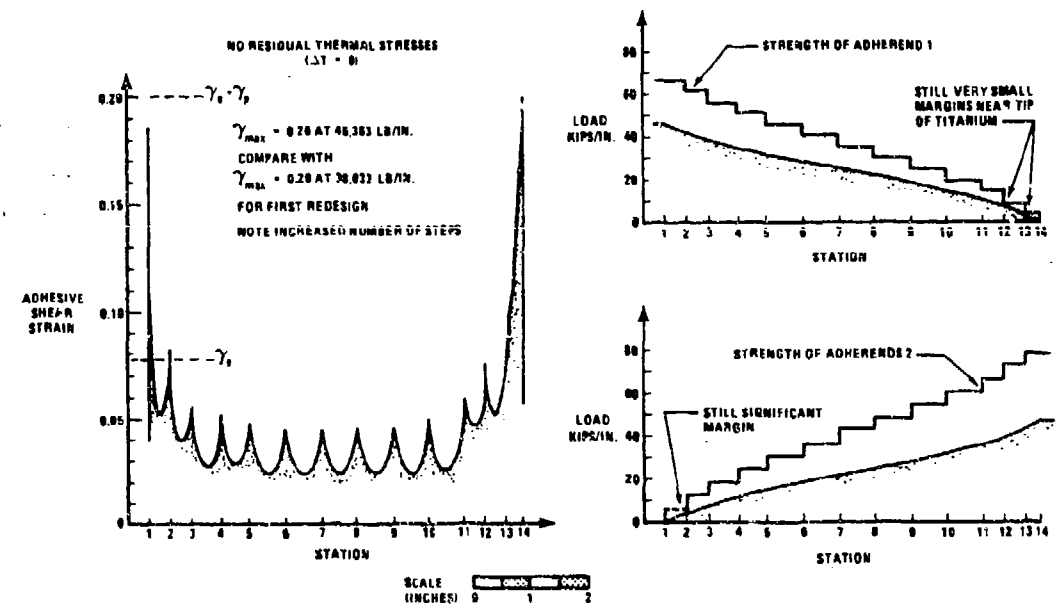

FIGURE 9. IMPROVEMENTS DUE TO SECOND REDESIGN OF STEPPED-LAP BONDED JOINT

also that, for this relatively thick stepped-lap bonded joint, the bond strength is still substantially less than the lesser adherend strength of 66300 lbs/in. and that still further refinements will be progressively less effective in increasing the bond strength. These examples suffice to demonstrate the design refinement techniques. The design iterations are much more straightforward for thinner adherends, which are subjected to lighter loads. For a real design, one would need to analyze the joint throughout the entire operational environment, and iterate the design for the most severe condition. A comparison of Figures 6 (and 7), 8, and 9 shows that the critical location in every instance is the thin end of the titanium. So it is here that further design refinements would be applied. These would take the form of a greater number of shorter steps, to keep the rate of load build up below that for the strength build up. However, a word of caution is necessary. The critical step in Figure 9 is already only 1/4 inch long, and step increments are limited by the finite thickness of the composite material, be it tape or cloth. It would be easy to continue this design iteration process to the degree that the precision demanded of the manufacturing techniques would be beyond any reasonable tolerances. Rather than use the program A4EI to such questionable ends, it would make more sense to do only one more design iteration, by thickening the end step to 0.040 inch to increase its strength, and the next step likewise to 0.080 inch and then to use the computer program to assess the strength losses to be expected due to reasonable manufacturing tolerances in chem-milling the titanium and laying up the fibrous composite. The results of such a final analysis, with all other variables as in Figure 9, were an elastic strength of 21032 lbs/inch, and an ultimate strength of 39957 lbs/inch, with the adhesive critical at the far end of the joint. These are, in fact, significant strength decreases with respect to the configuration analyzed in Figure 9, confirming that it is going to be difficult to improve upon that design.

One very important characteristic of the design of stepped-lap joints which is not apparent in Figures 5 through 9 is that experience has shown that the best such joints have 0^{o} fibers adjacent to the adhesive, rather than a 90^{o} or $\pm 45^{o}$ ply. The reason is that the transverse fibers tend to roll under the shear transfer loads and the resin splits between the fibers. This imposes a severe constraint on the options available to the designer in

regard to optimizing the joint details, particularly if the fiber pattern has been set by conditions outside the bonded joint area. It should be apparent that the joint area should be considered more in setting the fiber pattern. The fiber pattern must not deviate much from a uniformly dispersed quasi-isotropic pattern if the laminate is to be free from the weak cleavage planes associated with laminates in which parallel fibers are bunched together rather than interspersed.

Effect Of Residual Thermal Stresses From Bonding Dissimilar Adherends

When advanced fibrous composites are bonded to metal adherends at an elevated temperature to cure the adhesive and give it resistance to environmental attack, the metal tends to shrink during the cool-down. That induces residual stresses and strains in the adhesive for all but joints so short (half an inch or so) that they are alleviated by adhesive creep. The shrinkage also introduces tensile stresses in the metal and compression in the composite. These effects are shown in Figure 10 for the basic stepped-lap bonded joint shown in Figure 5. Figures 11 and 12 show what happens when

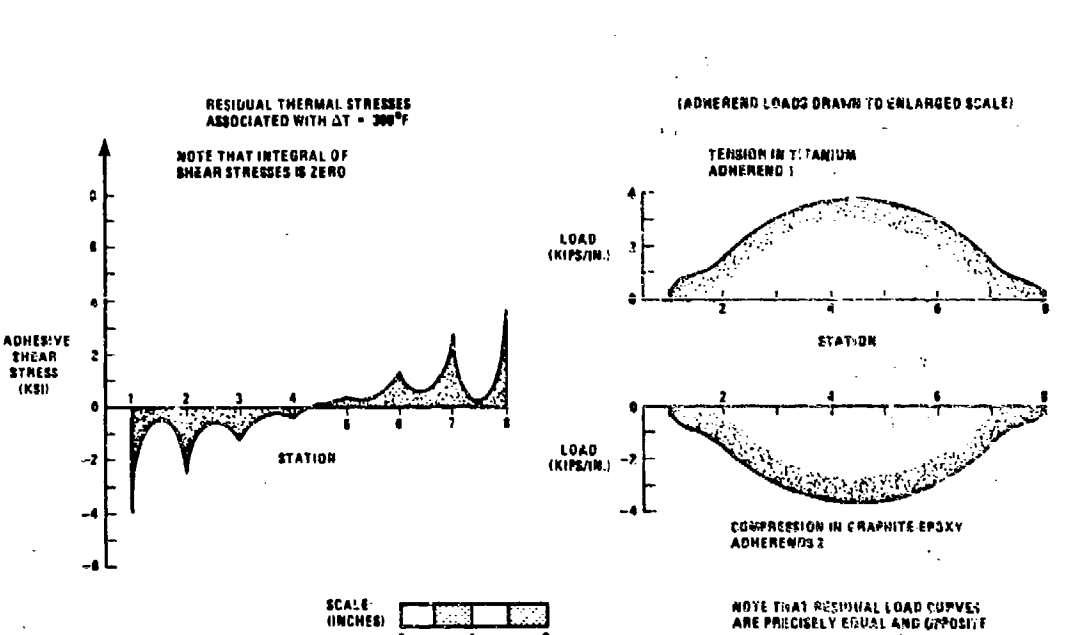

FIGURE 10. RESIDUAL THERMAL STRESSES FROM BONDING TITANIUM TO GRAPHITE-EPOXY

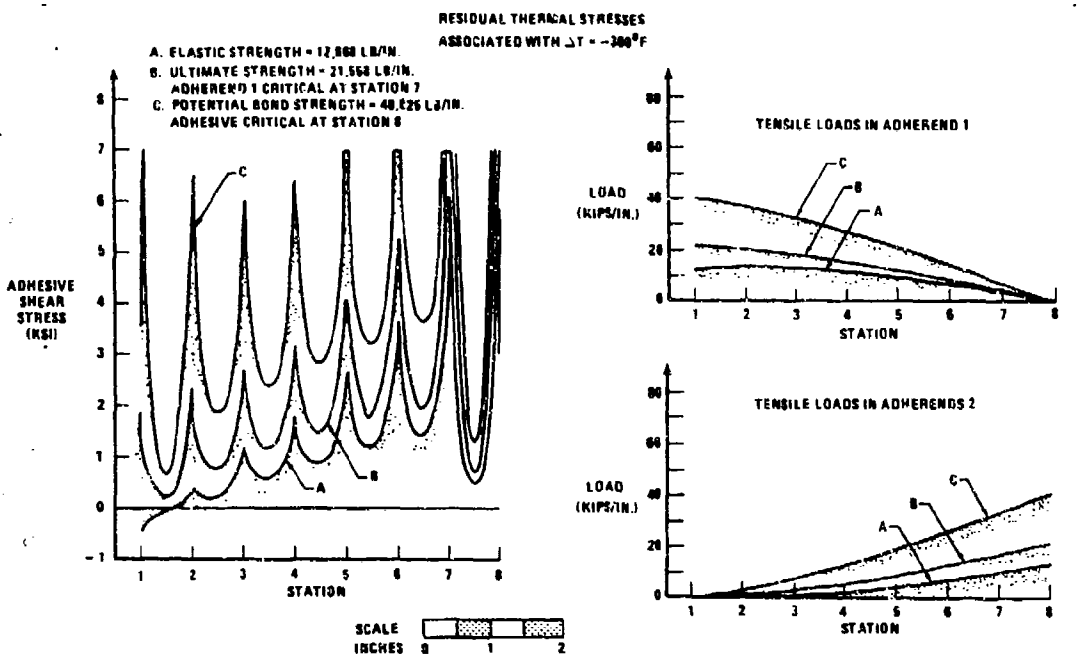

FIGURE 11. TENSILE LOADS ON STEPPED-LAP BONDED JOINTS WITH THERMAL MISMATCH

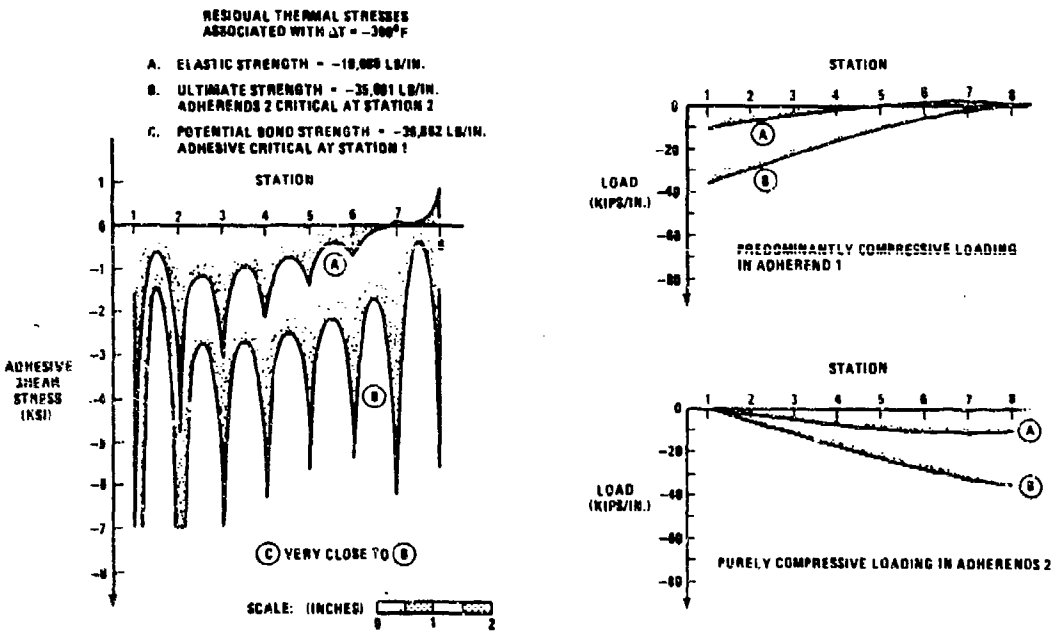

FIGURE 12. COMPRESSIVE LOADS ON STEPPED-LAP BONDED JOINTS WITH THERMAL MISMATCH

tensile and compressive shear loads are superimposed on the residual stresses shown in Figure 10. It is significant that the tensile shear stresses combine with the tensile residual stresses at station 8, on the right hand side of the joint while station 1, on the left, is critical for compressive loading. It is very clear that it is necessary to analyze for both the tensile and compressive shear loads separately, because the strengths are different, the critical locations are different and even the critical modes are different. The end step on the titanium joint is not at all critical under compressive loading, for example. While the residual thermal stresses tend to detract from the overall joint strengths, it is self-evident that they are helpful in regard to ensuring that there is some very lightly loaded adhesive to help resist the accumulation of adhesive creep.

2.5 EXPERIMENTAL EVIDENCE

The importance of having available a computer program like A4EI, or the earlier A4EG and A4EH codes, can be gaged from the premature failures which occurred at metal-to-composite stepped-lap bonded joints in several R&D programs over the years at various establishments. Some of these problems are discussed here, to explain them and to encourage their avoidance in the future. Since their history is irrelevant to the present discussion, no identification or credits are given here. Nevertheless, it should be noted that these are real problems and have occurred far too frequently.

Figure 13 shows what happens when the end step on the metal is made too long and too thin. It breaks off! Usually the metal yields under static loading, permitting a secondary failure elsewhere with no indication of this cause of load redistribution. The great bulk of evidence that the long thin end step is a problem has occurred in fatigue testing. Quite apart from the mechanical load transferred through the bond, there is also the tensile residual thermal stress, as shown in Figure 10, and the stress concentration due to the steps, which are more frequently chem-milled rather than machined. The test specimen shown in Figure 13 had a thickness of 0.030 inch on the end tab and a length of over an inch. The author's experience suggests that a length of only a quarter of an inch would have been more appropriate for a tab of that thickness, particularly if it were in double shear. The A4EI

program permits a systematic parametric study of such joints to be made for a small fraction of the cost of even one such test specimen. This can greatly reduce the need for test specimens and maximize the usefulness of those actually tested.

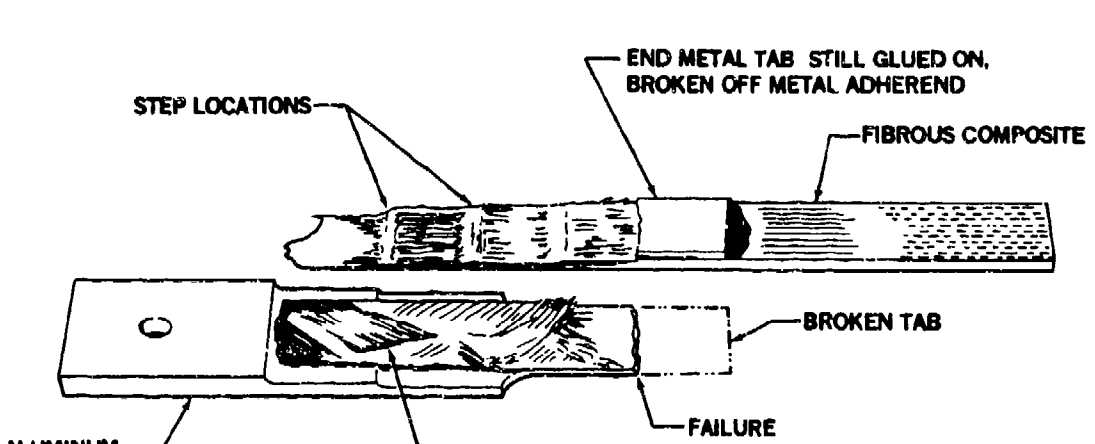

FIGURE 13. FAILURE OF STEPPED-LAP ADHESIVE-BONDED JOINT

Further experimental evidence on the use of the A4EG program to design stepped-lap titanium to graphite-epoxy bonded joints is given in Reference 6. This was a much easier task than similar work on the F-15 tail and F-18 wing and tail because, for the A-4 graphite-epoxy stabilizer program it was possible to use a highly ductile adhesive, Epon 951, and the titanium was only 0.25 inch thick. During several tests, at progressively more complexity, the failures were consistently in the fibrous composite outside the joint area. Tests on that same program, described in References 1 and 7, highlighted the potential problems that can occur due to wrinkles in the fibers at the tip of an embedded titanium plate. That is why the joint shown in Figure 5 includes a tapered fiberglass-epoxy wedge beyond the end step, co-cured with the basic graphite-epoxy laminate to eliminate both the wrinkling and the abrupt termination of such fibers if they had simply been butted up against the end step.

Quite apart from reducing the structural efficiency by carrying around excess

material, such abrupt termination of the fibers just beyond the tip of the titanium splice plate can actually weaken the strength to below that which would be attained had those plies been replaced by low-modulus filler material to prevent them from picking up load. This is explained in Figure 14, which is a simplification of a somewhat more complicated condition in which the delamination was actually initiated by the combination of shear and peel stresses. The example on which Figure 14 is based had a tip thickness in excess of 0.1 inch, with over 50 percent of the central plies terminated there being longitudinal. The consequent stress concentration was far worse than normal design practice permits. The number of plies which can be simultaneously terminated safely in a graphite-epoxy laminate, without fear of inducing delaminations, is closer to four rather than more than twenty, whether there is a joint in that vicinity or not. Likewise, it is important to thoroughly intersperse the cross plies rather than lumping them together, because of the substantial residual tensile stresses in the resin, which has typically two to three times the coefficient of thermal expansion of aluminum alloys. Just because a laminate is not warped, it does not mean that it is not pre-stressed. Any warpage is actually due to relief of such internal stresses which would otherwise be worse.

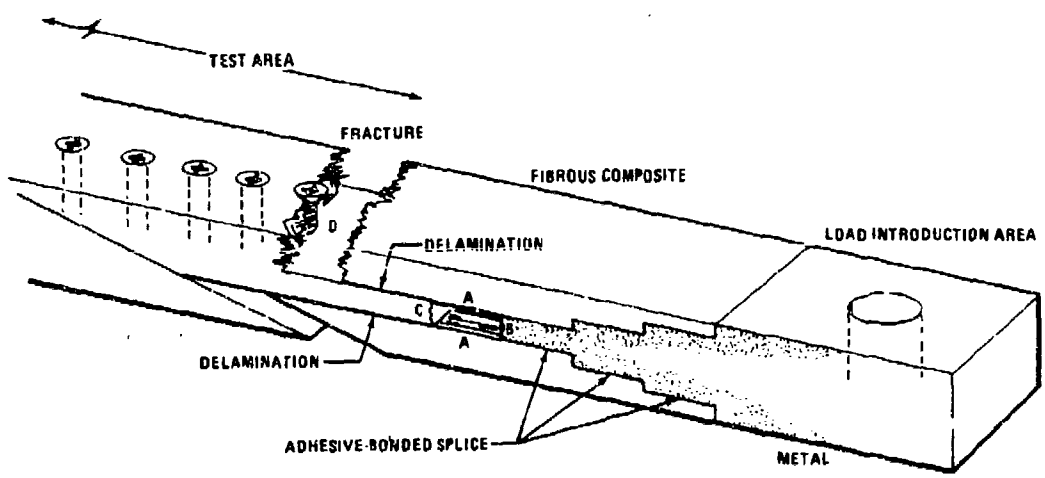

INITIAL FAILURE AT "A" BECAUSE THICKNESS "B" IS EXCESSIVE AND LOAD IN FIBERS "C" CANNOT BE UNLOADED THROUGH RESIN MATRIX

FINAL FAILURE, AT "D", IS BY NET SECTION TENSION ON THE TOP FACE AND SHEAROUT (NOT SHOWN) ON THE LOWER FACE

FIGURE 14. PREMATURE FAILURE OF STEPPED-LAP BONDED JOINT BY DELAMINATION

While on this subject, it is appropriate to digress a little and explain that a 90^{o} ply within a laminate cured at the usual $350^{o}F$ or $250^{o}F$ does not behave at all like a transverse test on a 0^{o} monolayer. In the latter case, the resin is free to contract laterally (perpendicularly to the fibers) rather than to develop internal stresses, while in the former case such lateral contraction is resisted by adjacent fibers in the 0^{o} or $\pm 45^{o}$ directions. Thus the 90^{o} layer within a typical laminate is prestressed and usually also pre-cracked. If too many such plies are bunched together, delaminations will occur, as discussed in Reference 8, even under tension-tension fatigue loading.

The purpose of mentioning some of the items above is to point out that if certain good design principles are not followed in designing bonded stepped-lap joints in fibrous composites, the analysis given here would become quite inadequate and would need to be replaced by a far more complicated model which checked not only for the adhesive and gross adherend behavior but also checked each and every resin interface within the laminate for possible failure there, instead.

2.6 LOAD REDISTRIBUTION DUE TO DISBONDS IN ADHESIVE IN STEPPED-LAP JOINTS

When titanium to fibrous composite stepped-lap joints are co-cured and bonded with an adhesive film, as is done on the F-18 and F-15 by McDonnell and was done on the A-4 R&D horizontal tail by Douglas, it is virtually impossible to manufacture a bad joint unless there is something like a bag failure which would ruin the laminate as well as the joint. However, if one were to precure all the details separately and then try to secondarily bond them, it would be relatively easy to have major disbonds caused by poor fit of the details, particularly if the joint is thick enough to warrant several steps. Indeed, such has been found to be the case elsewhere. The variable adhesive properties introduced into the A4EI program during the Primary Adhesively Bonded Structure Technology (PABST) program, as described in Reference 2, permit an assessment of the effects of such misfits in stepped-lap bonded joints. Three such examples of this are discussed below, again using the basic joint in Figure 5 as a reference.

Figure 15 shows the consequences of the two end steps being disbonded at the left end of the joint, Figure 16 shows the load redistribution due to the middle three steps beind disbonded, and Figure 17 shows what happens when the end two steps on the right are disbonded. It is immediately obvious that the

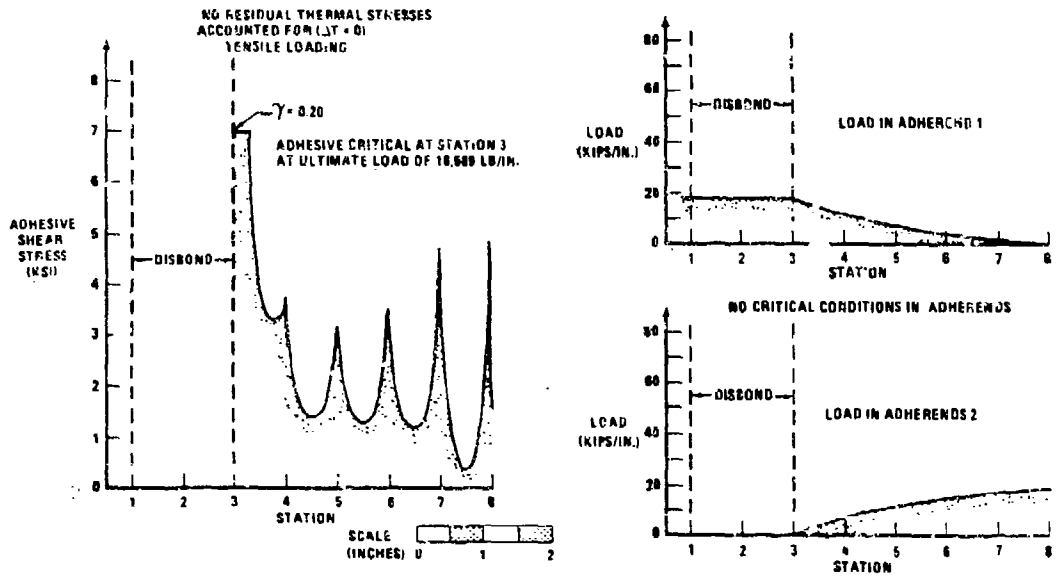

FIGURE 15. STRENGTH LOSS AND LOAD REDISTRIBUTION DUE TO DISBONDS IN STEPPED-LAP JOINTS

load redistribution due to the disbonds is far more substantial than shown in Figures 8 to 11 of Reference 2 for uniformly thick bonded adherends. The reason for this much greater sensitivity of the larger more complex joint to bond flaws is that there are no large areas so lightly loaded that the flaw could be missed or to which the load transfer could be moved. Figure 16 is particularly significant in the sense that the load redistribution around the central flaw is so intense that the critical adhesive conditions are no longer located at the ends of the overlap, but at the edge of the flaw.

Figures 15 to 17 have been prepared from the thermal-stress-free solutions and the predicted strengths are well down from the 34067 lbs/inch in Figure 6 for nominally perfect bonds in the same specimen. Table I enumerates some of the predictions when thermal stress terms are included. The strength losses

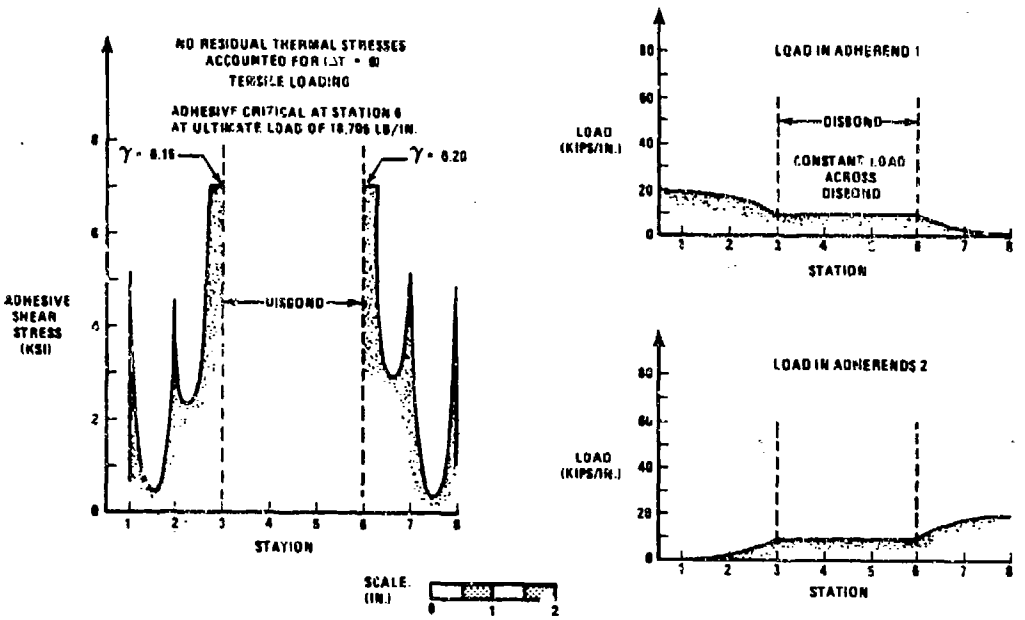

FIGURE 16. STRENGTH LOSS AND LOAD REDISTRIBUTION DUE TO DISBONDS IN STEPPED-LAP JOINTS

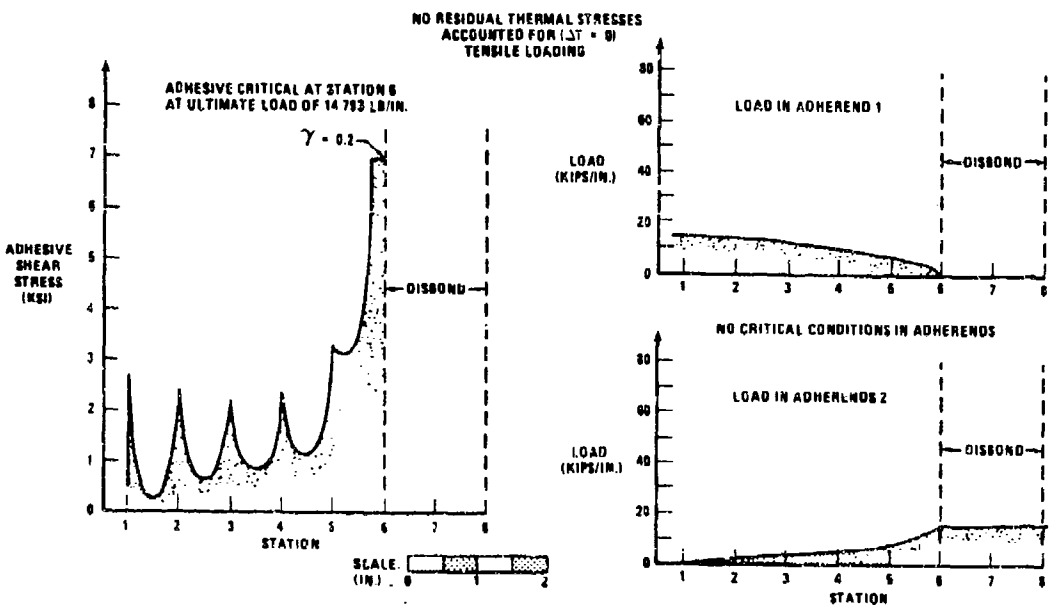

FIGURE 17. STRENGTH LOSS AND LOAD REDISTRIBUTION DUE TO DISBONDS IN STEPPED-LAP JOINTS

TABLE 1. STRENGTH OF VARIOUS FLAWED BONDED STEPPED-L ? JOINTS

BASELINE SPECIMEN, AS IN FIGURE 5, NO BOND FLAWS	LEFT END TWO STEPS DISBONDED, AS IN FIGURE 15	MIDDLE THREE STEPS DISBONDED, AS IN FIGURE 16	RIGHT END TWO STEPS DISBONDED, AS IN FIGURE 17
THERMAL STRESSES ASSOCIATED WITH $\Delta T = -300^{o}F$ ULTIMATE STRENGTH SOLUTIONS GIVEN			
TENSION			
STRENGTH = 21,658 LB/IN.	21,814	15,911	8430
MAXIMUM ADHESIVE SHEAR STRAIN = 0.106 AT STATION 8	0.110 AT 8	0.200 AT 6	0.200 AT 6
ADHEREND 1 CRITICAL AT STATION 7	1 AT 7	ADHERENDS NOT CRITICAL	ADHERENDS NOT CRITICAL
COMPRESSION			
STRENGTH = – 35,684 LB/IN.	–8699	–16,710	–17,974
MAXIMUM ADHESIVE SHEAR STRAIN = –0.193 AT STATION 1	–0 20 AT 3	–0.2 AT 3	–0.2 AT 6
ADHERENDS 2 CRITICAL AT STATION 2	ADHERENDS NOT CRITICAL	ADHERENDS NOT CRITICAL	ADHERENDS NOT CRITICAL

are even more substantial. Further analyses, reported in Section 4 of this report, have been made to predict how much of that strength loss could be recovered by bolting through the disbonded areas. Those solutions involve the use of the combined bonded-bolted joint analysis program A4EK.

Figures 15 to 17 fail to show one other important effect of disbonds in stepped-lap bonded joints only because the adherends are so thick and strong that the adhesive is the weak link. This other important effect is that, if the end steps are disbonded, the entire load is now carried in a reduced section of the adherends, just as if they had been notched or cut down outside a sound joint. This effect is shown in Figures 18 and 19 which is not for the same joint as used in Figures 15 to 17, but for a thinner joint with a more ductile adhesive. This effect could not be demonstrated for the thick joint in Figure 5. This situation of a disbond weakening the adherends more than the adhesive would be prevalent for well-designed joints between thinner adherends, in which the adhesive had a considerable margin with which to tolerate some reasonable level of disbonding.

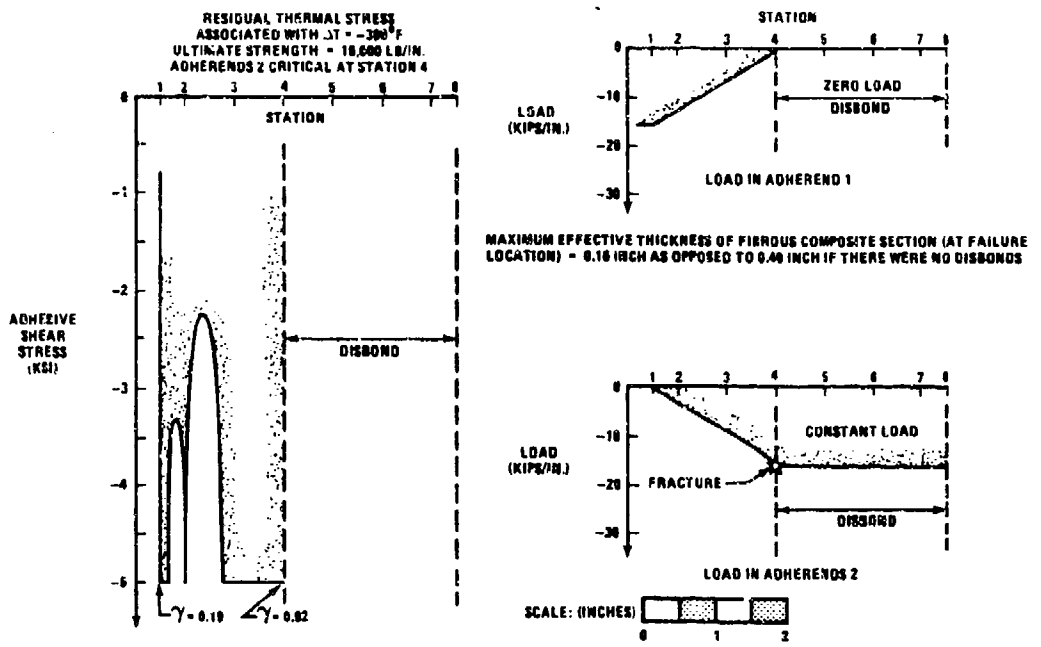

FIGURE 18. COMPRESSIVE LOAD ON SMALL STEPPED-LAP JOINT WITH DUCTILE ADHESIVE

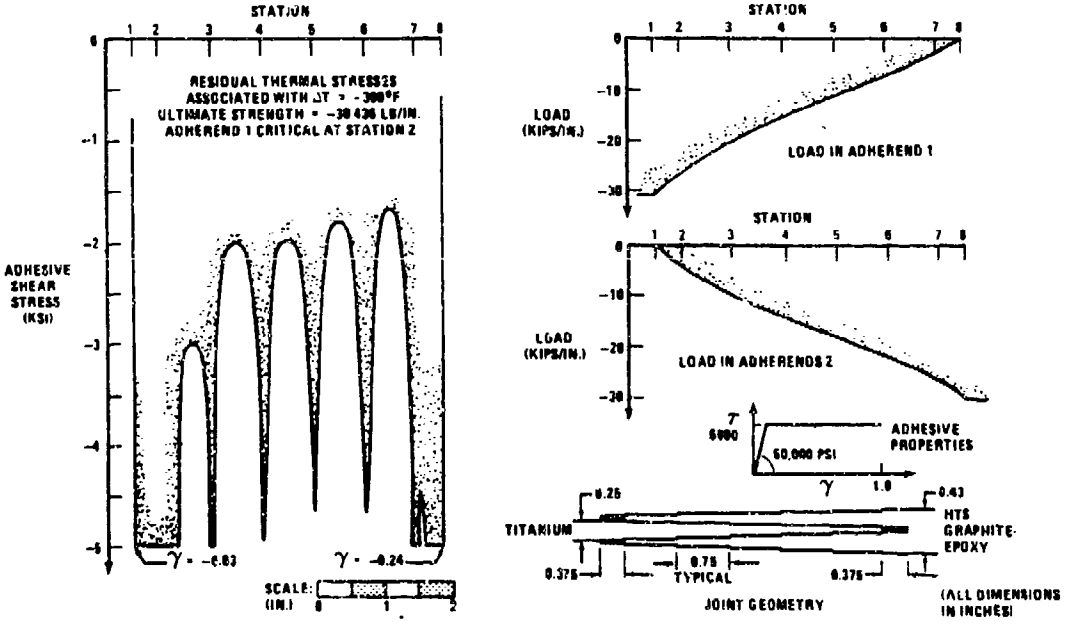

FIGURE 19. PREMATURE FAILURE OF ADHERENDS DUE TO DISBOND IN ADHESIVE

2.7 CHECKS ON THE ACCURACY OF THE SOLUTIONS

The logic within the computer program A4EI is now so complex, in comparison with the original A4EG version, that it is now difficult to devise sample solutions to exercise all options within the coding to verify its accuracy. The last bugs were not found until after over fifty complex joints had been analyzed with several different conditions for each. However, there are some techniques which have been developed which can be useful in maintaining the program.

The most obvious ones are mathematically trivial, but very important. The thermal-stress-free case of uniform adherends in a double-lap joint should give a precisely symmetric solution. Likewise, precisely anti-symmetric solutions can be devised with residual thermal stress problems. Also, a problem run with a tensile load and negative ΔT, for example, can be compared with what should be a precisely opposite answer for a compressive load and the positive ΔT. Such checks cannot verify that all parts of the program are operational, but they are an easy way of exposing a problem due to misreading a card, or to cards out of sequence, which could not be detected from a very complex solution because there is no basis for questioning it, unless it is grossly wrong.

2.8 CONCLUSIONS

The ability to analyze adhesive-bonded joints and account for variations in the adhesive, either in properties or geometrically, is a valuable asset. This is particularly true in regard to the load redistribution around flaws.

The computer program A4EI is particularly useful in optimizing the proportions of stepped-lap bonded joints, as between titanium edge members and graphite-epoxy laminates. Both analysis and test over many years have shown that the strength of such joints can be particularly sensitive to poor detailing of the end step of the titanium, in particular, as well as to any gross mismatch in adherend stiffnesses.

Since this is a continuum mechanics analysis, rather than one based on finite elements, the computer run times are extremely short. However, the actual run time depends on just where in a joint it becomes critical. Run times are typically five times as long if the joint is critical at the far end rather than at the near end where the analysis began.

The sample solutions described here show that the computer program A4EI will be a useful tool in analyzing adhesive-bonded stepped-lap joints and doublers, particularly because of its nonlinear capabilities, without which failure prediction is virtually impossible.

SECTION 3

NONLINEAR ANALYSIS OF MULTIROW BOLTED JOINTS IN FIBROUS COMPOSITE AND METAL STRUCTURES

3.1 INTRODUCTION

The analysis of the load sharing in multirow mechanically fastened joints in aerospace structure has, in the past, been limited to linear elastic solutions and empirical techniques. These have sufficed for typical ductile metals which are very forgiving and tend to deform without catastrophic failure and redistribute the load according to plastic, rather than elastic, behavior. Some of these existing analyses have been used very effectively to obtain great insight into the behavior of multirow bolted joints, even though precise failure predictions are lacking. The manner in which the end fasteners tend to pick up a disproportionate share of the load has long been understood. And any sculpturing to redistribute the load transfer more evenly will be just as effective at some indeterminate failure load as it is at some lesser specified load for which analyses have been run. These existing tools have contributed much to the art of designing mechanical splices and this is quite evident from a new analysis here of an efficient splice which had been designed a decade ago according to established techniques.

However, the advent of the greater use of advanced fibrous composite materials has necessitated the development of improved analysis methods for mechanically fastened splices. One reason for this is that fibrous composites are so brittle that a more precise load-sharing analysis is needed because there is no material yielding to mask approximations or even inaccuracies in the predictions. The analysis for that aspect could be linear. However, the same brittleness causes a need for a basic nonlinear feature in the analysis. Since the clearances around fasteners are sometimes about the same as the maximum possible stretching of fibers between the fastener rows, it is obviously necessary to account for any initial

clearances or preloads at the fasteners. Even if it should transpire that hole clearances in bolted fibrous composite structures are eventually shown to be unacceptable for much primary structure, this new analysis might well be the key to demonstrating such a conclusion. There is another need for including nonlinear behavior in the analysis of mechanically fastened joints in fibrous composites. This need is due to the non-catastrophic bearing damage that occurs in the immediate vicinity of fastener holes whenever the holes are not close enough together to fail by tension through the hole. Thus, even though fibrous composites are customarily regarded as linearly elastic to failure, they still need a nonlinear analysis for bolted or riveted joints.

While the justification for improving the existing analysis capability is greater for fibrous-composites than for ductile metals, it makes sense to include in the analysis developed any extra features necessary to permit a better analysis of bolted metal structures also. A better characterization of the load transfer distribution at typical fatigue loads can then be obtained. For this reason, the analysis developed here includes nonlinear behavior of the members between the fastener rows.

3.2 SYMBOLS

d	Fastener diameter, can vary along length
E	Young's modulus
$F_{0.7}$	Stress level in Ramberg-Osgood model
K_{el}, K_{pl}	Stiffness of element of bolt load versus deflection characteristic
k	Station identification
ℓ	Step length, or distance between adjacent stations
P	Fastener load, varies along length
p_1, p_2	Running shear loads, assumed constant along length
T_1, T_2	Internal loads in members, vary along length
T	Temperature
ΔT	Temperature change ($T_{operating} - T_{assembly}$)
t_1, t_2	Thicknesses of members, can vary along length
w_1, w_2	Widths of members, can vary along length

α_1, α_2	Coefficients of thermal expansion
δ, δ_1, δ_2	Displacements of members
ϵ	Strain in members
σ	Stress in members

Subscripts

o, +, -	Sign convention for displacements
1, 2	Identification of each member
k	Station number identification
e, p	Elastic and plastic values, respectively
ult	Ultimate value, at failure
fr	Contribution due to friction load transfer

3.3 LOAD-DEFLECTION CHARACTERISTICS FOR A SINGLE FASTENER

The transfer of load through mechanical fasteners (bolts and rivets) within a joint is characterized in terms of the relative displacement between the members at each fastener station. Figure 20 depicts the simplest possible mathematical model for such load transfer. The take-up of any initial clearance is shown to be friction free but, in principle, it would be quite straightforward to include a constant (Coulomb) force throughout that displacement increment. Any further load applied to the extremities of the joint induces a shear load in that fastener as the relative motion is resisted by the shear strength of the fastener. The initial load transfer is linear, as shown, but there is also usually a significant nonlinear contribution prior to failure. The straight-line non-linear behavior shown in Figure 20 is the simplest such representation possible. No more complex representations are necessary. In some instances it would be possible to have an ambiguous (nonunique) solution if a perfectly plastic (horizontal) nonlinear mathematical model were used, so it is preferable to adopt a positive slope, however small, in the model. In the case of a net- or interference-fit fastener, of course, there is no initial clearance to contend with while, for multirow joints, it is possible that the "other" fasteners may induce a positive or negative preload on the fastener under consideration.

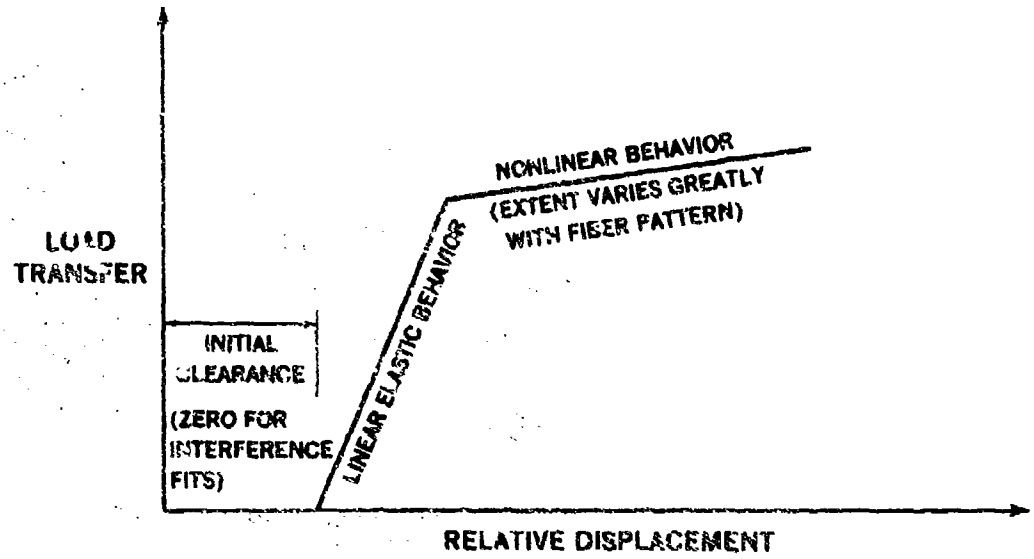

FIGURE 20. FASTENER LOAD-DEFLECTION CHARACTERISTICS

In order to implement such a load-deflection curve as in Figure 20 it is necessary to define also precisely what is meant by the relative displacement, between the members at each fastener. This can be understood by reference to Figure 21, or to its equivalent for double-shear fasteners. The points A and C move apart under the load P. Those points are sufficiently remote from the fastener, at station B, that the displacements at A and C can be considered to be uniform across the section. The relative motion between stations A and C can be considered as the sum of three components; the gross section stretching (or compression) in member 1 between A and B, the gross section stretching in member 2 between B and C, and the combination of the local distortions of the members in the vicinity of the fastener and the shear deformation (and/or rotation) of the fastener itself.

By isolating out the first two such components, one is left with what is referred to as the fastener flexibility. It is specific to a given fastener in particular materials, but is independent of the location chosen for stations A and C. Such characteristics are customarily deduced by measuring the relative motion between stations A and C and removing mathematically the amounts that the members 1 and 2 would have stretched over the increments AB and BC, respectively, had there been no fastener at B. It is important to

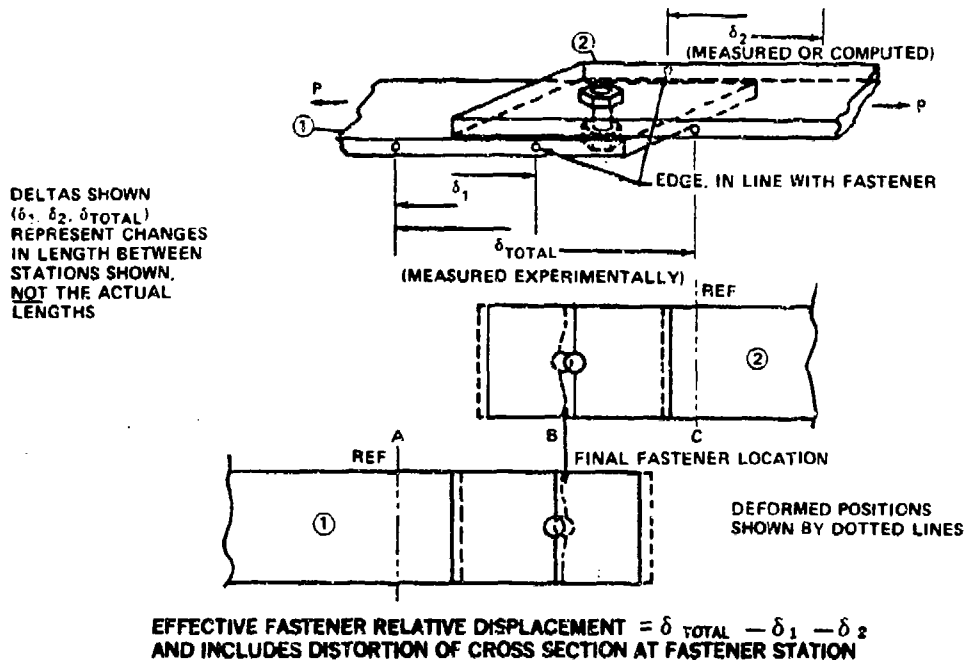

FIGURE 21. DEFORMATIONS IN MECHANICALLY-FASTENED JOINT

include the local distortion of the members around the fastener holes within the characterization of the fastener flexibility to simplify the analysis of such joints for the load sharing between fasteners, as is explained in the next section.

The load-deflection curve shown in Figure 20 applies for load in one direction only. The more general case, in Figure 22, includes also the characteristics for load in the opposite direction. It is customary to associate positive loads and deflections with tensile lap shear, as depicted in Figure 21. The elastic behavior for both tensile and compressive behavior is usually identical, so the initial elastic lines have the same slope. However, since the stress trajectories in each case are so different, as shown in Figure 23, one must provide for different proportional limits and nonlinear behaviors. The mathematical model shown in Figure 22 is appropriate for the fastening of both fibrous composite and metal members, with the use of suitable (different) coefficients to characterize the load-deflection curves.

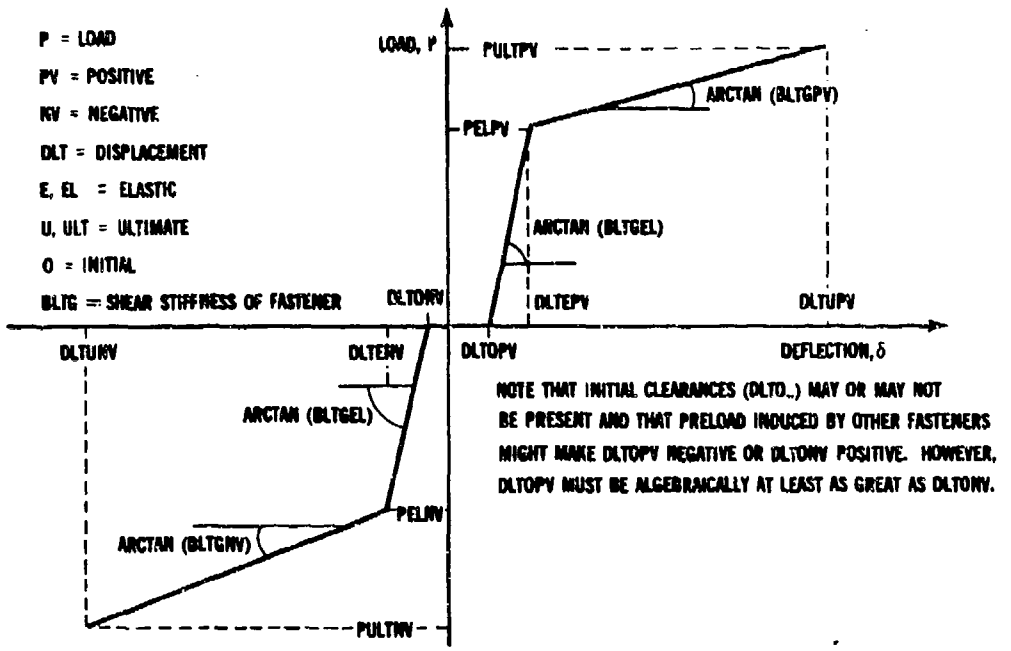

FIGURE 22. IDEALIZED FASTENER LOAD-DEFLECTION CHARACTERISTICS

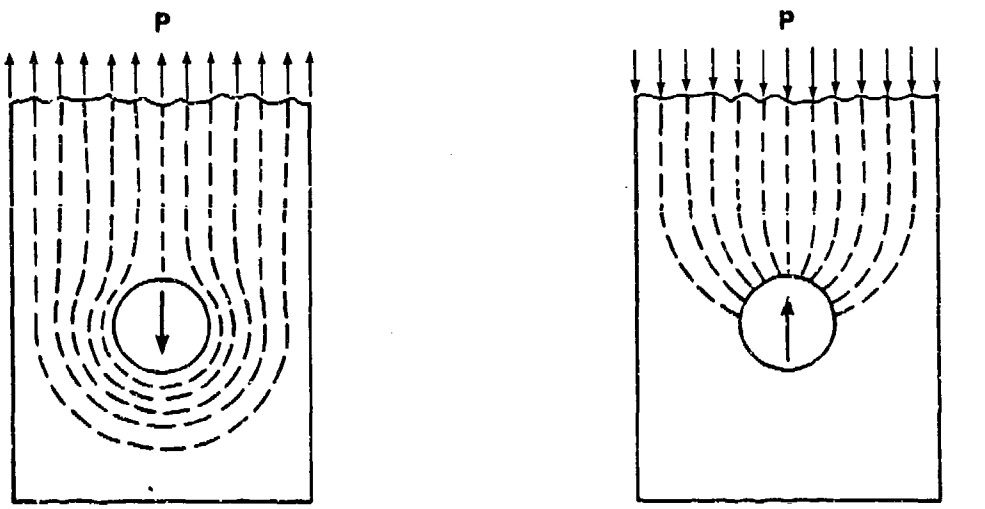

FIGURE 23. STRESS TRAJECTORIES AROUND BOLTS FOR TENSILE AND COMPRESSIVE LAP SHEAR

The mathematical description of the load transfer characteristic in Figure 22 is as follows:

$$P = 0 \qquad \text{for } \delta_{o-} \leq \delta \leq \delta_{o+}, \tag{54}$$

$$P = K_{el}(\delta - \delta_{o+}) \qquad \text{for } \delta_{o+} \leq \delta \leq \delta_{el+}, \tag{55}$$

$$P = P_{el+} \qquad \text{for } \delta = \delta_{el+}, \tag{56}$$

$$P = P_{el+} + K_{pl+}(\delta - \delta_{el+}) \qquad \text{for } \delta_{el+} \leq \delta \leq \delta_{pl+}, \tag{57}$$

$$P = P_{ult+} \qquad \text{for } \delta = \delta_{pl+}, \tag{58}$$

$$P = - K_{el}(\delta_{o-} - \delta) \qquad \text{for } \delta_{el-} \leq \delta \leq \delta_{o-}, \tag{59}$$

$$P = - P_{el} \quad (-ve) \qquad \text{for } \delta = \delta_{el-}, \tag{60}$$

$$P = P_{el-} - K_{pl-}(\delta_{el-} - \delta) \qquad \text{for } \delta_{pl-} \leq \delta \leq \delta_{el-}, \tag{61}$$

$$P = P_{ult-} \quad (-ve) \qquad \text{for } \delta = \delta_{pl-}. \tag{62}$$

The negative relations are needed both for compressive external loads and to cover the possibility of internal (self-equilibrating) loads induced by thermal mismatch between dissimilar members fastened together at one temperature and operated at a different temperature. They are also needed in the iterative analysis, described below, to cover those intermediate analyses prior to convergence.

Load transfer due to friction associated with tightly clamped assemblies can easily be accommodated in such a model. However, particularly in the case of fibrous composites with a resin matrix, the reliance upon frictional load transfer in long-life aerospace structure is questionable. The resin would creep to relieve the preload. Also, in the many structures which have countersunk fasteners to achieve a flush exterior, there is often not much clamp-up possible even in the short term. Leaving aside the questions of estimating the magnitude of any frictional load transfer, the modifications

to Equations (54) to (62) would be

$$P = P_{fr} = \text{constant} \qquad \text{for } 0 \leq \delta \leq \delta_{o+} \tag{63}$$

in place of Equation (54), and

$$P = P_{fr} + K_{el}(\delta - \delta_{o+}) \qquad \text{for } \delta_{o+} \leq \delta \leq \delta_{el+} \tag{64}$$

instead of Equation (55). Likewise, Equation (63) would be complemented by

$$P = - P_{fr} \qquad \text{for } \delta_{o-} \leq \delta \leq 0 \tag{65}$$

and Equation (59) would become

$$P = - P_{fr} - K_{el}(\delta_{o-} - \delta) \qquad \text{for } \delta_{el-} \leq \delta \leq \delta_{o-}. \tag{66}$$

The other equations would remain unchanged.

The preceding discussion concerns the load-transfer characteristics of either a single-fastener joint or of one fastener isolated out of a multirow joint. The next section of this paper addresses the subject of calculating just how the load is shared between multiple fasteners when there are redundant load paths. After that, it is necessary to consider the failure criteria, station by station, to identify just where any failure would occur, and at what load.

3.4 LOAD SHARING BETWEEN MULTIROW FASTENERS

A variety of analysis techniques is available for the solution of the problem of load sharing between multirow fasteners. Most are rendered unsuitable for this task because of a restriction to linear behavior. The method adopted here is chosen because it is compatible with the equivalent nonlinear adhesive-bonded analysis, Reference 1, with which it is later integrated, in Section 4 of this report.

The known boundary conditions are at both ends of the joint, while the unknown conditions are likewise not confined to one end. Therefore, in solving the problem iteratively, it is appropriate to start at one end of the joint (preferably that which is more critically loaded to improve accuracy) and to assume a value for some unknown there. The assumption may be of the total joint strength or the displacement at the first fastener (or the edge

of the joint) induced by a specified load. By then calculating progressively along the joint, satisfying both equilibrium and compatibility requirements, one can interpret the consequent predictions at the other end of the joint. The initial assumption can then be modified as necessary until all boundary conditions are satisfied at both ends of the joint. The development of this iterative technique is explained in References 1 and 2. Actually, unless the initial assumption is very close, or has been refined by prior iterations, the progressive calculations will diverge and the appropriate change to the previous estimate is recognized in terms of the nature of the divergence.

The establishment of the typical equations for each step of the joint is explained in Figure 24. The conditions of equilibrium are that, for member 1 between stations k and k+1

$$T_{1(k+1)} = T_{1(k)} - P_{(k)} + p_1 \ell_{(k)} \tag{67}$$

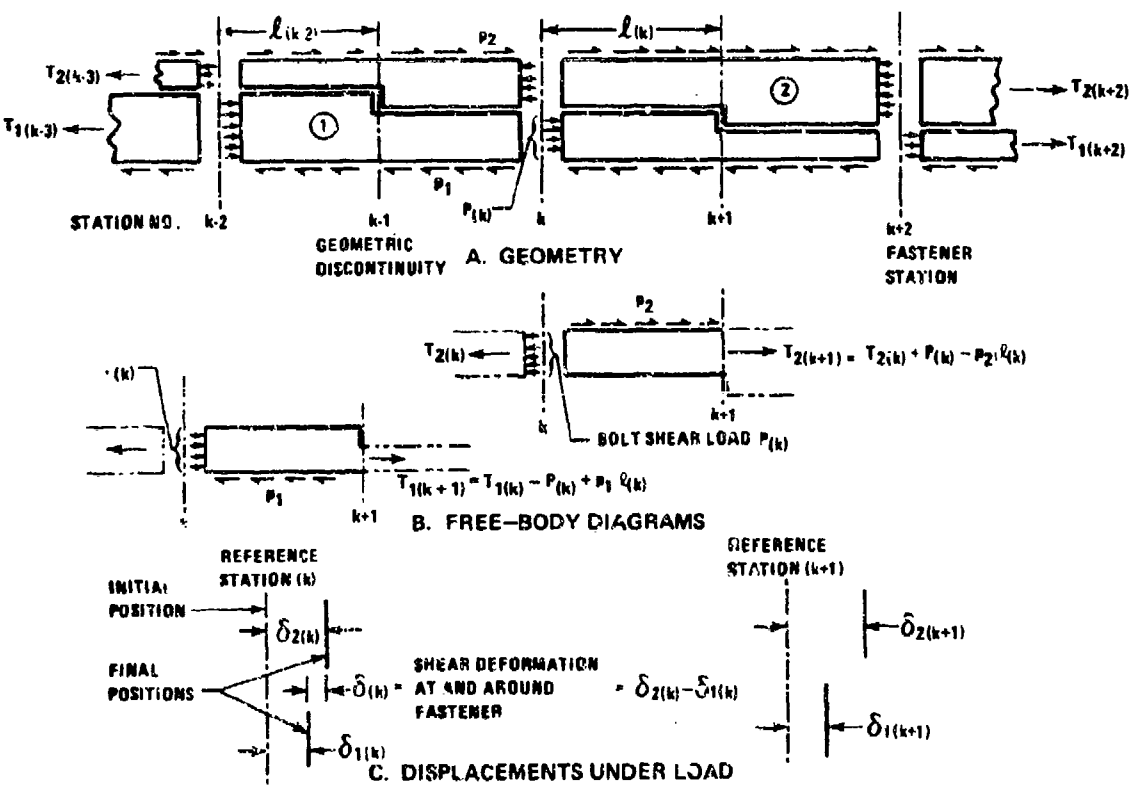

FIGURE 24. LOADS AND DEFORMATIONS ON ELEMENTS OF BOLTED JOINT

in which T_1 is the member internal load, being positive for tensile loads, P is the shear load transfer by that fastener and is positive for tensile lap shear, as shown. The remaining term $p_1\ell$ is usually absent from test coupons but represents the running shear load that may be present in such real structures as the splice at the root of a wing under bending loads. The sign convention for p_1, and p_2 likewise, is that each load is taken to be positive when it acts in the same direction as a tensile load in the member outside the joint area. Similarly, for the same element of member 2,

$$T_{2(k+1)} = T_{2(k)} + P_{(k)} - p_2\ell_{(k)}. \tag{68}$$

Figure 24 illustrates a single-shear application. In a double-shear joint, the two portions which would make up members 1 or 2 would be combined and the fastener load transfer P would be changed from single to double shear values. The form of Equations (67) and (68) would not be altered. Similarly, in what follows, the subscripts 1 and 2 refer to any appropriate summation of properties as well as of loads.

To ensure that the analysis complies with compatibility requirements, one must use the mechanical (and possibly thermal) properties of the members. Because of uniqueness requirements, it is mathematically not permissible at all to use any ideal elastic-plastic material characterization, even though that could sometimes be done for the fasteners, in terms of Figure 20. Effectively, what is required is the stiffness of each member between each adjacent pair of fastener stations, making due allowance for variations in width (as with lollipopping to reduce the load picked up by an end fastener) as well as in thickness. Figure 25 shows typical sculptured skin splices for the fuselages of pressurized transport aircraft. Because such skins are relatively thin, it is more effective to rout the edges of uniformly thick splices and doublers to improve the fatigue strength than to taper the thicknesses of such members. It is also much safer, in the sense that the cyclic variation in joint geometry along the splice permits any cracks which might be initiated from the holes to grow slowly into visible areas. That, in turn, permits more prompt repairs. Thicker members, such as wing skins, are customarily spliced by tapered members, as shown in Figure 26. The analysis developed here has the capacity to account for both of these techniques. It is appropriate to also include in the analysis provision for

thermally induced strains and some provision for the running shear load discussed above.

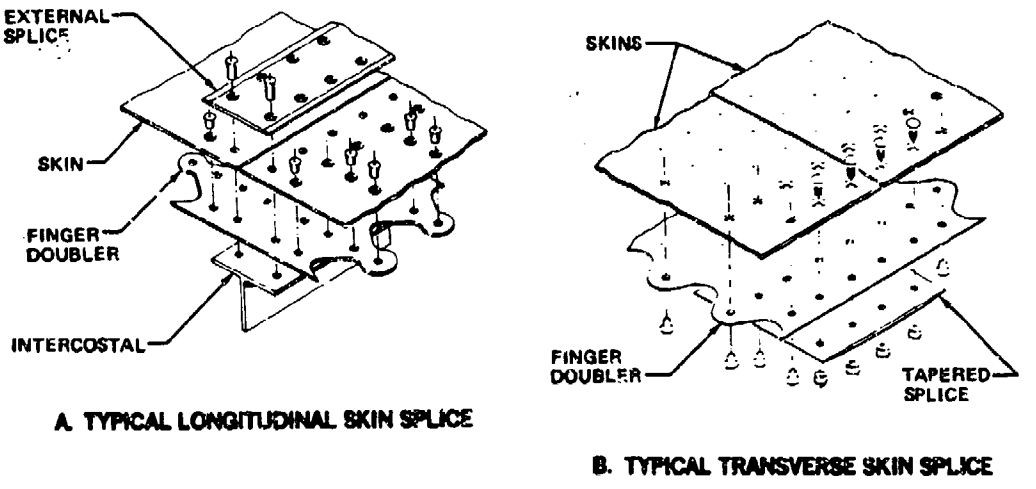

FIGURE 25. RIVETED FUSELAGE SKIN SPLICES

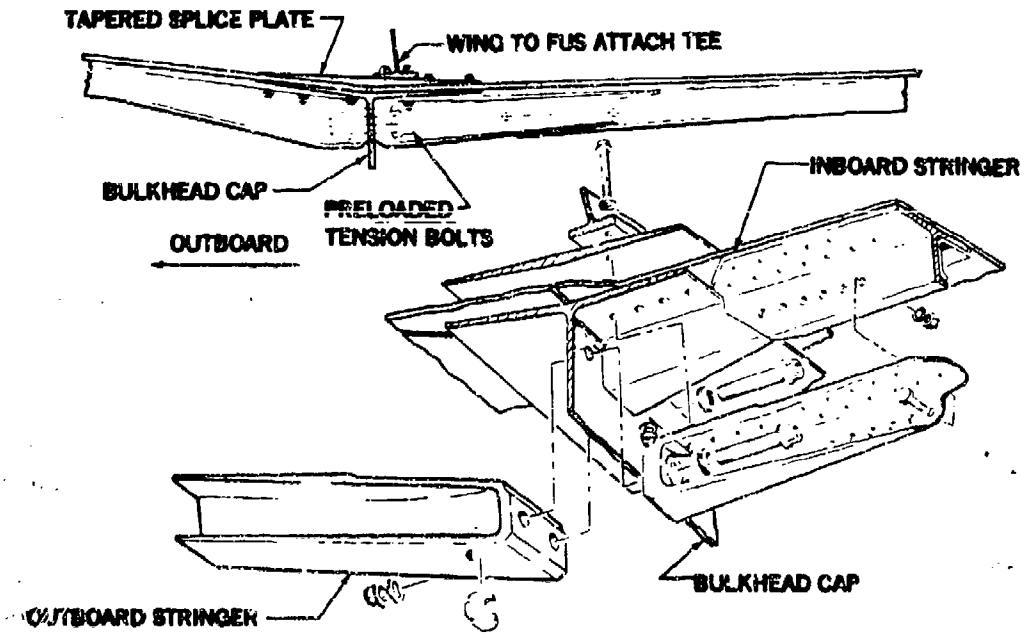

FIGURE 26. WING PANEL JOINT AT SIDE OF FUSELAGE

For fibrous composite materials, a linearly-elastic gross material behavior will suffice but, for ductile materials like aluminum alloys, one must include some nonlinear behavior to permit loading beyond the material proportional limit. The stiffness of each segment of the joint can be calculated to any level of accuracy desired but any improvement in accuracy beyond what can be achieved by the well publicised Ramberg-Osgood model (Reference 9) or even a two-straight-line (bilinear) model is likely to very small and not worth the added complexity. The nonlinearity of purely ±45° fibrous composites can be represented by the Ramberg-Osgood model. Other fiber patterns, containing some 0° fibers aligned with the load direction, can be treated as linearly elastic to failure.

The extension of the members between stations k and k+1 is given by

$$\delta_{1(k+1)} - \delta_{1(k)} = \alpha_1 \Delta T \ell_{(k)} + \varepsilon_1 \ell_{(k)} \tag{69}$$

and

$$\delta_{2(k+1)} - \delta_{2(k)} = \alpha_2 \Delta T \ell_{(k)} + \varepsilon_2 \ell_{(k)} \tag{70}$$

since, for uniformly stepped members, the strain can be considered to be uniform between stations, except for the local deformation around the fasteners, which is accounted for in Equations (54) to (62). In Equations (69) and (70) the thermally-induced strains derive from any temperature differential

$$\Delta T = T_{operating} - T_{assembly} \tag{71}$$

and the mechanically induced strains ε_1 and ε_2 are deduced on the basis of the member loads and the material behavior, as depicted in Figure 27.

Any running load is considered to be applied uniformly along the length of the joint and, in calculating the strains in Equations (69), the stretching is taken to be that which would be associated with the average member load in each segment. Since the fastener loads are treated as step discontinuities at each station, it follows from Equations (67) and (68) that the average loads causing the stretching of each member between stations k and k+1 are

$$\overline{T_1}_{(k)} = T_{1(k)} - P_{(k)} + p_1 \ell_{(k)}/2 \tag{72}$$

and

$$\overline{T_{2(k)}} = T_{2(k)} + P_{(k)} - p_2 \ell_{(k)}/2 \tag{73}$$

The corresponding stresses are

$$\sigma_{1(k)} = \overline{T_{1(k)}} \; / \; [w_{1(k)} t_{1(k)}] \tag{74}$$

and

$$\sigma_{2(k)} = \overline{T_{2(k)}} \; / \; [w_{2(k)} t_{2(k)}]. \tag{75}$$

For linearly elastic materials, such as fibrous composites, the equivalent strains would be

$$\varepsilon_{1(k)} = \sigma_{1(k)} \; / \; E_{1(k)} \tag{76}$$

and

$$\varepsilon_{2(k)} = \sigma_{2(k)} \; / \; E_{2(k)}. \tag{77}$$

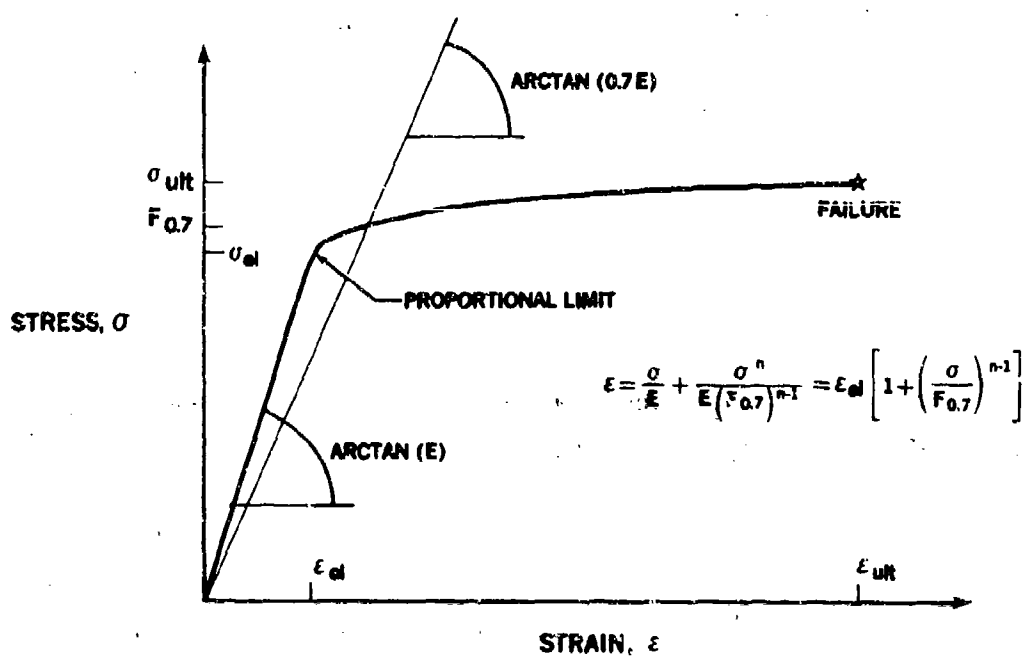

FIGURE 27. RAMBERG-OSGOOD NONLINEAR CHARACTERIZATION OF STRESS-STRAIN BEHAVIOR

In terms of the Ramberg-Osgood material characterization for ductile materials,

$$\epsilon_i = \frac{\sigma_i}{E_i} + \frac{\sigma_i^{\,n}}{(E\,F_{0.7}^{\,n-1})_i} = \frac{\sigma_i}{E_i}\left[1 + \left(\frac{\sigma_i}{F_{0.7}}\right)^{n-1}\right], \qquad (i = 1, 2) \tag{78}$$

Care must be exercised in using the formulations in Equations (78) because some of the published mathematical models do not agree precisely with the material properties given in MIL-HDBK-5. The discrepancies are usually small but it is necessary to input into the solution strength and strain failure properties at each station which are precisely consistent with Equation (78).

Having determined the member strains, per Equations (76) to (78) as appropriate, the relative displacement between the members, at the next station, follows for Equations (69) and (70) as

$$\delta_{(k+1)} = \delta_{2(k+1)} - \delta_{1(k+1)} \tag{79}$$

as shown in Figure 24. This, in turn, permits a new increment of fastener load transfer to be evaluated on the basic of Equations (54) to (62).

Actually, for the example shown in Figure 24, there would be no transfer of load at station (k+1). Therefore, between stations (k+1) and (k+2), Equations (67) and (68) would be modified to read

$$T_{1(k+2)} = T_{1(k+1)} + p_1 \ell_{(k)} \tag{80}$$

and

$$T_{2(k+2)} = T_{2(k+1)} - p_2 \ell_{(k)}. \tag{81}$$

However, Equations (69) through (79) would be applied in precisely the same manner for the next increment of the joint.

In analyzing such a multirow joint, one can specify the load(s) in members 1 and 2 at the start (left end) of the joint and seek such a value of the first fastener load that the boundary conditions are satisfied at the far (right) end of the joint. Alternatively, in seeking the elastic and ultimate joint strengths, one can specify the displacement differential between the members

at the first row of fasteners and iterate on the assumed applied load until satisfaction of the boundary conditions at the other end of the joint indicates the convergence has been attained.

The application of the methods described above, for tensile loading, to situations in which the applied loads are compressive is straightforward, requiring only some sign changes and modifications to the Ramberg-Osgood relations (78). The same method can be adapted also to in-plane shear loading, just as was done in Reference 2 for bonded stepped-lap joints, by replacing the various Young's moduli E by the shear moduli $G = E/2(1+\nu)$. While the analysis can thus be made to compute the load sharing for a specified applied load, the lack of suitable test data make it difficult to predict the failure strength for in-plane shear loading.

3.5 FAILURE CRITERIA AT FASTENER HOLES

Having computed the bearing loads and bypass loads at each station throughout the joint, it is still necessary to assess whether or not that combination is capable of causing the joint to fail. In the case of conventional ductile metal members, this customarily is a simple problem since only minimal interaction is considered between the two load components. With fibrous composites, however, that is not so. The use of a linear or kinked interaction for composites is explained in References 10 and 11, and illustrated in Figure 28 for tensile loading. The linear interaction for narrow strips is the consequence of a tensile (through-the-hole) failure regardless of the ratio of bearing to bypass load. The use of wider strips, or greater bolt spacing, is seen to permit distinct bearing and tension failure modes, so a two-straight-line interaction is necessary. The question of just what constitutes the optimum width-to-diameter ratio, in the sense of maximizing the joint strength, is discussed fully in Reference 11. In most cases it is found that having the bolts just a little too close together to permit bearing failures maximizes the strength. However, sometimes a weaker joint is preferred, on the basis that bearing failures are more forgiving. That aspect of joint design in composites is beyond the scope of this paper. For the present it suffices to say that any analysis of multirow structural joints in fibrous composities should cover both possibilities.

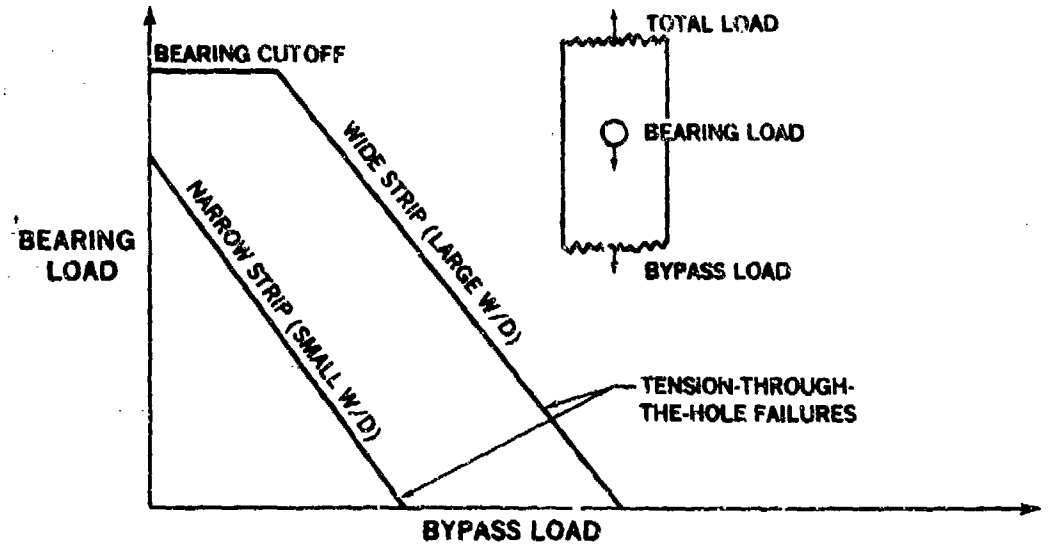

FIGURE 28. BEARING/BYPASS LOAD INTERACTION FOR LOADED BOLTS IN ADVANCED COMPOSITES

Figure 28 has been prepared for the most usual test case, tensile loading. However, the general case must include compression as well, as in Figure 29.

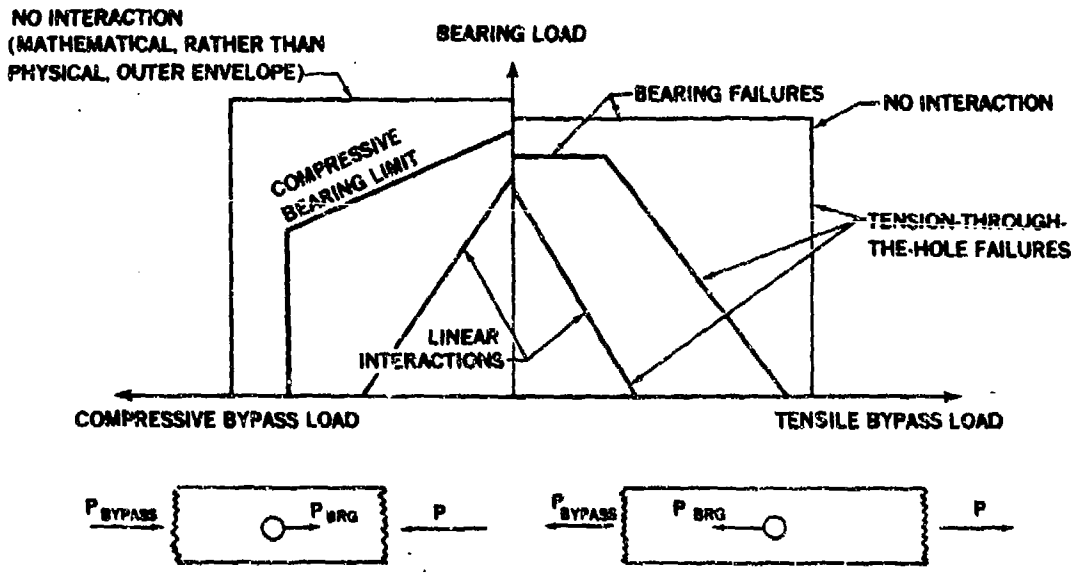

NOTE: ONLY TWO BASIC CONDITIONS POSSIBLE. OTHERS ARE MIRROR IMAGES OF THESE TWO.

FIGURE 29. EXTREMES OF BEARING-BYPASS LOAD INTERACTIONS

It is important to note that, as shown in the bottom of Figure 29, all possible seemingly different combinations of bearing and bypass load can in fact be reduced to one of only two cases, by identifying as the bypass load the numerically smaller load on one side of each fastener station. For fibrous composite materials, these bearing-bypass interactions are strongly dependent upon the fiber pattern as well as the material constituents and, in the case of tension-bearing interactions, are dependent on the geometry as well. It is evident, however, that each of the interactions can be defined by three points with straight line interpolation, as shown in Figure 30.

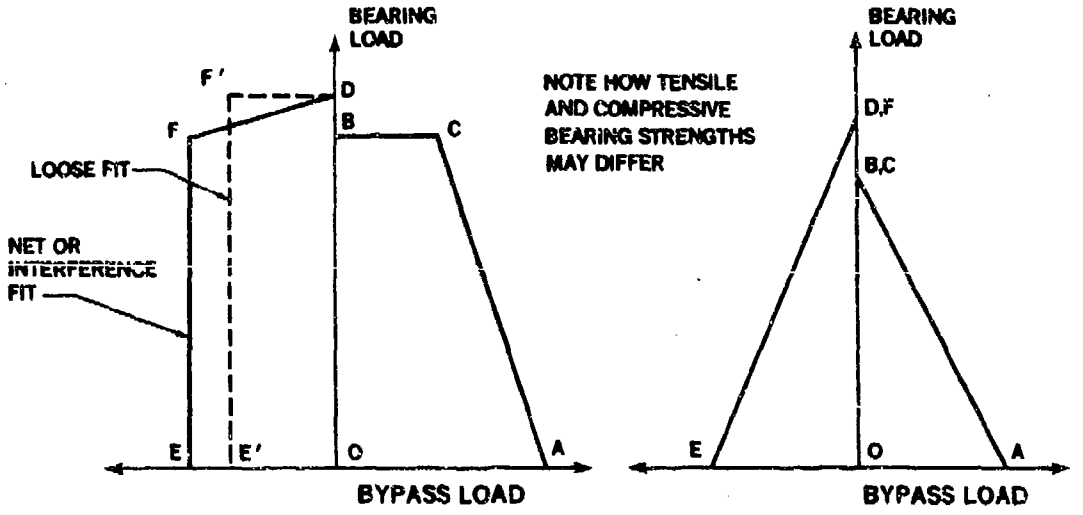

FIGURE 30. IDENTIFICATION CODE FOR BEARING-BYPASS LOAD INTERACTIONS

The physical explanation of the various line segments in Figure 30 is as follows. Along AC, the criterion is that the total load (bearing plus bypass) is sufficient to fail the net section while, along BC, there would be a local bearing failure, which would transfer load to other fasteners. The line EF represents a gross-section compressive failure through the filled fastener hole while, along E'F', the inability to transmit direct bearing through a loose fastener reduces the compressive load capacity because of the reduced effective section. Along FD, the combination of bearing and bypass stress is sufficient to induce a bearing failure. The heights of the points B and D above the origin O are strongly dependent on whether the load is

transferred through simple shear pin, a countersunk fastener, or protruding head fasteners with washer. Likewise, one difference between single- and double-shear attachments would be apparent in the different locations of points B and D. The generation of curves such as in Figure 30 for fibrous composites relies on either testing or empirical interpretation of prior test data.

The rectangular outer envelopes in Figure 29 are only mathematical curiosities which, nevertheless, must be included in the computer coding to be able to recognize improperly input data. Since the tensile bypass load shown is the difference between the total net section load and the bearing load there must be some interaction for even the most ductile materials. This is explained in Figure 31. The physical limits on the envelopes shown in Figure 31 are that the net section strength is constant for tensile load and is not reduced by any applied bearing load while, for compression, the total bearing allowable is constant and is the sum of the applied bearing and bypass (or carry-through) stresses. The computer program is coded to detect

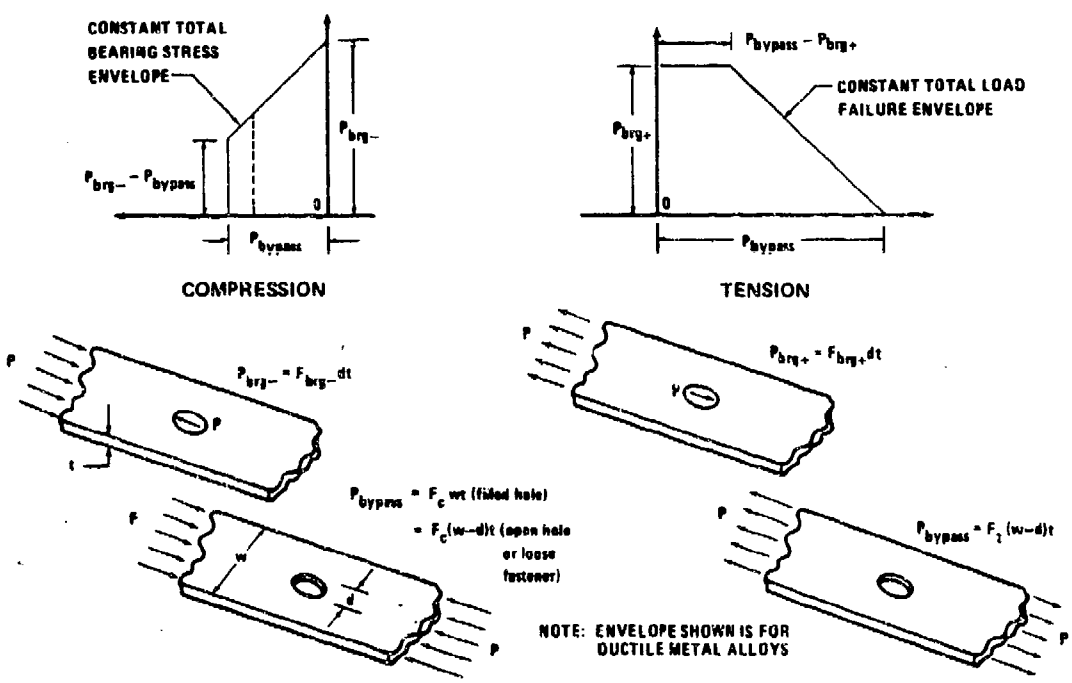

FIGURE 31. OUTER ENVELOPE OF BEARING-BYPASS LOAD INTERACTIONS

any violation of this situation. If possible, incorrect input data is modified and noted. If not, the solution is aborted.

Obviously, the likelihood of a failure at some intermediate station between fasteners is remote because of the lack of any bearing stress there, but the computer coding should cover that possibility for such a case as improperly proportioned sculpturing to soften the load on the end fastener, along the lines of Figure 25. Since the joint strength varies from station to station, the failure criteria must be determined for each location. For fibrous composites, the methods described in References 10 and 11 can be used. The standard methods for evaluating the equivalent properties for ductile metals are described in References 12 and 13. It should be noted that it is customary to express the failure criteria differently - gross section strains for fibrous composites and net section stresses for ductile metals.

3.6 EXPERIMENTAL DETERMINATION OF INPUT DATA FOR COMPUTER ANALYSIS

The analysis above has been coded as the Fortran IV digital computer program A4EJ which is described in Volume II of this report where complete user instructions are provided. In comparison with the earlier program A4EI for stepped-lap bonded joints and doublers, there is a considerable increase in the amount of data needed to define the problem for bolted joints. Unfortunately much of the data must be generated on the basis of tests that are specific to individual fasteners in particular members and must be repeated for different thicknesses, diameters, fiber patterns, and so on. Further, many of the past tests on this subject, as in References 10 and 11, were conducted with less ambitious recording of the data because the needs established here had yet to be identified. It is hoped that, now that the analysis has been developed, it will be possible to plan a new test program for bolted and riveted joints in fibrous composite structures.

Despite this seemingly unpromising situation for the present, there is a considerable body of experimental and empirical data available for the mechanical attachment of metal structures. Reference 14 contains an empirical formula for the load-deflection characteristics of individual fasteners.

$$K_{el} = E \Big/ \left[\frac{A}{d} + \frac{B}{t_1} + \frac{B}{t_2} \right] \tag{82}$$

where E is Young's modulus of the members being joined, d is the fastener diameter, and t_1 and t_2 are the member thicknesses.

Established values of the coefficients A and B are

$A = 5.0$, $B = 0.8$ for aluminum rivets (83)

$A = 5.0/3$, $B = 0.86$ for steel fasteners (84)

and the the author of Reference 14 has recommended the use of

$A = 5.0/1.6$, $B = 0.82$ for titanium fasteners. (85)

Whenever members of different moduli are fastened together, it would seem to be appropriate to use the lower modulus as the primary value of E and to adjust the thickness of t_1 or t_2 to compensate for the higher modulus. Until there is a significant data base established to endorse or refute the use of Equation (82) for fibrous composites, it should be used with caution. But, in the absence of other verified information, there would seem to be little alternative to the use of that or similar formulae.

Now, having established the slope of the linear portion of the load-deflection characteristic in Figure 22, it remains to establish the proportional limit and the nonlinear behavior. The end of the elastic curve can be estimated as the yield bearing strength of the weaker member at each fastener station. This strength P_{el} will obviously vary along the length of a stepped joint as the member thicknesses progress from the unbalanced ends of the joint to the balanced middle. The ultimate strengths P_{ult} can be established the same way. However, the slopes K_{pl} of the nonlinear portions are not as well defined.

Obviously, there is much testing remaining to be done to make full use of this analysis, but the considerably increased definition available in the solutions demands a commensurate increase in the input data.

3.7 SAMPLE SOLUTIONS

Three examples illustrate the capabilities of this new analysis program. One concerns a design for fibrous composite structure while another is an after-the-fact analysis of a thick metal splice and the third is a design study in thin metal splices.

Graphite-Epoxy Wing Spar Cap Splice

Figure 32 summarizes the results of an analysis, by the A4EJ computer program, of a design for a spar cap splice at the side of a fuselage for a large transport aircraft which might be built from advanced composites. Because of the high aspect ratio of the wing, the load intensity is much more severe than on any existing application, with the possible exception of the F-18 wing skin root fittings, which is presumably much more heavily loaded than are any of the horizontal tails on the F-15, F-16, or F-18. The total splice length shown in Figure 32 is 20.25 inches and, with three rows of bolts perpendicular to the thirteen shown in each row, it is quite a massive joint.

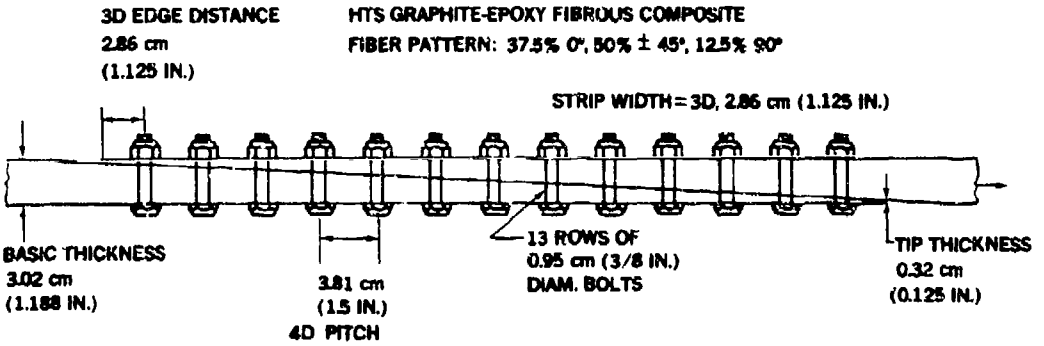

PREDICTED FAILURE LOAD=225.5 kN (50703 LB)
PREDICTED GROSS SECTION FAILURE STRAIN=0.0039
PREDICTED NET SECTION FAILURE STRESS=349.4 MPa (50.7 ksi)
PREDICTED FAILURE MODE: TENSION THROUGH FIRST FASTENER HOLE
PEAK BOLT LOAD (AT ENDS)=22.7 kN (5093 LB)
MINIMUM BOLT LOAD (IN MIDDLE)=14.8 kN (3317 LB) } :RATIO 1.5

FIGURE 32. BOLTED COMPOSITE JOINT

One very significant result shown in Figure 32 is that the predicted gross section failure strain is 0.0039, roughly half way between the loaded hole strain level of 0.0035 and that for unloaded holes of 0.0042. One should not, therefore, expect any significant improvement in strength to be possible as the result of even the most thorough redesign. The other significant finding is that, because the members cannot possible be tapered down to a point, and the first fastener could not be located there anyway, the load distribution is not uniform. The end bolts pick up 1.5 times as much load at those in the middle. Actually, that ratio would have much higher still had there been no tapering at all. The significant point to be recognized here is that it is not possible to design a linearly tapered multi-row mechanically fastened joint which approaches the uniformity in load transfer of a bonded scarf joint.

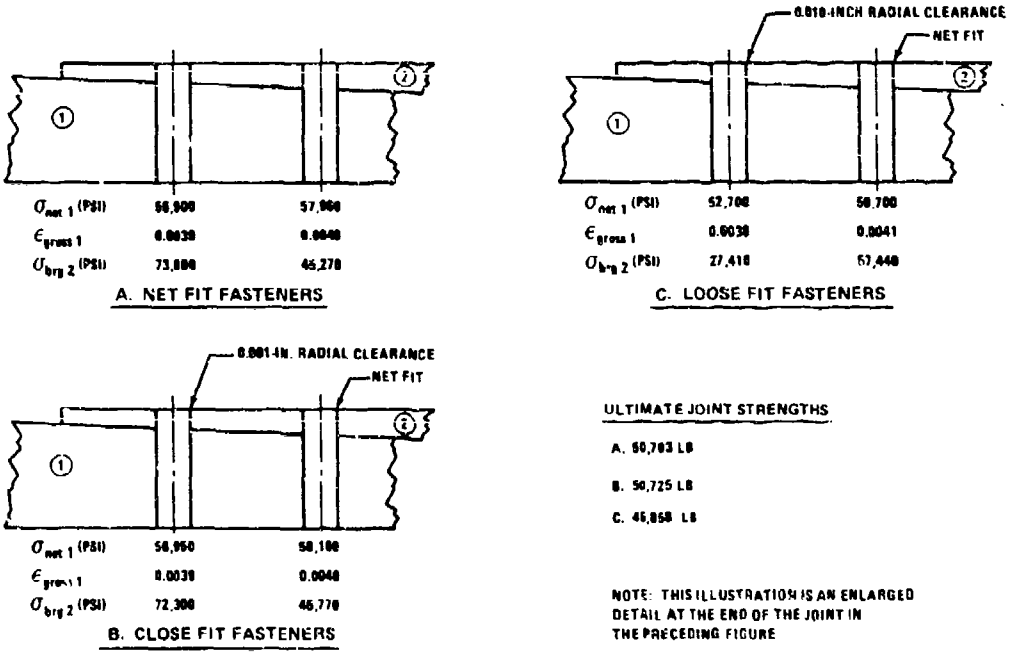

FIGURE 33. INFLUENCE OF HOLE CLEARANCE ON STRENGTH OF BOLTED JOINTS

Figure 33 records some perturbations on the basic solution in Figure 32 due to minute and gross clearances around the end fasteners. The 0.001 inch radial clearance actually increases the strength because it softens the end fasteners and decreases their bearing loads slightly. The gross clearance of

0.010 inch around the end fasteners, on the, other hand, unloads them so much that more of the basic load is carried through to the next fastener station, where the thickness has been reduced and the laminate strength also. It is clear that, in tapered splices like this, it is important that the outermost fasteners in particular are not loose. Otherwise there will be a disproportionate loss of strength. In metal structures, however, there would be enough yielding to redistribute the loads and increase strength prior to failure.

Metal Wing Skin Splice

The splice shown in Figure 34 is one of many splices actually tested in the development of the wing skin splice at the side of the fuselage for a large transport aircraft. The fasteners near the tip of the splice plates are of

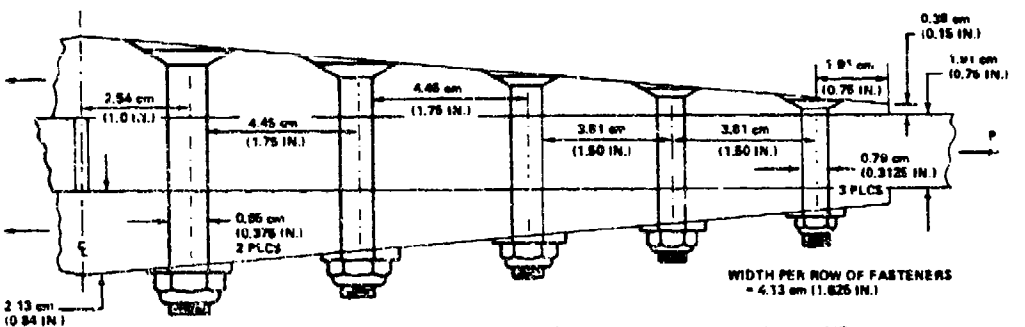

• RESULTS OF NONLINEAR ANALYSIS AT APPLIED GROSS SECTION STRESS OF 275.8 MPa (40 KSI)

FASTENER (kN)		51.6	37.0	34.2	39.8	54.4	
LOADS (LB)		11,605	8,323	7,694	8,947	12,232	
NOTE BALANCE BETWEEN END FASTENER LOADS, DUE TO THICKENING OF SPLICE STRAPS							
SKIN NET	(MPa)	85.4	146.6	193.5	256.2	341.9	276.1
SECTION STRESSES	(KSI)	12.379	21.254	28.060	37.165	49.575	40.041
SPLICE STRAP	(MPa)	179.5	169.6	164.7	165.6	151.6	
NET SECTION	(KSI)	26.027	24.592	23.885	24.012	21.975	

STRESSES PEAK BEARING STRESSES ON RIGHT END FASTENER: 360.0 MPa (52.2 KSI) IN SKIN; 636.5 MPa (92.3 KSI) IN SPLICE

• TEST FAILURE IN SKIN THROUGH RIGHT END FASTENER, WHERE BOTH NET TENSION AND BEARING STRESSES ARE PREDICTED TO BE HIGHEST

• ANALYSIS PREDICTED ULTIMATE FAILURE AT GROSS SECTION SKIN STRESS OF 350.3 MPa (50.8 KSI)

FIGURE 34. BOLTED METAL JOINT

lesser diameter than the others to equalize the load sharing. The success of this design, using older methods established at least ten years prior to this analysis, can be gaged from the predicated net section failure stress of 50.8

ksi, in comparison with the design target of 52 ksi. The seemingly disproportionate thickness of the splice plates where the skins butt together is needed to try and equalize the load transfer at each end of the overlap.

The first and last bolts shown do transfer close to the same load. Figure 34 indicates some of the quite extensive internal definitions of the load transfer and stress states within the joint that this analysis can provide.

Metal Fuselage Skin Splice

The thick tapered splice shown in Figure 34 is unsuitable for use in the much thinner fuselage structure, so it is more usual to employ scalloped or lollipopped edges on splice plates and doublers there, as shown in Figure 25. This is true for bonding such structures also. Apart from the difficulty of handling thin tapered strips without damaging them, there is a further reason for preferring a wavy edge to the splices. The variation along the edge makes earlier crack detection possible, minimizing both the likelihood of catastrophic failure and the size of repair needed. A skin crack could grow far longer before detection if it were concealed under a uniform tapered doubler rather than periodically exposed for visual inspection by a routed sculptured edge.

Figure 35 presents a comparison between different fuselage skin splice designs, with a basic uniform splice with the same number of rivets for reference. Since it has been shown in Reference 11 that the load on a fastener induces a hoop stress around the hole of the same order of magnitude as the average bearing stress, the fatigue life of the lollipopped designs should be much greater, as has often been shown by test. The skin is most frequently critical through the first row of attachments. The reasons for omitting every second fastener in that outermost row are that it increases the static stength of the joint, because of the reduced net area loss, and it means that any cracks which may initiate have further to grow before they could join up and rip the skin apart. These advantages outweigh the consequent increase of bearing stress on those end fasteners, with respect to having had twice as many fasteners to share that load.

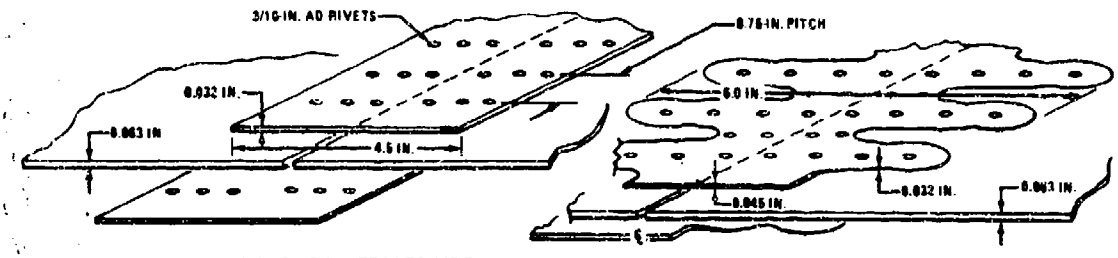

3 FULL ROWS OF RIVETS PER SIDE

RIVET LOAD (LB)	224	182	224	
BEARING STRESS (KSI)	19	15	19	
SKIN STRESS (KSI)	8.3	11.5	17.0	13.3

2 FULL AND 2 HALF ROWS OF RIVETS PER SIDE

RIVET LOADS (LB)	213	188	183	285	
SKIN BEARING STRESS (KSI)	18	15	16	24	
SPLICE BEARING STRESS (KSI)	12	11	16	24	
SKIN STRESS (KSI)	6.8	9.6	11.8	15.2	13.3
SPLICE STRESS (KSI)	10.7	14.8	9.0	5.6	

INTERNAL LOADS FOR COMMON 1-P LOAD OF 840 LB/IN.

NOTES
1. ULTIMATE STRENGTHS ARE 2820 LB/IN. FOR BASIC JOINT AND 3410 LB/IN. FOR LOLLIPOPPED SPLICE, CORRESPONDING WITH REMOTE SKIN STRESSES OF 46 AND 54 KSI, RESPECTIVELY.
2. EACH SPLICE HAS THE SAME NUMBER OF RIVETS.
3. FURTHER OTIMIZATION OF REFINED SPLICE COULD ENHANCE FATIGUE LIFE BY REDUCING END FASTENER LOAD, BUT ULTIMATE STHENGTH WOULD NOT BE IMPROVED.

FIGURE 35. COMPARISON BETWEEN BASIC AND REFINED FUSELAGE SKIN SPLICES

The softening by scalloping which, is shown in Figure 35, is also applied to slightly thicker structure, where stringers are spliced, for example. The computer program A4EJ now makes it possible to perform parametric studies to optimize the proportions of all such design details. It might even be possible now to design by analysis rather than test, for the first failure to occur in the splice plate, which is easier to replace than the skin.

In thin sheet-metal structure, it is common to have multiple splice elements which do not all start at the same fastener location. There are therefore two or more rows of fasteners which are subjected to peak loads. Once the use of this program A4EJ has been mastered, it is possible to obtain a reasonable representation of the internal loads in such splices, as shown in Figure 25, by selectively lumping the skin and doubler together to cover one end of the joint, while the doubler and splice would be lumped together to characterize the other end. This takes two runs and obviously will not cope with all such situations. There is a need, therefore, to try and modify the existing coding to account for multiple splice elements some day. The limit to such work is anticipated to be in the computer run times. For example, if

it takes 100 iteration cycles to solve a problem with a single (or symmetric) splice, it would take 10,000 cycles if there were two splice plates of different widths. That must be weighed against the cost of inputting two models to approximate the problem with two runs on the present program. The author believes that there is a case for a three-member splice analysis, but not for any more than that, even though the recoding effort would be the same. Eventually designers must face up to standardized design concepts within the capability of then current analyses for any future project or incur the ever increasing expense in money and time of specific detailed finite-element analysis or physical testing, for gains that are often imperceptible with respect to simpler concepts if done well.

Improvement Of Bolted Joint Designs To Enhance Fatigue Lives

None of the examples discussed above would qualify as a poorly designed joint, so they provide no standards against which other joints can be assessed. It is appropriate, therefore, to include a comparison between a multirow bolted joint in which no design finesse at all was employed and one in which a reasonable degree of expertise had been applied. This comparison is evident in the different designs and analyses shown in Figures 36 and 37. These joints are idealized in the sense that there would have to be support structure to react the eccentricity in load path and that the bolt failure in Figure 36 could easily be avoided by a double-strap splice design with the bolts in double shear. Nevertheless, there are several important conclusions to be drawn from these examples.

While the uniformity of load transfer in Figure 37 is far superior to that shown in Figure 36 (within 4 percent for normal operating loads), the inefficiency in Figure 36 is nowhere near as severe as similar analyses in adhesively bonded structures would suggest. The forty percent inefficiency shown would become much higher for thinner more extensible members and for more rows of bolts, however, but would probably never approach the 10 to 1 ratio needed between the peak and minimum adhesive shear stresses in durable bonded joints.

The ultimate strengths of the two joints shown in Figures 36 and 37 differ by

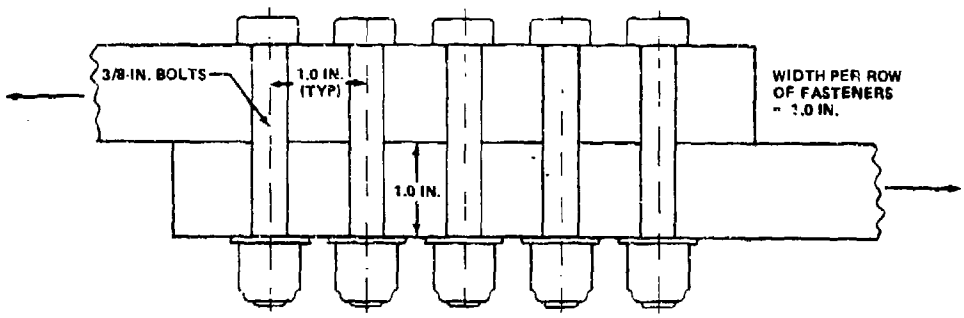

TOTAL LOAD (LB/ROW)	INDIVIDUAL FASTENER LOADS					RATIO P_{MAX}/P_{MIN}
10,000	2,337	1828	1669	1828	2,337	1.40
20,000	4,675	3656	3338	3656	4,675	1.40
30,000	7,032	5472	4992	5472	7,032	1.41
40,000	9,588	7162	6500	7162	9,588	1.48
43,042 (ULTIMATE)	10,490*	7597	6867	7597	10,490	1.53

*SHEAR FAILURE (HIGHEST ASSOCIATED NET SECTION ALUMINUM STRESS = 68.9 KSI)

NOTE: COMPATIBILITY OF DEFORMATIONS AGGRAVATES NONUNIFORM LOAD DISTRIBUTION AS LOAD IS INCREASED, BECAUSE MEMBERS YIELD ONLY AT HIGHLY LOADED ENDS, NOT EVERYWHERE.

FIGURE 36. BOLT LOAD DISTRIBUTION IN POORLY-DESIGNED MULTIROW BOLTED JOINT

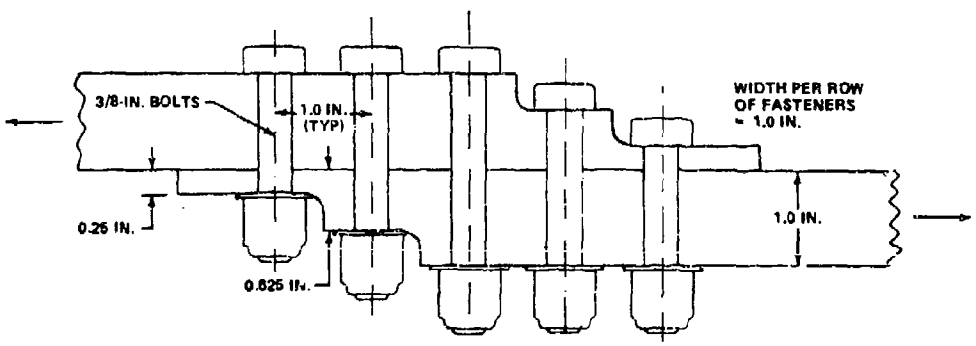

TOTAL LOAD (LB/ROW)	INDIVIDUAL FASTENER LOADS					RATIO P_{MAX}/P_{MIN}
10,000	2030	1995	1951	1995	2030	1.04
20,000	4060	3989	3902	3989	4060	1.04
30,000	6105	5973	5844	5973	6105	1.04
40,000	8257	7882	7722	7882	8257	1.07
46,387 (ULTIMATE)	9709	9044	8881	9044	9709	1.09

ULTIMATE FAILURE IN NET SECTION OF ALUMINUM (AT AVERAGE STRESS OF 74.2 KSI) AT OUTERMOST ROWS OF BOLTS. NO BOLT FAILURES.

FIGURE 37. BOLT LOAD DISTRIBUTION IN IMPROVED DESIGN FOR MULTIROW BOLTED JOINT

only 8 percent. While that represents a significant improvement, the inevitable criticality of the net section at the outermost fasteners makes it very difficult to make major improvements to the ultimate strength of joints by techniques which yield substantial benefits in the fatigue resistance of the joint. The fifteen percent reduction in bearing stress on the outermost fasteners in Figure 37 could easily double the number of load cycles neeeded to fail the joint in Figure 36.

Figure 37 represents only a single estimate of proportions to improve the joint in Figure 36. Yet it came within 4 percent of a perfect load transfer. This implies that the theoretical benefits of scarf joins (which are in practice not fully obtainable because of the finite thickness at the outermost bolts) can be approached very closely with relatively far less effort. In other words, the benefits from a little bit of design finesse are substantial and should always be sought. Conversely, the residual benefits to be gained from precise optimization are disproportionately small in comparison with the effort expended to improve on the first refinements.

In the example shown, it is obvious that reducing the diameter of the outermost fasteners would not enhance the joint strength because the bolt strength would decrease faster than the stiffness. In a similar design for a double-shear joint, however, the computer program A4EJ would provide a rapid estimate of any benefits to be gained by such a modification.

It is most unlikely that a joint with such an abrupt load transfer as shown in Figure 36 would be designed today. However, that situation could arise in service due to a fatigue crack grown through a continuous member like a wing spar cap, for example. Thus, the new analysis can be used also to investigate the damage tolerance of bolted structures as well as the load transfer in the virgin structure.

3.8 CONCLUSIONS

The nonlinear behavior and increased internal definition of this new bolted joint analysis represent considerable extensions beyond the prior state of the art.

This increase in analysis capability in turn demands a more extensive experimental data base for input. Some such information may be provided also by other analysis programs for individual loaded fasteners in specific stress fields.

Even without precise data, however, the program can be very effective for parametric studies using only estimated input values.

Since this is a continuum mechanics analysis, rather than one based on finite elements, the computer run times are extremely short. The amount of input needed is significantly greater than for the earlier stepped-lap bonded joint analysis program A4EI because of the increase in number of parameters needed to define the behavior at each station.

The sample solutions described here show that the computer program A4EJ is a useful tool in analyzing multirow bolted joints, in both fibrous composite and metal structures.

SECTION 4

NONLINEAR ANALYSIS OF BONDED/BOLTED JOINTS

4.1 INTRODUCTION

Separate nonlinear analyses for the load transfer in adhesive-bonded joints and multirow bolted joints are given in Sections 2 and 3 of this report. When adhesive bonding is used in conjunction with mechanical fastening, one cannot sum the individual joint strengths because the individual stiffnesses of each load path differ. So also do the strains to failure. The function of the analysis method reported here is to be able to characterize the combined load transfer, accounting for the compatibility of deformations. Depending on one's point of view, one purpose of this investigation may be regarded as exposing once and for all the futility of combining bolting and bonding, to increase joint strength, by means of a nonlinear analysis so thorough that there can no longer be any doubts about the inefficiency of such a combination. However, that would not be a reasonable attitude to adopt because, in a broader context, there is a very legitimate need to know such things as the consequence of installing a fastener through a bonded joint not to augment the shear transfer but to tie in to some other structure or fitting. Also, of course, the introduction of load in test coupons through a bolt via bonded-on reinforcing doublers is a widespread standard practice.

By far the biggest justification for the development of such a combined bonded/bolted joint analysis capability is to be found in imperfect structures. Here there are many classes of problems in which the combination of bonding and bolting offers unique advantages, and these provide the real payoff from this new capability. The sample solutions presented in this report have been selected specifically to explain such applications as well as to illustrate the capabilities of the analysis program. The first group of these applications is the repair of what was originally intended to be purely adhesively bonded structure but which has suffered from either flaws

which occurred during manufacture or from damage in service. Such a combination was even employed as a standard production fix for a design/manufacturing problem on one modern aircraft. The second group of these applications is the enhancement of the damage tolerance of thick bonded structures, particularly those made from fibrous composites. The prior understanding of fail-safety due to the combination of rivets and bonding has been far less than adequate, so the opportunity is taken here to present a thorough discourse on this subject in the process of illustrating the capabilities of the analysis program. Briefly, for light-loaded structure, adhesive bonding provides a fail-safe load path to overcome the weakness caused by tearing along a line of fasteners. For heavily-loaded structure, on the other hand, mechanical fasteners can be very effective in preventing widespread unzipping triggered by what was initially quite localized load redistribution around a damaged or defective bond.

There is no discussion here of the derivation of the analysis methods used in the new FORTRAN IV digital computer program A4EK because that has already been covered fully in Sections 2 and 3 of this report. The combined program is capable of much but not all of what the separate programs A4EI and A4EJ can do and the reader is referred to the user manual and listings of the computer codes (Volume II of this report) for full details. The biggest difference in analysis capability is that the absence of adhesive bonding permitted the inclusion of nonlinear adherend behavior as well as nonlinear load-deflection curves for the fasteners in the bolted joint program A4EJ, while for the bonded/bolted program A4EK, the adherend deformations must remain linearly elastic to be able to compute the load transfer through the adhesive bond. Since prior work has shown that gross yielding of the adherends triggers progressive failure of adhesive bonds, this is not considered a significant limitation. The shorter length of the purely bonded analysis program A4EI has permitted the inclusion of an extra subroutine to massage the input data and improve the computer run times. Thus, these three new programs each have unique capabilities. However, the earlier stepped-lap joint analysis programs A4EF, A4EG and A4EH have no capabilities not found in the A4EI program. Yet their more limited capabilites are associated with a far shorter computer code so that they may be more desirable for small computers or for subroutines in bigger programs on larger computers.

4.2 REPAIR OF DEFECTIVE BONDED JOINTS BY MECHANICAL ATTACHMENTS

Section 2 of this report contains several sample solutions of the load transfer through a substantial titanium to graphite-epoxy adhesive bonded joint. These include both the basic nominally perfect joint and three different disbonds. The purpose of this section is to show how the addition of mechanical fasteners, in the form of 5/16-inch titanium bolts, can modify the original solutions. The basic joint geometry is shown in Figure 38. The composite laminate is 0.81 inch thick, while the titanium is 0.51 inch thick, and the overlap is 5.0 inches. It was shown in Section 2 of this report how, by progressive redesign, the joint strength could be increased significantly by optimizing the proportions. However, these refinements are not compatible with the use of bolts to provide an alternative load path with which to repair local disbonds due to misfit during manufacture or damage in service. So the original equally-stepped geometry is used in these new examples, with only a shortened end step on the titanium.

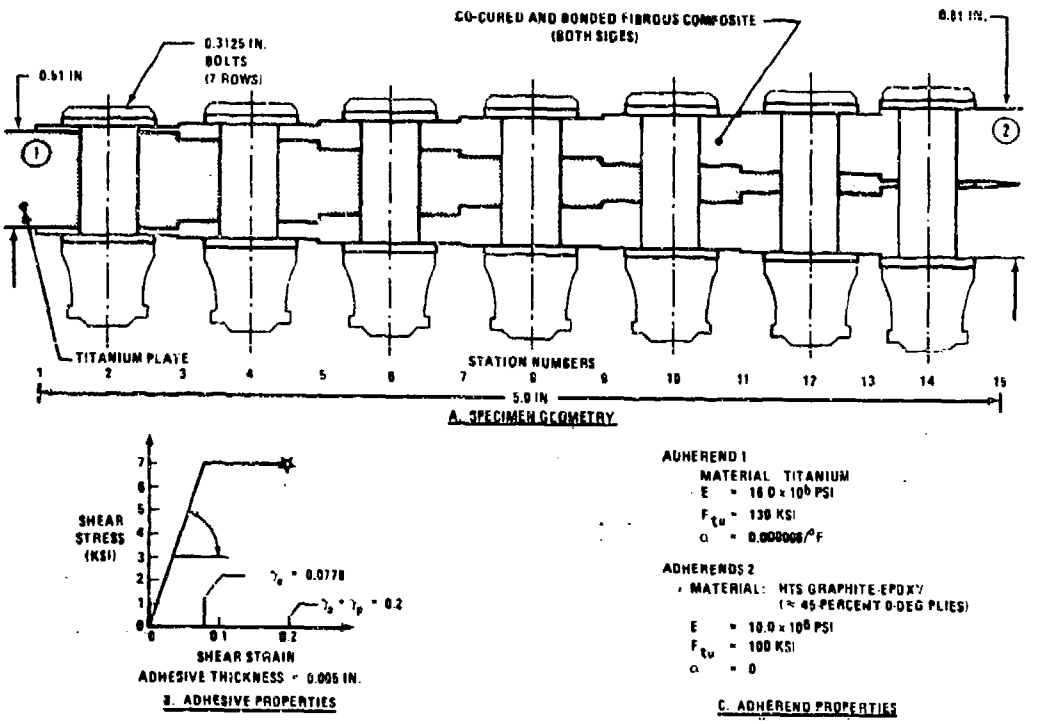

FIGURE 38. STEPPED-LAP BONDED/BOLTED JOINT

Figure 39 describes the load transfer through the bonded-bolted joint and is directly comparable with Figure 25 in Section 2 for a purely bonded joint. The addition of seven rows of fasteners to this joint is actually predicted to decrease the joint strength, from 34,322 lb/in. to 33,096 lb/in., as revealed by comparing Figure 39 with the equivalent solution here in Figure 40 for precisely the same joint without any fasteners. The reason for this decrease is a change in failure mode and location. While other examples might show a small increase in strength, the assessment of load transfer given in Figure 39 makes it clear that the addition of fasteners to an unflawed adhesive-bonded joint does not increase the joint strength significantly. In the example shown in Figure 39, the adhesive transfers over 98 percent of the total load. That may seem surprising, since it shown in Figure 41 that the fasteners acting alone, without any adhesive, could have transferred 28,380 lb/in., or 83 percent as much as the adhesive alone. The reason why the combination does not work well together is the gross dissimilarity in stiffness between the two load paths. Taken together, these three solutions seem to make a strong argument against the combination of

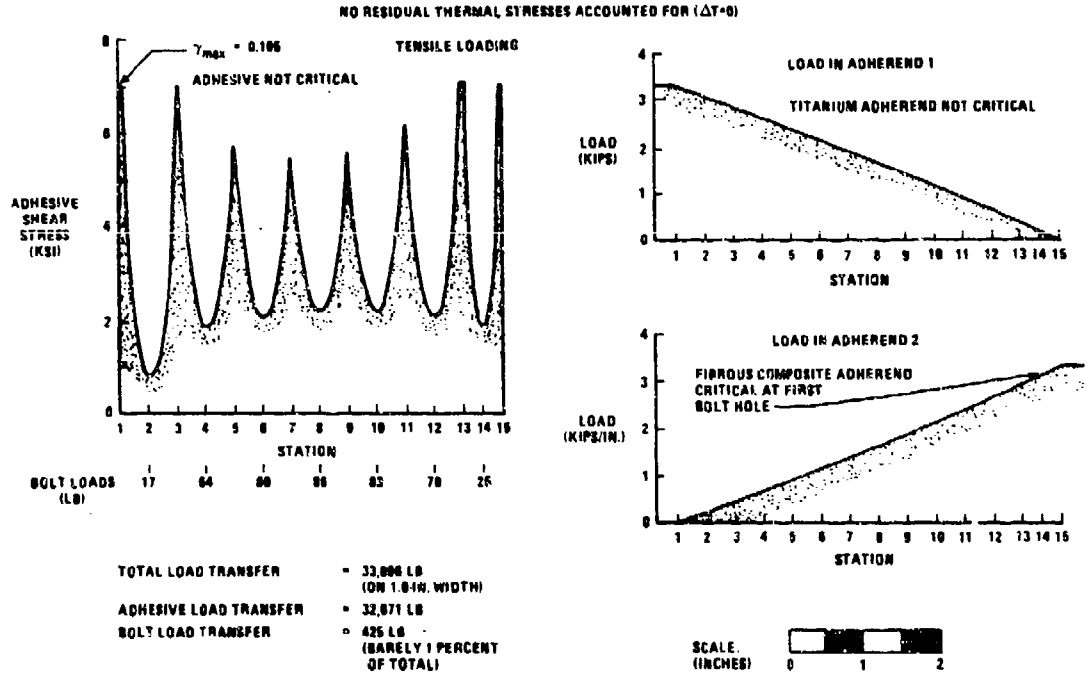

FIGURE 39. LOAD TRANSFER THROUGH BONDED/BOLTED STEPPED-LAP JOINT WITH NO FLAW

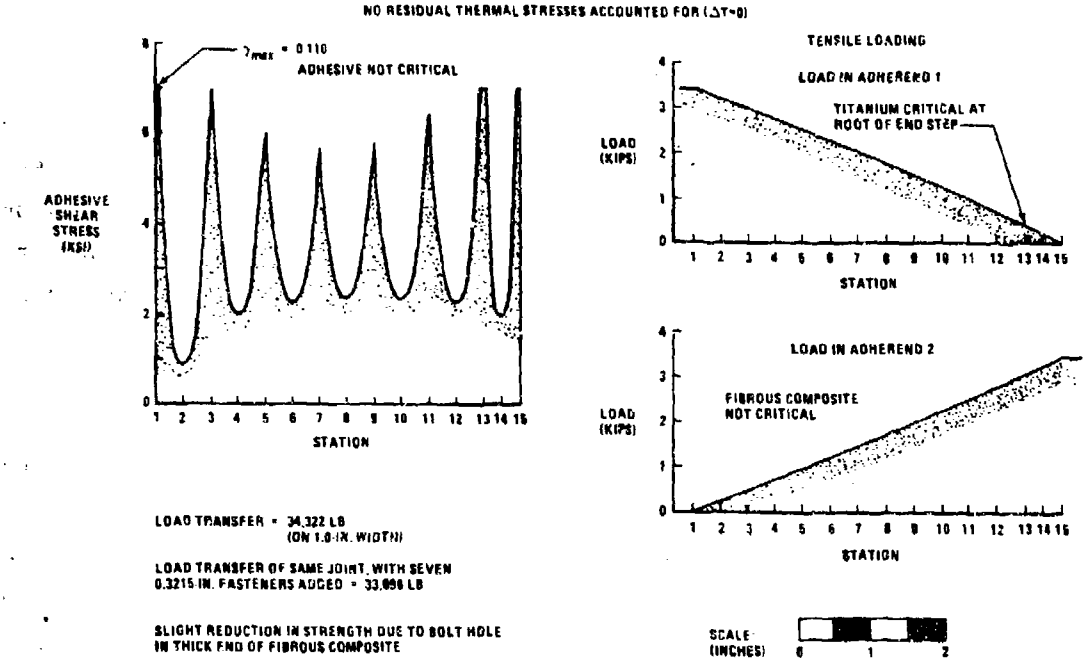

FIGURE 40. LOAD TRANSFER THROUGH ADHESIVE-BONDED STEPPED-LAP JOINT WITH NO FASTENERS

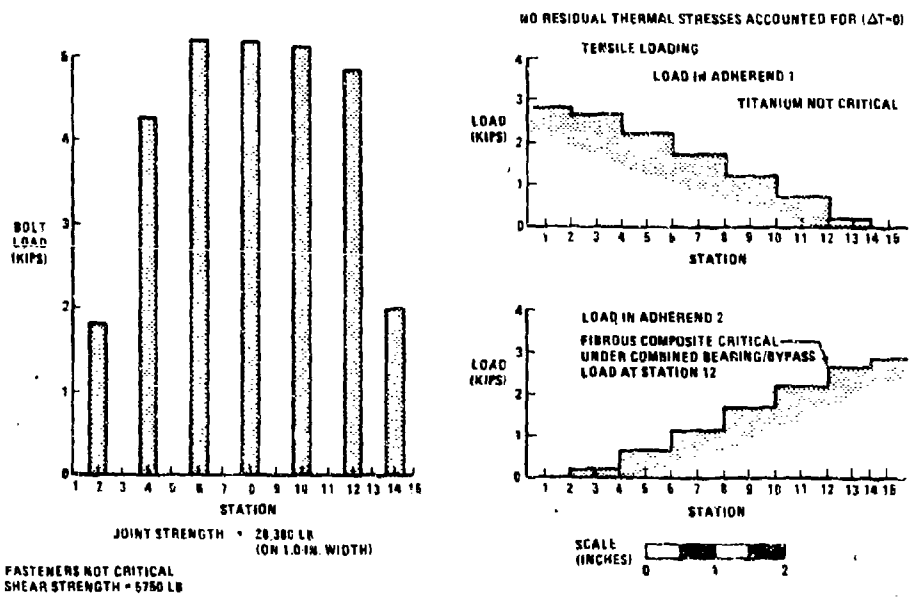

FIGURE 41. LOAD TRANSFER THROUGH BOLTED JOINT WITHOUT ANY ADHESIVE

adhesive bonding and mechanical fasteners. Such a pessimistic prediction has been found to be true for several joint geometries investigated during the course of this work. A well manufactured, well designed bonded joint is very difficult to improve upon, particularly when one considers the design refinements described in Figures 8 and 9 of Section 2 of this report to increase the bonded joint strength. Such techniques as the special shortened end step on the titantium plate are not quite compatible with the subsequent additions of rivets or bolts.

Before proceeding to the more fruitful applications of combined bonding and bolting, below, it is appropriate to comment on a surprising feature of Figure 41. The end bolts pick up much less load than do those in the middle. This is in marked contrast with the behavior of adhesive-bonded joints, where the load transfer peaks at the ends. The reason for this alleviation in Figure 41 is that the end steps are quite thin and, therefore, those fasteners have a much lower effective stiffness than those nearer the middle of the joint. If the members being bolted together were uniformly thick, the end fasteners would incur a disproportionate share of the load, just as for bonded joints.

When the bolts are used to substitute for defective or damaged bonds, the pessimistic picture above changes dramatically. This is shown in Figures 42, 43, and 44, which are directly equivalent to Figures 15, 16 and 17 of Section 2 of this report for flawed bonded joints without fasteners. The strength increases due to such bolted repairs are seen to be substantial even though they remain much weaker than the baseline joint in Figure 39 or 40. What is of special interest in Figures 42, 43 and 44 is that the fasteners still transfer so little of the load. Their effectiveness follows from relieving the stress and strain concentrations in the adhesive immediately adjacent to the flaw, rather than in the load they transfer themselves. In other words, the benefit from the presence of the bolts is that they permit the remaining adhesive to work more effectively. The strengths of the unrepaired flawed bonded joints are shown in the lower left corners of Figures 42, 43 and 44 for comparison. (While the geometry of the joint in Figure 38 here and Figure 5 of Section 2 is slightly different because of the shortened and titanium step here, the effects are insignificant, as can be

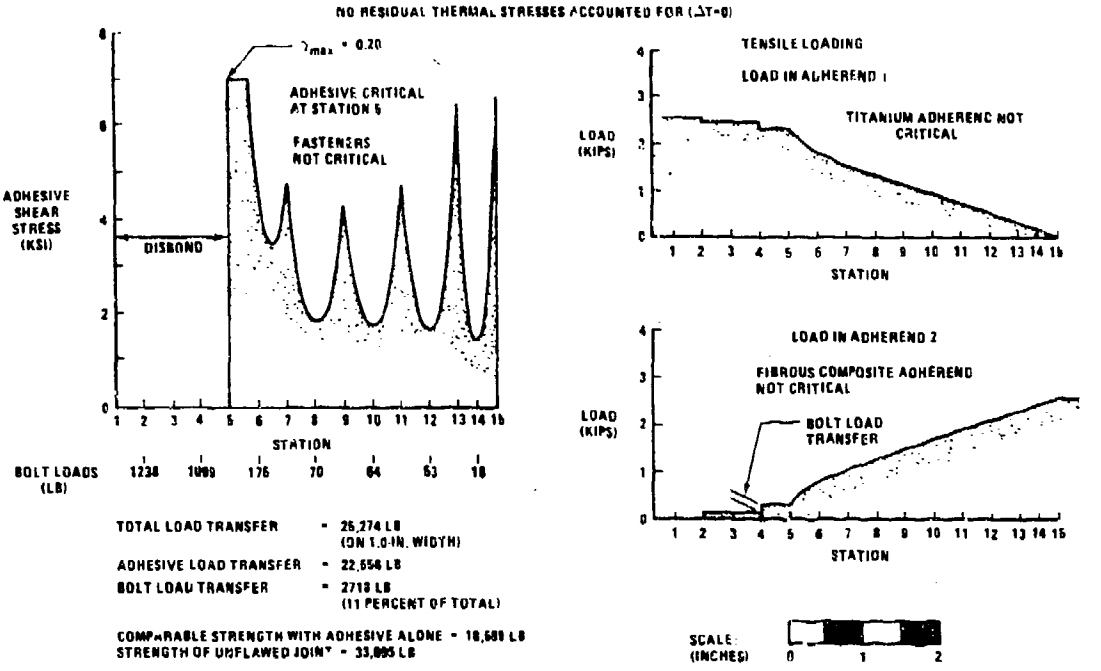

FIGURE 42. LOAD TRANSFER THROUGH FLAWED BONDED JOINT REINFORCED BY BOLTS

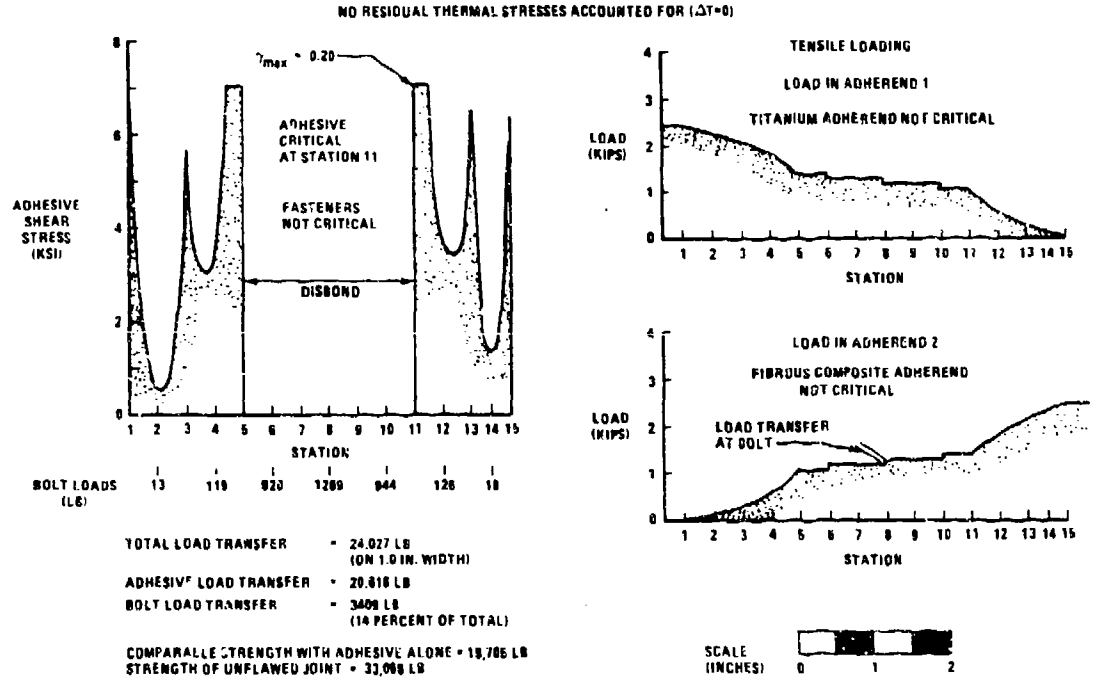

FIGURE 43. LOAD TRANSFER THROUGH FLAWED BONDED JOINT REINFORCED BY BOLTS

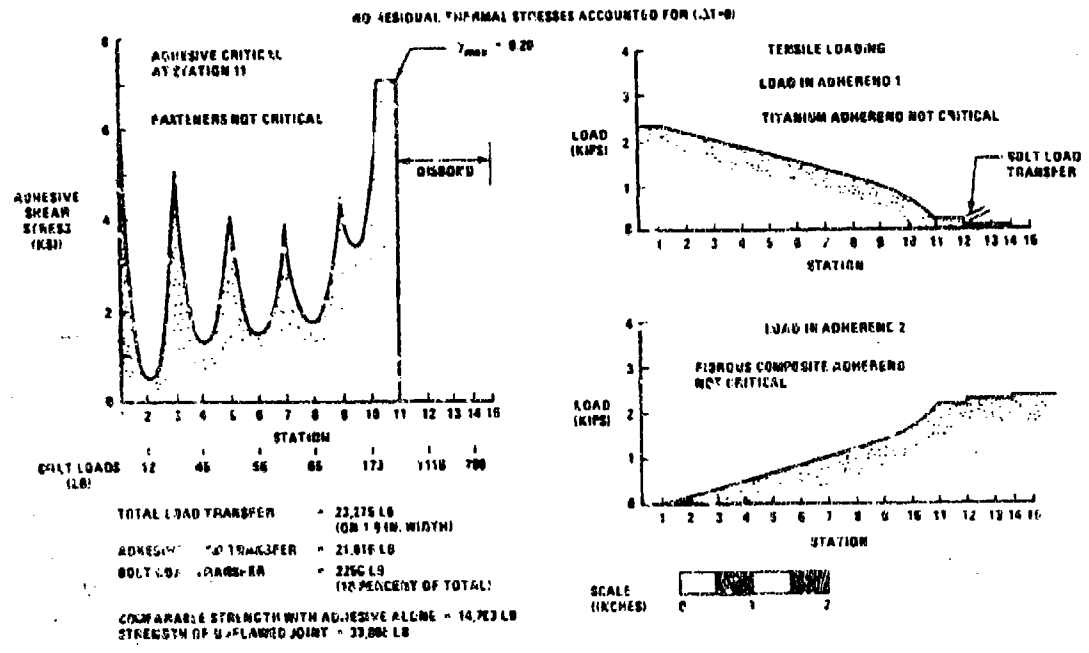

FIGURE 44. LOAD TRANSFER THROUGH FLAWED BONDED JOINT REINFORCED BY BOLTS

seen by comparing the purely bonded joint analyses - 34,322 lb. in Figure 40 here and 34,075 lb. in Figure 6 of Section 2.)

While it is true that the predicted strength for the fasteners alone, in Figure 41, is greater than for any of the repaired bonded/bolted joints in Figures 42, 43, and 44, it should be acknowledged that Figure 41 represents an ultimate load condition, with substantial damage to the laminate at much lower load levels. The bonded/bolted repaired joints would last much longer in service than the same joint with no adhesive. It is not clear whether the repaired joints would default to the greater ultimate strength with fasteners alone because the weak link with fibrous composite adherends is not the adhesive - it is delamination of the adherends - so the initial failure might well trigger quite a different final failure.

This use of the combination of bonding and bolting for repairs is thus seen to expose very real benefits which the assessment of the nominally perfect bond in Figure 39 could not reveal.

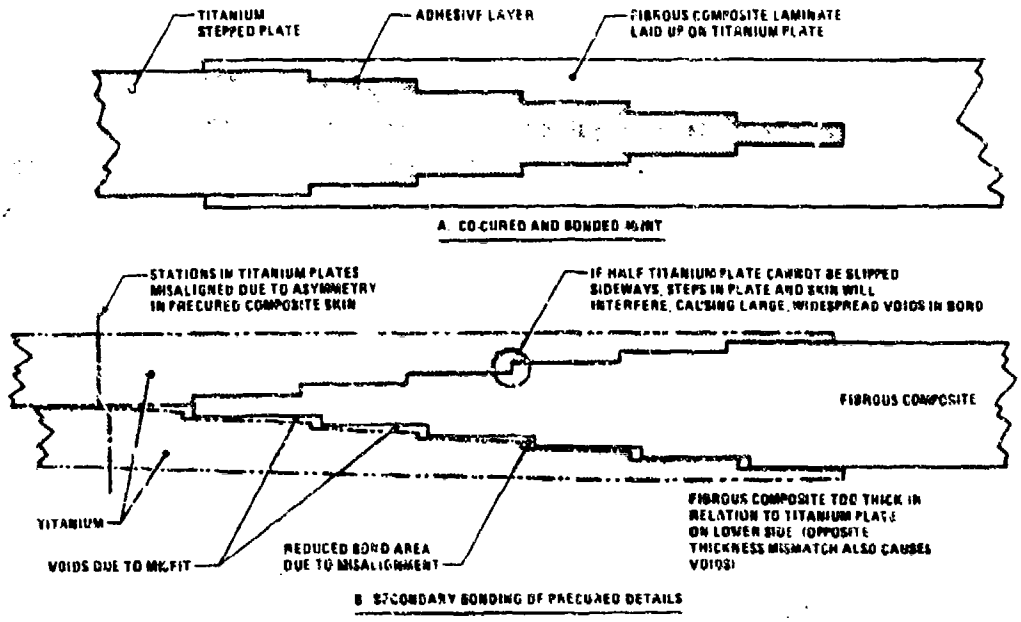

FIGURE 45. POTENTIAL MANUFACTURING PROBLEMS WITH STEPPED-LAP BONDED JOINTS

The likelihood of needing such repairs due to manufacturing difficulties can be minimized by the selection of the design and fabrication concept. This is explained in Figure 45, in which the central titanium stepped plate used in conjunction with co-cure and bonding of the fibrous composite virtually ensures an excellent fit without any of the difficulties likely to be encountered with the bonding together of pre-cured details. Even sandwiching the pre-preg between split external titanium plates will not result in a top quality bond because there is no escape path for any volatiles generated during the cure, even if the fit were otherwise perfect.

4.3 REPAIR OF DAMAGED STRUCTURE BY BONDING AND BOLTING

The new analysis methods can be applied also to the repair of general damage to structure, particularly for fibrous composite structures, regardless of whether such damage occurred at the site of an existing joint or not. Since any such patch can be regarded as two joints back-to-back, the same theory and analysis methods apply. However, for the repair of local damage, there are redundant load paths in the sense that the interrupted load is shared between the surrounding intact structure and the repair member itself.

Actually, if the repair is too stiff, it could even attract more load locally than the original structure encountered. This is not the place for a full discourse on the topic of the details of bonded repairs and the pitfalls to be avoided, but the most basic principles must be explained to make the present discussion effective.

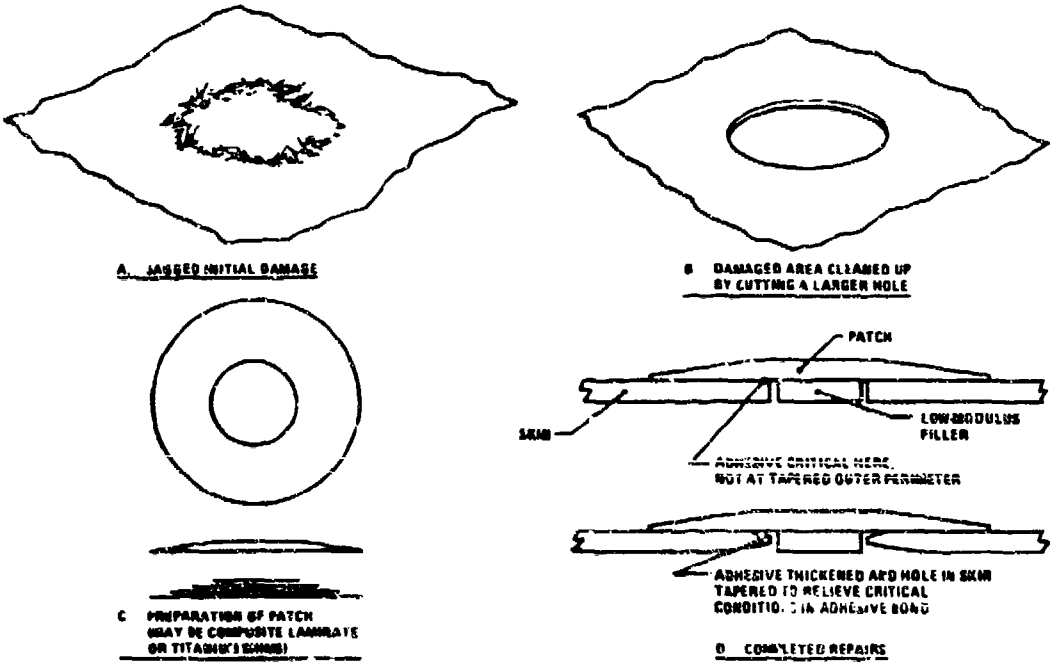

FIGURE 46. ADHESIVE-BONDED REPAIR OF DAMAGE TO FIBROUS COMPOSITE STRUCTURES

The usual procedure in the repair of local damage to fibrous composite structure is shown in Figure 46. The damaged area is first trimmed to a smooth contour. Depending on the application, the resulting hole may or may not be filled. Finally, the damaged area is covered by a larger patch, to transmit some (or all) of the load which had been interrupted by the damaged area. There are two potential sites at which the bond may become critical. One is at the outer perimeter of the patch and the other is at the edge of the hole. The fact that care must be taken at both locations is often overlooked. There have been premature failures, with excellently detailed runouts at the edge of the patch, which were due to the abrupt thickness

discontinuity at the edge of the hole. The understanding of this problem has been complicated by the fact that what seems to have been the very same repair concept which had been tested satisfactorily in small scale had failed when scaled up. While the bond area had been scaled up, the adhesive thickness had not been and that omission changed the relative strength of the adhesive and adherends, resulting in a pronounced change in failure mode. Therefore, one should expect to relieve the stress concentrations at both perimeters of the adhesive bond annulus, as shown in Figure 46, to develop the maximum strength from such a bonded repair.

Having attended to such design details for bonded repairs, the next step is to analyze the repair concept. By inspection, the most severely loaded location is a unit strip along a diameter of the hole, in line with the principal load direction. Before the analysis of that strip can be performed, however, it is necessary to establish how much of the load remains in the skins, to be diverted around the hole, and how much passes through the patch, over the hole. Strictly, one would need a finite-element analysis to establish that precisely, but the method described in Figure 47 provides a

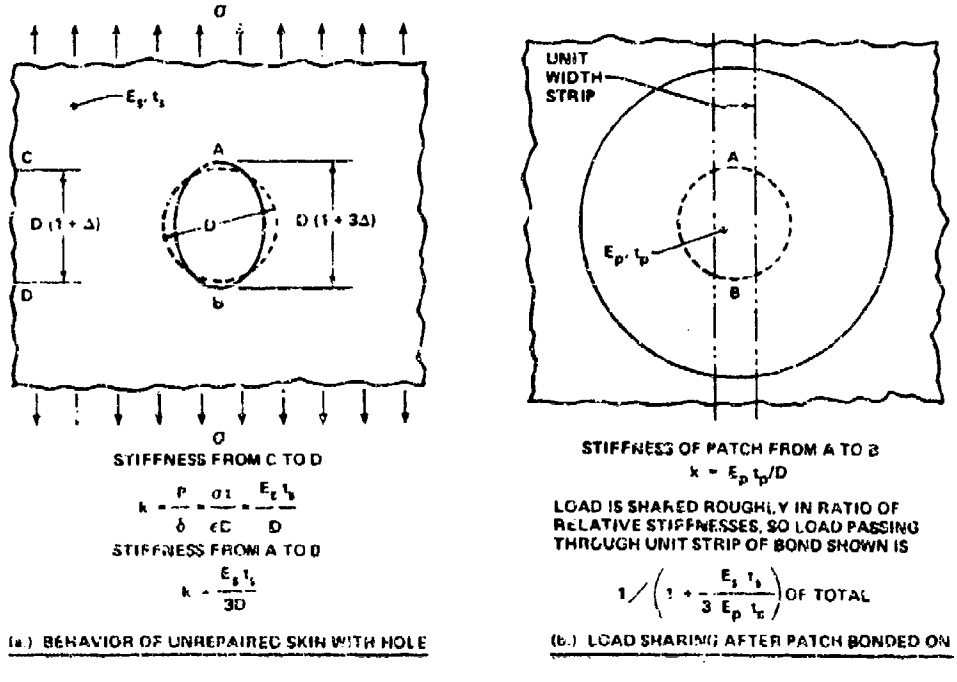

STIFFNESS FROM C TO D

$$k = \frac{P}{\delta} = \frac{\sigma t}{\epsilon C} = \frac{E_s t_s}{D}$$

STIFFNESS FROM A TO B

$$k = \frac{E_s t_s}{3D}$$

(a.) BEHAVIOR OF UNREPAIRED SKIN WITH HOLE

STIFFNESS OF PATCH FROM A TO B

$$k = E_p t_p / D$$

LOAD IS SHARED ROUGHLY IN RATIO OF RELATIVE STIFFNESSES, SO LOAD PASSING THROUGH UNIT STRIP OF BOND SHOWN IS

$$1 \Big/ \left(1 + \frac{E_s t_s}{3 E_p t_p}\right) \text{ OF TOTAL}$$

(b.) LOAD SHARING AFTER PATCH BONDED ON

FIGURE 47. SIMPLIFIED METHOD OF ANALYSIS OF LOAD SHARING WITH BONDED REPAIRS

reasonably close approximation which can be evaluated with nc more than a pocket calculator. The load intensity along the strip to be analyzed can then be established by load sharing in proportion to the relative stiffnesses of the load paths, as shown in part B of Figure 47.

A simple but particularly powerful rule to remember in this kind of assessment is that a hole in an isotropic plate under uniaxial loading increases in diameter or radius precisely three times as much as the same length in an area remote from the hole, as shown in part A of Figure 47. Thus, the stiffness of the load path diverted around an open hole is only one third as great as for the original structure. This softening is quite beneficial, since it diverts load away from the damaged area. The deduction of the factor three follows from the classical analysis of the stress field around an open hole in an infinite plate given in Reference 15. With the relation between the load in the patch and the remote stress level thus established, these new analysis programs can be used to analyze either purely bonded or bonded/bolted repairs. A sample solution is shown in Figure 48 to illustrate the capabilities of the A4EK program in this context. On their own, the bolts would be predicted to be capable of an even greater load transfer, of 9581 lb. per inch instead of 9535 lb. per inch for the combination. Again, however, it should be noted that the 9581 lb. is an ultimate value, attained only after substantial damage around the bolt holes, while the 9535 lb. strength would be achieved with no such damage.

The bolts in the repair shown in Figure 48 would often be the most practical way of locating the patch and clamping the parts together, particularly if they are thick. That would leave only the need for application of heat to cure the adhesive. The reliable in-service repair of fibrous composite structures by adhesive bonding alone is not as simple as it seems at first sight, however. One major problem which is already recognized in many quarters is that the small amount of moisture absorbed by laminates causes inferior bond or co-cured laminate strengths unless it is first removed by careful drying out. The impracticality of doing so in some cases, particularly for large thick composite structures, means that high-strength bonded repairs cannot always be relied on. Therefore, the repair of large composite structures may be forced to depend on mechanical fastening and an

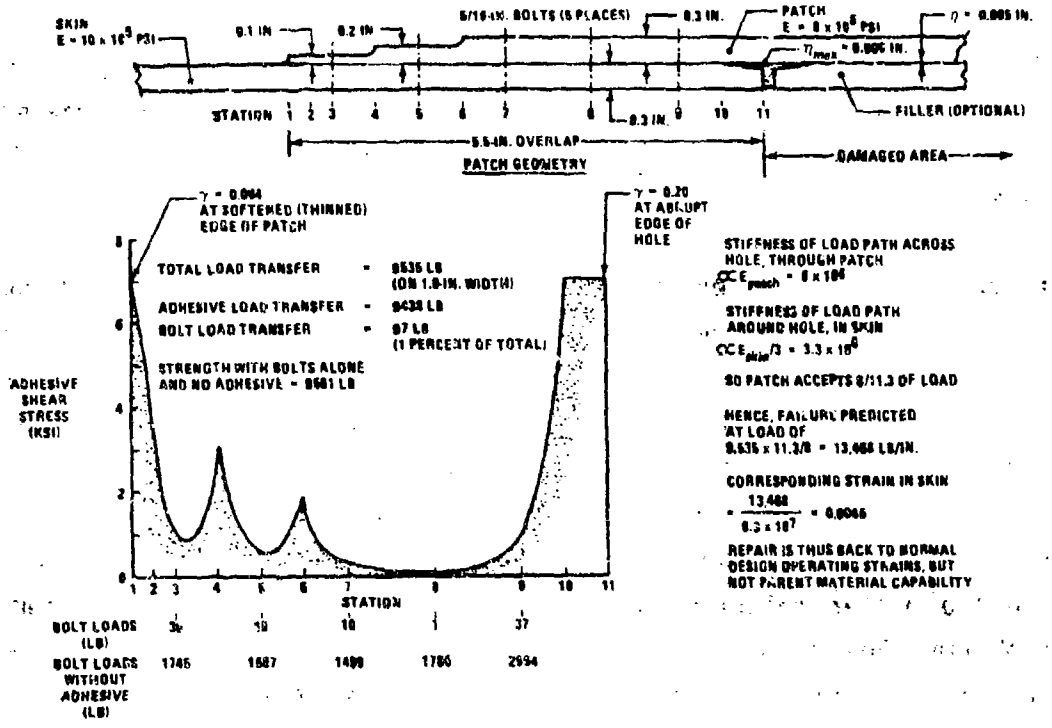

FIGURE 48. LOAD TRANSFER THROUGH BONDED/BOLTED FIBROUS COMPOSITE PATCH

adhesive bond of only about half its normal strength. (In that case, the predicted strength above would be reduced to 6777 lb. per inch.) In the case of thin composite laminates, on the other hand, purely bonded repairs are quite practical, because the bond starts out much stronger than thin adherends, the drying out prior to bonding is both quicker and easier.

4.4 COMBINATION OF BONDING AND BOLTING IN FAIL-SAFE STRUCTURES

There is a quite widespread misconception that mechanical fasteners can be considered to always provide fail-safety for adhesively-bonded joints. In actual fact, they can do so only in relatively few instances in well-designed bonded structure and not many more in poorly-designed structure. The key to the differences in behavior lies in the relative strength of the adhesive and the adherends. This is explained fully in Reference 16. Briefly, whenever the bond is stronger than the members being joined, no fail-safe load path is needed because the failure must run outside the bond area (where any rivets

would be located) before it could propagate. In such a case, rivets to backup the bond would be superfluous because, even in the area adjacent to any disbond or damage, the adherends are simply not strong enough to fail the adhesive.

In the case of thick members bonded together with such a simple joint concept that the adhesive is the weak link, a local disbond could cause a widespread and catastrophic unzipping of the bond. Mechanical fasteners through such a bond would provide a degree of fail-safety and could represent an improved structure. Certainly, no adhesive bond should ever be used without such reinforcement whenever the bond would be weaker than the members being joined. In some such cases, the use of a complex joint geometry would provide the better solution, by increasing the joint strength and removing the weak-link fuse from the structure. That is not always possible, however, particularly for fibrous composite structures, as is explained in the next section, so there are some structures for which the strongest and most damage-tolerant structure is obtained by bonding and bolting together. It should be understood that, even so, the ultimate strength of the intact structure is effectively defined by the adhesive alone, and the fasteners remain virtually unloaded until some damage has occurred to cause a load redistribution, as shown in Figure 49.

Whereas rivets or bolts can therefore be considered as fail-safe load paths for thick bonded structures, the converse is true for thin structures. This can be appreciated for Figure 50 by starting with the riveted, bond-free case as a baseline. The fasteners cause a weakness in the members being joined, like a seam of perforations along the joint. And the nature of such structure is that the more fasteners are broken (or the longer is the skin crack), the more severe is the load in the adjacent skin and fasteners. These conditions permit a catastrophic tearing whenever the damaged area is large enough or the load sufficiently high. Those unsatisfactory characteristics can be avoided by including adhesive bonding as well, both as a stronger alternative load path and as a means of reducing both the skin stress and the bearing stress along the fastener seam. It is fair to say, then, that the adhesive bond is then acting as the fail-safe load path for the rivets! In actual fact, the rivets or bolts are then superfluous

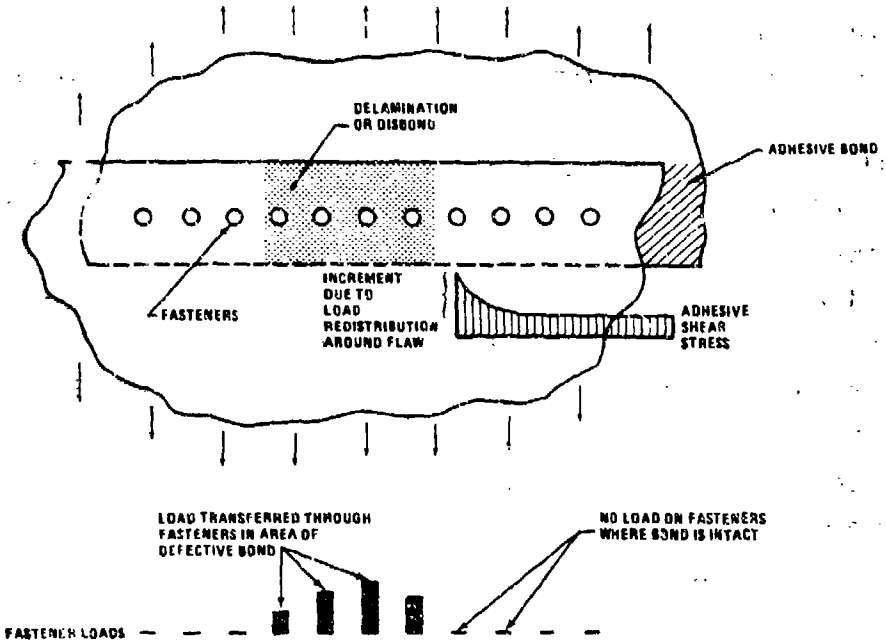

FIGURE 49. INDEPENDENT ACTION OF FASTENERS AND ADHESIVE IN LOAD REDISTRIBUTION DUE TO BOND FLAW

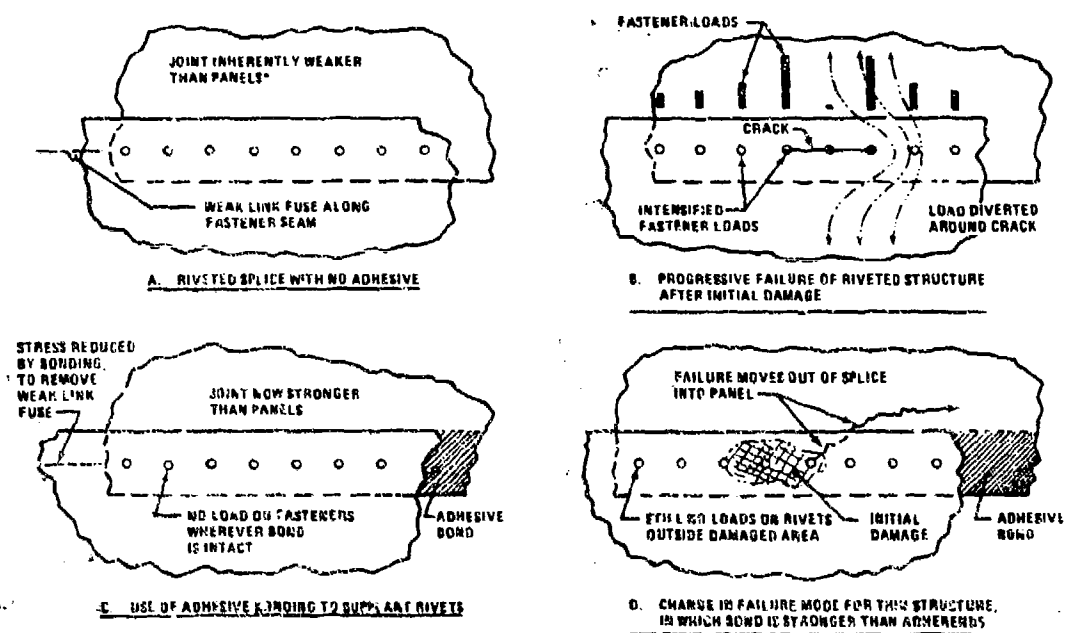

*NOTE: IF SPLICE AREA REINFORCED BY ADHESIVELY BONDED DOUBLERS, WEAK LINK IS MOVED OUT OF SPLICE INTO BASIC PANEL, AS IN D

FIGURE 50. USE OF ADHESIVE BONDS TO PROVIDE FAIL-SAFETY FOR RIVETED JOINTS IN THIN STRUCTURE

whenever the bond is stronger than the adhesives and should be eliminated to save weight and cost and to remove possible sites for damage initiation.

If so-called chicken rivets are added to a design only because of doubts about the reliability of the surface preparation or quality control for bonding, that cost would be better spent on improving the bonding techniques to remove the doubts. There are sufficient good service records of bonded structures to have full confidence in bonding alone, proved that the design and manufacture are done properly. Advanced composite structures have done much to expand the use of adhesive bonding in highly-loaded structure because they are so brittle that the structural efficiency of purely bolted or riveted composite structures is often unacceptably low. That is one reason why so much such structure is purely bonded.

4.5 ANALYSIS OF FAIL-SAFETY OF BONDED/BOLTED STRUCTURES

The section above contains an explanation of why the combination of bonding and bolting can be the most appropriate for thicker structures, particularly when made from fibrous composites. The purpose of this section is to illustrate the use of the new analysis program A4EK to characterize such a situation.

Figure 51 shows the area of concern representative of a bonded/bolted spar cap and skin combination in fibrous composite construction. Even under normal operating loads, the total load would be some tens of thousands of pounds. Now, if either the skin or the spar were to be broken, but not the other, a resin interface adjacent to the bond would be overloaded and tend to unzip. The only restraint would be the fasteners which have much more shear strength than the resin or possibly even the adhesive. The adhesive itself is not the weak link because it is so much tougher and stronger than the resin matrix. Therefore, the resin properties are used in the analysis in place of those for the adhesive. The analyses of this problem shown in Figures 52 and 53 show that the structure would indeed start to unzip and that the fasteners are capable of arresting such delaminations before they spread very far. This behavior is directly analogous with that reported in Reference 17 for purely bonded stiffened metal structures. In fact,

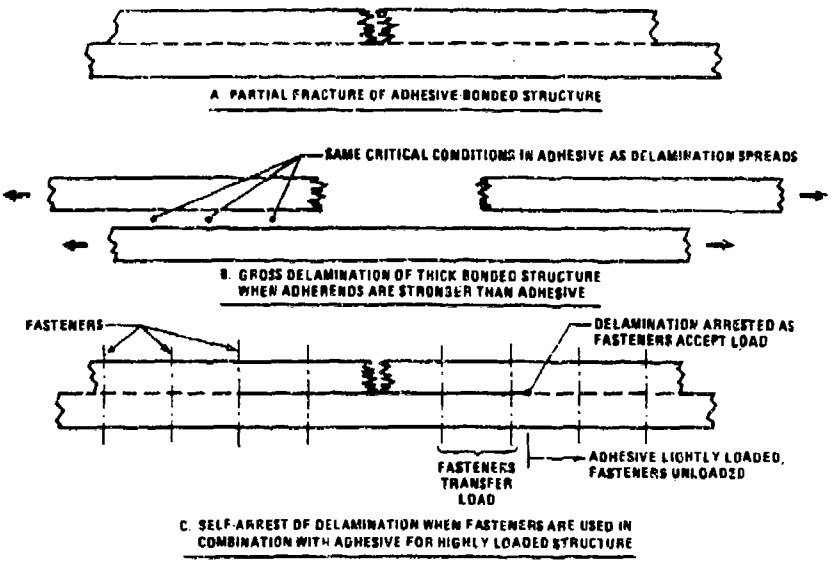

NOTE: IF ADHESIVE WERE STRONGER THAN ADHERENDS, THERE WOULD BE NO DELAMINATIONS. THE SECOND MEMBER WOULD SIMPLY FAIL AT THE SAME LOCATION AS THE FIRST. IN THAT SITUATION, FASTENERS WOULD NEVER FEEL ANY LOAD AND WOULD BE SUPERFLUOUS

FIGURE 51. NEED FOR FAIL-SAFE FASTENERS IN THICK BONDED STRUCTURES

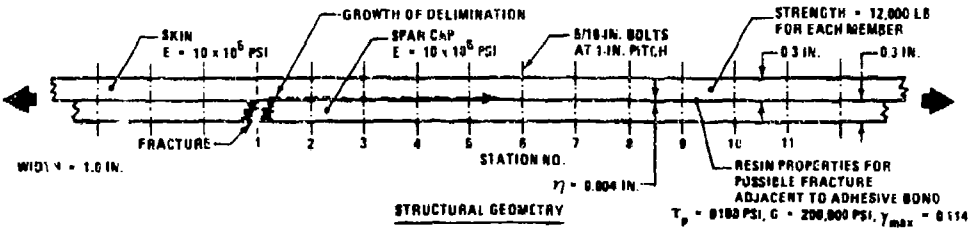

STATION NUMBER	1	2	3	4	5	6	7	8	9	10	11
1 ZERO DELAMINATION; FAILURE AT 6313 LB											
ADHESIVE SHEAR STRESS (KSI)	9180	74	0	0	0	0	0	0	0	0	0
FASTENER LOAD (LB)	0	1	0	0	0	0	0	0	0	0	0
2 1.0 IN. DELAMINATION, FAILURE AT 9003 LB											
ADHESIVE SHEAR STRESS (KSI)	0	0	9180	74	0	0	0	0	0	0	0
FASTENER LOAD (LB)	0	285	1	0	0	0	0	0	0	0	0
3 2.0-IN. DELAMINATION, FAILURE AT 10,468 LB											
ADHESIVE SHEAR STRESS (KSI)	0	0	0	9180	74	0	0	0	0	0	0
FASTENER LOAD (LB)	0	1783	231	1	0	0	0	0	0	0	0
4 3.0 IN. DELAMINATION; FAILURE AT 12,000 LB*											
ADHESIVE SHEAR STRESS (KSI)	0	0	0	0	9180	36	0	0	0	0	0
FASTENER LOAD (LB)	0	2662	1137	163	0	0	0	0	0	0	0
5 4.0-IN. DELAMINATION; FAILURE AT 12,0- 0*											
ADHESIVE SHEAR STRESS (KSI)	0	0	0	0	0	6530	20	0	5	0	0
FASTENER LOAD (LB)	0	2782	1304	600	84	0	0	0	0	0	0
6 NO ADHESIVE BOND, FAILURE AT 12,000 LB*											
FASTENER LOAD (LB)	0	2863	1505	785	412	219	113	58	31	12	0

*LIMITED BY ADHEREND STRENGTH

FIGURE 52. USE OF BOLTS AS FAIL-SAFE LOAD PATHS IN BONDED STRUCTURES

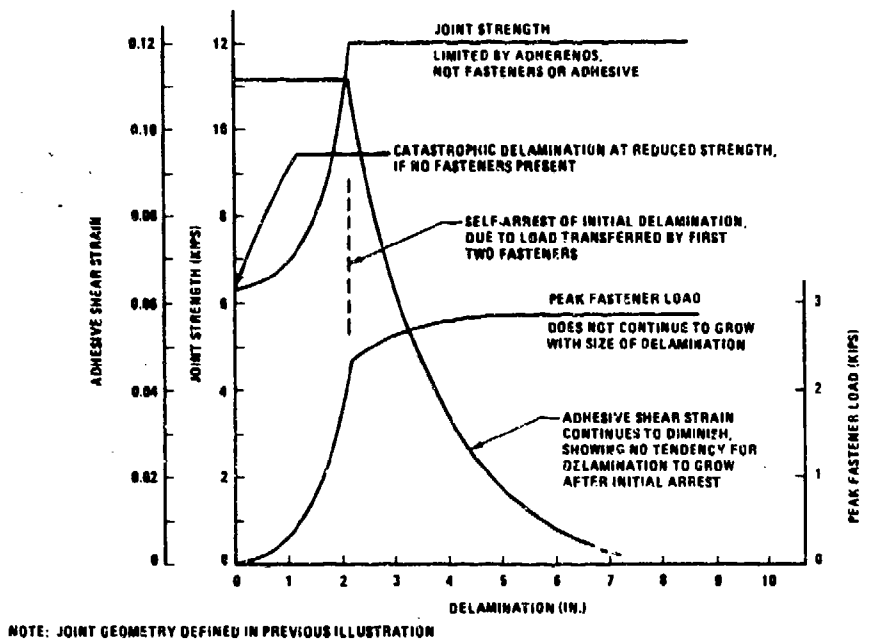

NOTE: JOINT GEOMETRY DEFINED IN PREVIOUS ILLUSTRATION

FIGURE 53. DAMAGE CONFINEMENT BY COMBINATION OF BONDING AND BOLTING

stiffnesses calculated by the A4EK program for various joint geometries and assumed or known disbonds could be fed into the pocket-calculator solutions in Reference 17 to expand the capabilities of each individual analysis.

Several significant observations can be drawn from Figures 52 and 53. The problem analyzed in Figures 52 and 53 is a good example of the need for fail-safe fasteners in thick, highly-loaded bonded structures. Local damage to one member would result in catastrophic failure due to unrestrained delamination if the structure were only bonded, without fasteners. The presence of the fasteners confines the delaminations to quite a small area, making repairs quite practical. While the bond alone is not as strong as the adherends, the fasteners are and they can reduce the loss of strength due to the initial damage to only a loss of effective area without any notch factor. The contribution of the adhesive in this case is so slight that the combination of fasteners with a good sealant would perform just as well as with the adhesive, particularly since the delamination tends to occur in a laminate rather than in the bond. The choice between adhesive and sealant should then be based on producibility considerations to maximize the quality

of the structure. It is important that the bonding medium should flow neither so little as not to wet the surfaces nor so much as to flow out all over the place. So the ideal material for such an application will have the cure cycle most compatible with the available heat-up rate for a given application.

4.6 CONCLUSIONS

The new nonlinear analysis of bonded/bolted joints is particularly useful in the context of damaged or imperfect structures. The method can be used to analyze the residual strength of such structures.

These analyses have confirmed that bonding and bolting together do not achieve any significant advantage over adhesive bonding alone in well-designed intact structures.

The A4EK program makes possible the analysis of the bonded/bolted repair of damaged or defective bonded structures by matching the various deformations through each load path.

The question of using fail-safe rivets in bonded structures is more complex than is generally recognized and a thorough explanation of the entire story is provided. Rivets are usually superfluous in lightly loaded structure, but bolts can be very valuable for heavily loaded bonded structures.

REFERENCES

1. L. J. Hart-Smith, "Adhesive-Bonded Scarf and Stepped-Lap Joints", Douglas Aircraft Company, NASA Langley Research Center Report CR-112237, January 1973.

2. L. J. Hart-Smith, "Further Developments in the Design and Analysis of Adhesive-Bonded Structural Joints", Douglas Aircraft Company Paper 6992, presented to ASTM Symposium on Joining of Composite Materials, Minneapolis, Minnesota, April 1980; published in ASTM STP 749.

3. M. K. Smith, L. J. Hart-Smith and C. G. Dietz, "Interactive Composite Joint Design", Douglas Aircraft Company, USAF Technical Report AFFDLTR-78-38, April 1978.

4. L. J. Hart-Smith, "Adhesive-Bonded Double-Lap Joints", Douglas Aircraft Company, NASA Langley Research Center Report CR-112235, January 1973.

5. L. J. Hart-Smith, "Advances in the Analysis and Design of Adhesive-Bonded Joints in Composite Aerospace Structures", Douglas Aircraft Company Paper 6224, presented to SAMPE 19th National Symposium and Exhibition, Anaheim, California, April 1974.

6. L. J. Hart-Smith, "Adhesive-Bonded Joints for Composites - Phenomenological Considerations", Douglas Aircraft Company Paper 6707, presented to Techonology Conference Associates Conference on Advanced Composite Technology, El Segundo, California, March 1978.

7. C. E. Thompson and L. J. Hart-Smith, "Composite Material Structures - Joints", Douglas Aircraft Company IRAD Report MDC-J0638, July 1971.

8. T. K. O'Brien, "Characterization of Delamination Onset and Growth in a Composite Laminate", NASA Langley Technical Memorandum 81940, January 1981.

9. W. Ramberg amd W. R. Osgood, "Description of Stress-Strain Curves by Three Parameters", NACA TN 902, 1943.

10. L. J. Hart-Smith, "Bolted Joints in Graphite-Epoxy Composities", Douglas Aircraft Company, NASA Langley Contract Report NASA CR 144899, January 1977.

11. L. J. Hart-Smith, "Mechanically-Fastened Joints for Advanced Composites - Phenomenological Considerations and Simple Analyses", Douglas Aircraft Company Paper 6748, presented to Fourth DOD Conference on Fibrous Composites in Structural Design, San Diego, California 14-17 November 1978.

12. F. P. Cozzone, M. A. Melcon and F. M. Hoblit, "Analysis of Lugs and Shear Pins Made of Aluminum and Steel Alloys, Product Engineering, Vol. 21, pp. 113-117, May 1950.

13. M. A. Melcon and F. M. Hoblit, "Developments in the Analyses of Lugs and Pins", Product Engineering, Vol. 24, pp. 160-170, June 1953.

14. T. Swift, "The Effects of Fastener Flexibility and Stiffener Geometry on the Stress Intensity in Stiffened Cracked Sheet", Douglas Aircraft Company Technical Report MDC-J6502, February 1974. Also published in "Prospects of Fracture Mechanics", Noordhoff International Publishing Co., Leyden, Netherlands, pp. 419-436, 1974.

15. S. Timoshenko and J. N. Goodier, "Theory of Elasticity", McGraw-Hill, New York, Second Edition, 1951, pp. 78-80.

16. L. J. Hart-Smith, Differences Between Adhesive Behavior in Test Coupons and Structural Joints", Douglas Aircraft Company, Paper 7066, presented to ASTM Adhesives D-14 Committee, Phoenix, Arizona, March 1981.

17. L. J. Hart-Smith, "Adhesive Bond Stresses and Strains at Discontinuities and Cracks in Bonded Structures", ASME, Jnl Eng Matls & Tech, Vol. 100, pp. 16-24, January 1978.

APPENDIX

This appendix (AFWAL-TR-81-3154, Vol II) has been intentionally omitted from this report because the computer software contained therein is limited to DOD agencies only. Other requests for the software should be submitted in accordance with AFSC Sup 1 to AFR 300-6 (DOD Dir 4160.19 dtd 2 Apr 73). Requests must be submitted to AFWAL/FIBRA, Wright-Patterson AFB, OH 45433.